Three-Dimensional Modeling of Biologically Relevant Fluid Shear Stress in Human Renal Tubule Cells Mimics *In Vivo* Transcriptional Profiles

By

Emily Jones Ross

Dissertation

Submitted to the Faculty of the

Graduate School of Vanderbilt University

in partial fulfillment of the requirements

for the degree of

DOCTOR OF PHILOSOPHY

in

Chemical and Physical Biology Program

January 31st, 2022

Nashville, Tennessee

Approved:

Billy G. Hudson

Nancy J. Cox

Anthony Capra

Emily Hodges

ACKNOWLEDGEMENTS

To those who made an impact on my scientific career:

Big thank you to my mentor, Dr. Nancy Cox, my committee chair, Dr. Billy Hudson, and my committee members, Drs. Emily Hodges and Anthony Capra for believing in me – a graduate student without a lab to call home and a passion for finishing this degree. Nancy, you are my science career savior and role model, all-in-one. Without your positive energy and assistance during some very delicate circumstances, I would not be finishing this thesis or my Ph.D.

Thank you, Drs. Rick Myers and Sara Cooper, for your encouragement and support in publishing my article, which allowed me to defend my graduate work. Under your guidance, I developed many skills through the publication process. Most importantly, you mentored me (and continue to mentor me). You both are truly amazing advisors, and I cannot express how much I appreciate everything you have done for me.

To the Myers, Cooper, and the former Jacob lab members – thank you all for the knowledge and scientific experience you shared with me. The Myers, Cooper, Cooper, Mendenhall, and Absher labs – our Friday morning lab meetings have been a continuous source of help and insightful questions. My paper and research would not have come together without your input. Also, I want to specifically recognize the efforts of the HudsonAlpha Institute during these challenging COVID-19 circumstances. Thank you for making sure we continually received financial and medical support during these difficult times.

I am beyond grateful to Jenna, Debbie, Prabhakar, and the supportive people at SynVivo (past and present) - my project was successful because of your training and allowing me to work in your lab space.

To Dr. Emily Gordon and (soon to be Dr.) Timley Watkins, thank you for all of your willing guidance and expertise in research and data analysis. Your kindness and tireless work effort are true inspirations. Plus, all of the meals, coffee/tea breaks, walks, Zoom calls, and text messages kept me sane.

Drs. Howard Jacob and Joe Lazar, please accept my sincere gratitude for taking in a graduate student with minimal experience in the field of genomics and genetics. Working on the SHROOM3 project in your lab taught me a lot of molecular biology techniques (such as primer design, CRISPR-Cas9, etc.), knowledge about genetics, and how to deal with difficult people. These skills will continue to help me throughout my career. Moreover, thank you for the research and intellectual freedom to develop my own thesis project and focus on creating a kidney proximal tubule microfluidic 3D model. I am disappointed that I could not finish my thesis work as your 11th graduate student. I wish you luck in your future endeavors; I am sure you will achieve your goals.

At Vanderbilt, I cannot thank my Chemical & Physical Biology department enough. Drs. Bruce Damon and Ivelin Georgiev, and Patty Mueller have been continuously supportive of completing my degree. I appreciate the assistance of my previous advisors, Drs. Gregg Stanwood and Sandy Rosenthal, and the amazing people in the Chemistry Department who contributed to my master's degree and graduate career. During my purgatory at FSU, thank you, Lisa Anderson, for all your supportive help and for being my

friend. Our coffee, lunch, and biscuit breaks were the only positive thing in my life while in Florida.

During my time in the Rosenthal lab, my colleagues ensured I was constantly engaged and entertained along the way. Specifically, I would like to thank Drs. Jerry Chang and Oleg Kovtun for their advice and assistance in teaching me the foundations of research and critical thinking. Because of both of you, I use cell culture techniques like a champion! I am proud and honored to be included in the beloved sub-group called "the bio-side." I would also like to thank Drs. James McBride, Melissa Harrison, Noah Thompson, and Mike Goodman for their helpful discussions and guidance in areas I was not knowledgeable about. In particular, I cannot express my gratitude enough for the exceptional friendships in graduate school. My friendship with Vanessa Bright goes beyond her short lab rotation – I always look forward to the times we can catch up. The musical concerts, Mellow Mushroom happy hours, TA and tissue culture room "therapy" sessions, breakfast/lunch/dinner/coffee breaks, and the encouraging words with smiles have made graduate school bearable. Also, a special thanks to those who helped me with data acquisition and advice, specifically Kasia Derewacz and Dr. M. Wade Calcutt, for their aid with the somatostatin project.

I am so grateful to all of the people who influenced my career path while working in the biotech field before graduate school – Open Biosystems/Thermo Fisher Scientific and Conversant. Working alongside experienced scientists and being mentored by many extraordinary people was a huge inspiration to pursue my degree. As well as those who educated and advised me throughout my undergraduate experience at the University of Alabama in Huntsville and Clemson University. Thank you, Dr. Ward, for convincing

other students and me that we had the ability and were “smart enough” to major in chemistry. Thank you, Dr. Bernhard Vogler, for suggesting that I apply for the NSF research experience for the undergraduate program and for putting up with me during your organic chemistry class – you had the patience of a saint. The UAH chemistry department for allowing me to get my first teaching experience. Finally, thank you to Drs. Maria Ragland Davis and Gopi Podila, for my first research experience in their labs and letters of recommendation to graduate school. You are both greatly missed.

Thank you for the financial support because this work would not have been possible without the aid of Vanderbilt University, Vanderbilt Institute of Chemical Biology, and HudsonAlpha Institute of Biotechnology.

To those who supported me in my personal life:

Outside of the lab, plenty of people kept me sane and happy. I am indebted to my wonderfully supportive family and friends. Without their patient listening and encouragement, the completion of this dissertation would have been much more difficult for all involved. Thank you to my brother David “Goobie” for being in my corner for support. My parents for always wanting what was best for me and my life. My adopted Brouillette family, your support and kindness is a blessing to my life. To my grandmother, Mama – two theses down and no more left! You supported me throughout it all!

I want to specifically thank my husband, Derek (a.k.a. Ky), for his love, patience, and rock-solid support throughout our adventures together, especially the final months of my Ph.D. You love me for all of me. One of the best feelings is finding someone who gets “you”. A person who lets you be vulnerable and honest, who encourages you, and never

tells you that you are “too much of this” or “too little of that.” Because to that person, you are just enough of everything they love and cherish. Thank you for being my person.

From my lap or closely lying nearby: Bailey, Harli, and Ryker closely supervised the writing of this thesis (thanks for the needed interruptions, animal babies).

Most importantly, I could not have completed any of this work without the help of my Lord and Savior. He is the reason I survived and made it through to the other side (Philippians 4:13 and Job 19:25-27).

TABLE OF CONTENTS

LIST OF FIGURES

LIST OF TABLES

LIST OF ABBREVIATIONS

AKI – acute kidney injury

Ad5 – adenovirus type 5

ABC – ATP-binding cassettes

AQP4 – aquaporin-4

CKD – chronic kidney disease

ESRD – end-stage renal disease

eGFR – estimation of glomerular filtration rate

FSS – fluid shear stress

FACS – fluorescence-activated cell sorting

HEK – human embryonic kidney (HEK293)

HPV – human papillomavirus 16

hTERT – human telomerase reverse transcriptase

iPSC – induced pluripotent stem cells

ICAMs – intercellular adhesion molecules

LAP – leucine aminopeptidase

MDCK – Madin–Darby canine kidney

MATE – multidrug and toxin extrusion proteins

MRPs – multidrug resistance proteins

OAT – organic anion transporters

OCT – organic cation transporters

OK – opossum kidney

P-gp – P-glycoprotein

PKD – polycystic kidney disease

LLC-PK1 – Lilly Laboratories cell-porcine kidney

PDMS – polydimethylsiloxane

PT – proximal tubule

PTCs – proximal tubule cells

RT-PCR – real-time polymerase chain reaction

RPTEC – renal proximal tubule epithelial cells

SLC – solute carrier transporters

2D – two-dimensional

3D – three-dimensional

ZO-1 – Zona occludens-1

CHAPTER I

General Kidney Introduction and Background

1.1 Kidney Physiology and Function

The kidney is essential in the homeostasis regulation of the human body. It enables physiological and regulatory functions, including regulating blood pressure by controlling extracellular fluid volume, maintaining pH balance, keeping appropriate electrolyte balance, hormone production, and waste and xenobiotics removal[1]. The kidneys are composed of three main segments: the renal cortex (outer section), medulla (middle section), and renal pelvis (inner drainage area). Nephrons (from the Greek *nephros*, meaning "kidney"), the kidney's functional units, are located in the renal cortex and between the renal cortex and renal medulla. The kidneys are complex organs with complex architecture, where blood vessels converge into a filtering compartment, the glomerulus, and adjacent tubular structures produce and collect urine[2]. Multiple unique cell types can be subdivided into five functional sections of the nephron – Bowman's capsule (containing glomerulus), proximal tubule, the loop of Henle, distal convoluted tubule, and collecting duct[3] (see Figure 1.1).

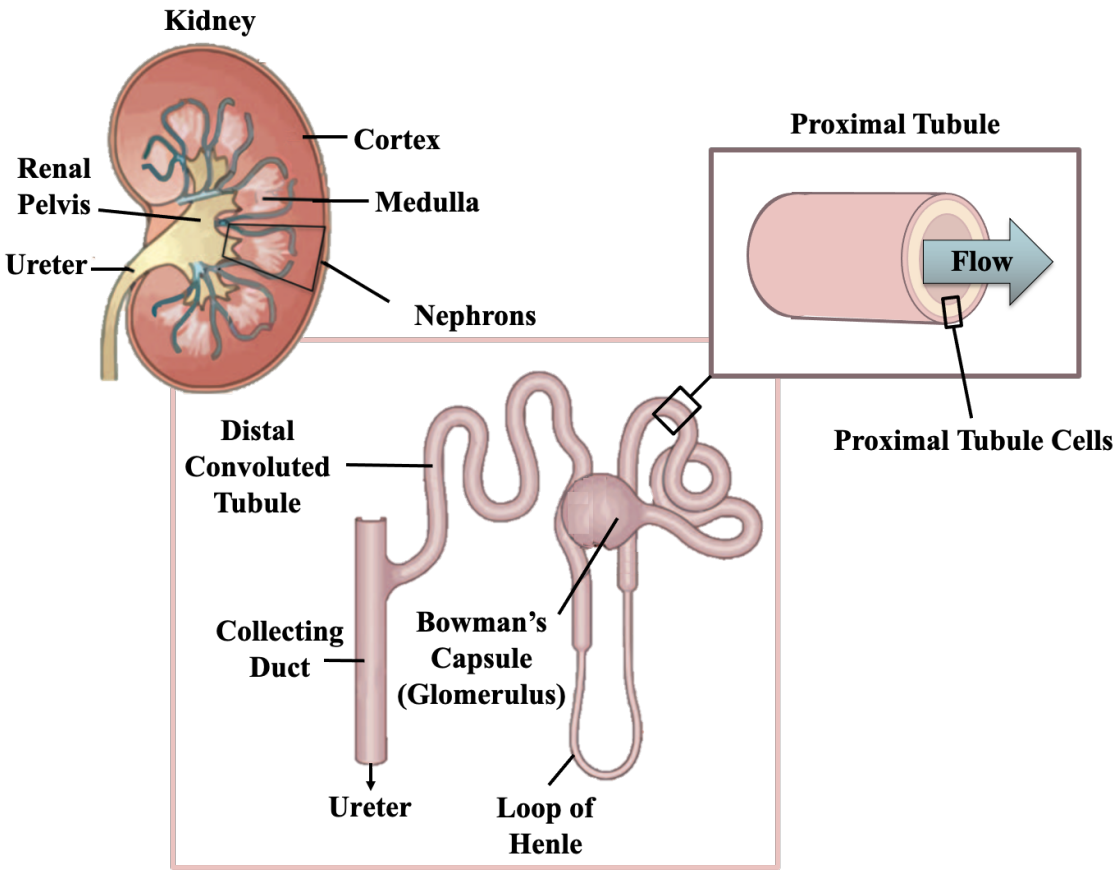

Figure 1.1 Diagram of the human kidney

The Bowman's capsule (or capsula glomeruli, or glomerular capsule) expands at the closed end of the nephron, and the cup-like structure encases a bundle of capillaries known as the glomerulus. It is the beginning of the filtration process and the site where the blood is entering the glomerulus through a highly pressurized, wide afferent arteriole and exits through a narrow efferent arteriole. This hydrostatic pressure creates a build-up of forces, and small molecules can pass from the blood into the capsule (known as the ultrafiltrate). Furthermore, inside the capsule is an elaborate physical filtration system or the filtration membrane. This consists of the innermost endothelium that lines the glomerular capillaries. The lining is a fenestrated or porous endothelium that penetrates through the endothelial cells. The next layer is the glomerular basement membrane, a

shared basement membrane between the two epithelial layers (endothelium and podocyte). The outer epithelium of the capsule is lined with podocyte cells; these specialized cells have an elaborate interdigitating processes or interlocking foot processes that are analogous to fingers of two clasped hands[4]. This elegant barrier permits passage of water, ions, and small molecules from the bloodstream into the Bowman's space (a molecular weight less than 20 kDa)[5]. In a healthy kidney, large components (molecular weight >70,000kDa) such as proteins and intact cells remain in the blood while small molecules, including nutrients that help nourish those cells, are allowed to pass[5]. The nephron capsule membrane extends to the renal epithelial proximal tubules, the primary site of reabsorption and metabolism within the kidney. My thesis will focus on developing a microfluidic device modeling the human proximal tubule (thus, the physiology of this part of the kidney will be discussed in greater detail below). The newly strained ultrafiltrate then progresses into the loop of Henle; the site of water and ions (including sodium, chloride, potassium, magnesium, calcium) are reabsorbed, and urinary concentration takes place. From there, the distal convoluted tubule fine-tunes the electrolyte content of filtrate by facilitating further sodium and chloride reabsorption, potassium secretion and further adjusts potassium, magnesium, and pH balance by hydrogen and bicarbonate ions. Once the filtrate has passed through the nephron, it is transferred into the collecting duct; the final site of electrolyte hemostasis, regulation, and concentration. The filtrate passes through the collecting ducts, which all join together in the renal pelvis of the kidney to form the ureter, ultimately traveling to the urinary bladder to be excreted.

1.2 Renal Proximal Tubules and Proximal Tubule Cells Physiology and Function

The kidney's proximal tubule (PT) is the extension of the Bowman's capsule devoted to the reabsorption of approximately 65% of the glomerular filtrate and performing other secondary functions, such as filtration, reabsorption, and excretion of substances passing through the PT[6]. The PT is subdivided into two main sections: the proximal convoluted tubule (*pars convoluta*) and the proximal straight tubule (*pars recta*). From these two main sections, proximal tubule physiology is classified as three morphologically and functionally distinct segments (S1, S2, and S3). The first segment (S1) extends from the Bowman's capsule and comprises the initial convoluted portion of the PT. The PTCs in this segment has a simple tall cuboidal epithelium, with a tall brush border (microvilli) on the apical membrane, and S1 basolateral membrane forms extensive lateral invaginations with adjacent cells. The S2 segment consists of the rest of the convoluted tubule section and the initial portion of the straight tubule. The S3 segment comprises the remainder of the proximal tubule before progressing to the loop of Henle.

Although there is variation between species, in mammalian kidneys generally, including humans, the S1 segment has a much broader physical diameter and greater complexity. This trend continues throughout the PT, with S1 > S2 > S3 as the filtrate passes towards the next refinement steps. This greater complexity seen in S1 compared to the other two segments includes cells with wider brush-border membranes with a greater number of microvilli on the surface. This leads to increased endocytic compartments and greater luminal surface area for transport and endocytic function. Furthermore, the S1 segment also has more extensive invaginations on the basolateral membranes, a larger network of mitochondria, increases in Golgi apparatuses in the cytoplasm, compared with the S2 and S3 segments of PT. Thus, it is not surprising that the S1 segment possesses the

highest capacity for ion, solute, amino acid, and active transport[6]. All three segments are considered a single collective proximal tubule within this thesis unless otherwise noted. The PT and PTC also play an active role in transporting xenobiotics, including drugs and their metabolic waste products, and are essential in reabsorbing drugs from the glomerular filtrate. These processes result in the exposure of the PTC to many potentially harmful compounds, making them an easy target for drug-related toxicity. Furthermore, due to their high metabolic rates and exposure to toxic agents, PTC is more exposed to hypoxia and chemical insults than other nephron segments. Transporter influx of the PTC can take place at the basolateral and apical membrane of the cells. These transporters are members of the solute carrier family (SLC). Necessary transporters include the organic cation transporter 2 (OCT2/SLC22A2) and the organic anion transporters 1 and 3 (OAT1/SLC22A6, OAT3/SLC22A8). Transporter efflux is mediated at the apical membrane via active ATP-binding cassettes (ABC) transporters, such as P-glycoprotein (Pgp/ABCB1), multidrug resistance-associated proteins 2 (MRP2/ABCC2), MRP4 (ABCC4), and breast cancer resistance protein (BCRP/ABCG2) (transporters are discussed in Chapters II and III). In addition, multidrug and toxin extrusion transporters 1 (MATE1/SLC47A1) and MATE2-K (SLC47A2) may play pivotal roles in detoxification through efflux facilitation[7–9]. Renal drug metabolism is less prominent than in the liver but is still physiologically important and involves cytochrome P450 (CYP) and Phase II enzymes[10].

A highly distinctive morphological feature of the PTC compared to other epithelial cells within the body is a unique brush border formed by densely packed microvilli. The presence of these microvilli in PT has greatly increased the luminal surface area of the cells, thereby facilitating their reabsorptive function. However, it has become more well

recognized and established that these cell-surface microvilli are also putative filtrate flow shear stress sensors within the lumen. The PT and proximal tubule cells (PTC) *in vivo* are exposed to continuous, relatively high luminal fluid shear stress (FSS) and a transepithelial osmotic gradient. In humans, precise measurements of FSS on PTC are lacking because urinary flow decreases along the proximal tubule as a result of tubular reabsorption. The FSS in the initial portion of the tubule was estimated based on the single-nephron glomerular filtration rate (GFR). In humans, the FSS is estimated to vary between 0.5 dyne/cm^2 and 1.2 dyne/cm^2, but can reach about 1.6 dyne/cm^2 in diseased individuals[10]. Studies performed under FSS even levels below those biologically relevant demonstrated that flow over the cells is a key modulator of cellular signal transduction, for which primary cilia functions as mechanosensing receptors. Flow affects PTC in multiple ways, including the organization of cytoskeleton and actin filaments, cell-cell junctional complex, cilia, expression of tight junction proteins (ZO-1), and adherens junction (E-cadherin) proteins[11].

Furthermore, studies have demonstrated FSS-dependency for gene and protein expression (for example, cubilin, megalin, intercellular adhesion molecules (ICAMs), vascular cell adhesion molecule 1 (VCAM-1), Phase I (CYP P450), Phase II enzymes (glutathione S-transferase, GST), and some multidrug resistance proteins (MRPs) and Phase III transporters (SLC))[12–16]. Additionally, functional changes can be seen after exposure to FSS. These changes include but are not limited to ion reabsorption (sodium and HCO3 transport), H+-ATPase activities, and receptor-mediated endocytosis[16–18].

Previous studies demonstrated that PTC cell-culture models systems exposing cells to FSS recapitulate *in vivo* proximal tubule morphology and function better than traditional static cell culture conditions. However, these studies do not always represent a level of FSS

relevant to biological conditions with existing publications using an FSS rate of 0.01 to 2.0 dyn/cm^2[19–23]. In addition, many existing PTC FSS studies have employed animal cells for their model systems, not utilized human proximal tubule cells. Likewise, existing methods have limited reproducibility of the model devices due to variability of fabrication and laboratory-to-laboratory device production. More information on two-dimensional, static models, and comparison to three-dimensional cell culture devices are discussed in length within the section below, Introduction to Current Proximal Tubule Cellular Models.

1.3 Kidney Disease and Renal Function

In 2013, kidney disease was the ninth leading cause of death in the United States[24]. Furthermore, chronic kidney disease (CKD) affects approximately 14 percent of the general population, and each year CKD kills more people than breast or prostate cancer[24,25]. The annual cost of this disease is over $30 billion dollars creating a significant burden on Medicare and healthcare spending[24–26]. There are two types of kidney disease, chronic kidney disease (CKD) and acute kidney injury (AKI), both of which may lead to kidney failure. A known risk factor for AKI is CKD, and there is research showing AKI is an accelerator for CKD[27]. Certain medications and drug therapies have been shown to cause AKI. These injuries result in a loss of function of the nephron, the kidney unit responsible for reabsorption and secretion of water and solutes from the blood. The PT, a section of the nephron, is a highly active site for this reabsorption and secretion and plays a key part in kidney-drug interactions. Renal drug transporters are primarily localized to proximal tubule cells PTC. These cells come into contact with nephrotoxic compounds, have high quantities of mitochondria, and few antioxidant defenses, making the PT susceptible to injury. The increased vulnerability towards injury makes the PT a crucial location for

kidney research. In order to study CKD, mechanisms, and effects of treatment interventions, many models have been developed. However, the lack of accurate predictive cell culture models and time-consuming/expensive animal studies have created a need for better-recapitulating kidney function *in vitro*. Given the wide range of and complex architecture of kidney functions, models that recapitulate these functions in a controlled system are valuable for studying diseases such as CKD. The complexity of this transport machinery makes the investigation of processes such as CKD pathology and drug efficacy for countering CKD, and more commonly, drug toxicity/secretion a challenge. Our goal is to facilitate improved experiments with our new model system.

1.4 Race and Gender Differences in Kidney Disease

Recently CKD, AKI, and End-Stage Renal Disease (ESRD) have been recognized as a global public health problem[28–31]. Issues associated and outcomes with CKD, AKI, and ESRD are characterized by marked differences in occurrence, frequency, and complications regarding gender, age, race/ethnicity, socioeconomic status, and geographic boundaries[28,32–34]. Some traits may indicate protection or an increased risk for certain health practices and medical conditions, suggesting there is much to learn beyond the traditional risk factors contributing to CKD and associated [35–38]. ESRD is a more dramatic example of health inequalities, with rates for minorities ranging from 1.5 to 4.0 times those of age-adjusted white counterparts, despite similar rates for the early stages of CKD[37,39–42]. Although CKD is associated with increased premature mortality rates, adjusted ESRD survival rates are unexpectedly improved for minorities[29,43]. Despite progress made, many diverse factors that influence the initiation and progression of CKD and the disparities therein are not fully understood. Although modifiable risk factors, such as culture,

socioeconomic status, and access to medical care contribute to a large proportion of CKD disparities, additional risk factors, from emerging biomarkers to providing structured and coordinated health care delivery, remain to be defined more clearly. Currently, the National Kidney Foundation and American Society of Nephrology established a task force in 2020 to reassess the inclusion of race in the estimation of glomerular filtration rate (eGFR, currently the gold standard to measure level of kidney function and determine kidney disease stage) in the United States and its implications for diagnosis and subsequent management of patients at risk for, kidney diseases[44]. These reviews and reports are a step in the right direction to help detail the process, assess current evidence, and values defined regarding the use of race to metrics of diagnosis.

Despite evidence of gender-specific disparities in epidemiology and pathophysiology in all stages of CKD, the majority of research and studies ignore the issue of gender[45]. The incidence of ESRD is 50% higher in adult men than in women, even though there is a slightly higher prevalence of CKD in women[25,34,46]. However, there are fewer women on renal replacement therapy than men and men may progress to ESRD more rapidly[34,46]. These gender differences in rates of CKD progression may be influenced by potential antifibrotic and antiapoptotic effects of estrogen or proinflammatory deleterious effects of testosterone, together with unhealthier lifestyles, might cause kidney function to decline at different rates[45,47]. Women are referred later for kidney replacement therapy and receive fewer arteriovenous fistulas than men receive, irrespective of race. Women are also less likely to receive kidney transplants as compared with men but are more likely to donate a kidney[47–49]. Further findings may also provide insights into gender differences, including looking at the effects of longer life expectancy on the natural decline of glomerular

filtration rate (GFR) with age, as well as potential overdiagnosis of CKD through the inappropriate use of GFR equations, might be in part responsible for the greater prevalence of CKD in women[47].

Gender differences can even influence transporter expression and, hence, drug kinetics, which creates the potential for toxicity screen results to differ between sexes[50]. In rats, for example, sex differences have been observed in the expression of tubule transporters and tight junction proteins, including claudin 2, AQP1, NCC, and ENaC108[51]. There are undoubtedly significant sex differences in renal blood flow and kidney function; however, the studies focused on understanding the human sex-related differences at genetic, transporter/receptor abundance, and overall physiological level.

Overall, a current hypothesis leading to men and women with CKD differs from the underlying pathophysiology of the disease and its complications, presenting different symptoms and signs, responding differently to therapy, and tolerate/cope with the disease differently[46]. Recommendations for medical management of CKD patients are currently made gender-blind, even though gender seems to impact underlying physiology[45]. Addressing gender differences and disparities in research is an important and overlooked area in the care of patients with kidney disease.

1.5 Development of a Living Kidney Membrane

Tissue engineering and stem cell research have paved the way for regenerative medicine, allowing to repair or replace damaged organs[52,53]. Significant successes in the medical research community towards reconstructing skin, bone, cartilage, and muscle, leading to clinical applications, have been made[53–57]. Continuous research efforts seek strategies to generate virtually every organ in the human body[55]. Nonetheless, the more

complex the organ – for example, the human kidney – the more complex the challenges. The current treatment of chronic kidney disease (CKD) has been replacement therapy, either by kidney transplantation or hemodialysis[58]. Kidney transplants may provide a solution for patients; however, organ availability, compatibility issues, lifelong requirements of monitoring, and pharmacological intervention to prevent organ rejection create expensive complications for the patients. Furthermore, hemodialysis blood purification treatment can improve the quality of life from the disease, although it does not represent a permanent solution and carries a significant burden for patients and their families[59]. Therefore, more treatment options and overall prevision is needed for this prevalent disease.

An adult human kidney can repair after injury, but rather than structural regeneration this involves rapid cellular turnover within the nephrons, either via proliferation of mature cells or the expansion of a residual tubular progenitor. However, no new nephron formation occurs in adults. Indeed, the repair responses that are seen after chronic injury with this reduced epithelial repair trigger tubulointerstitial fibrosis[60]. This lack of regenerative capacity after birth suggests that the kidney is an ideal organ to recreate using directed differentiation, albeit a challenging one. Progress towards this outcome has been slower than for some organ systems. One possible approach is using a bioartificial kidney that uses synthetic fibers lined with cells. Arguably, it aims at replacing function and not regenerating the kidney. Nonetheless, it could restore renal function using dialysis and kidney cells[61–63]. As will be discussed later in the Chapter, cell source is a pressing matter, and ensuring proper cell phenotype and function is vital. Other promising strategies in renal regeneration rely on the recellularization of kidney scaffolds, either by

decellularized scaffold-mediated renal regeneration or engineered by biological fabrication[54,64,65]. Finally, recreating kidney-like structures in vitro is showing promising preliminary results[66]. Both renal progenitors and induced pluripotent stem cells (iPS) successfully generate phenotypically accurate kidney organoids[62,66,67]. Generating these kidney organoids and testing renal progenitor cells in vitro presents opportunities for regenerative medicine and the improvement and refinement of current experimental methods[67–70]. Renal progenitors can be used to test the toxicity of a variety of compounds in cells cultured in 3D model systems. Although organoids are anatomically correct and express the desired renal markers, these renal constructs have limited use when mimicking kidney structures and functions[68,71]. The organoids are currently in an early stage of development and understanding their full potential.

1.6 Introduction to Current Proximal Tubule Cellular Models

Traditionally, *in vitro* PT studies are conducted under static conditions on two-dimensional (2D), plastic tissue culture plates, or in two-compartment containers separated by semi-permeable membranes. This included a transwell design – a membrane insert used for cell cultures, which allowed the formation of a compartmentalized system and cells to become polarize[23,72,73]. This category of cellular culturing system permitted co-cultures in independent compartments that can communicate through the release of signaling molecules through the transwell-mesh. However, due to the high cost, low-throughput design, and the failure to model many of the *in vivo* functional and physical aspects of kidneys, these devices have not been widely adopted across studies.

Since the late 90's the use of three-dimensional (3D) models has risen. Mainly, Fluid Shear Stress (FSS) is present within the lumen of the PT as the filtrate passes through

to the loop of Henle. Microfluidic devices provide a promising 3D model for PT since the cells are exposed to an FSS microenvironment which better mimics those found *in vivo*. The PTC grown in a traditional 2D static cell culture often lack or rapidly loses critical phenotypic and functional features, such as cell polarity, necessary apical brush borders, and significant receptor-mediated transport[72,74]. These features are critical kidney cell functions and actuate model studies. The use of FSS has been demonstrated to induce intracellular signaling and transporter function more reflective of the *in vivo* setting[14,16,67]. To overcome the limitations of existing 2D systems, we propose in this thesis to develop, demonstrate, and validate a microfluidic in vitro PTC model that better emulates human *in vivo* systems and diseased conditions by retaining key phenotypic and functional cellular aspects of human PTC.

Moreover, this 3D PTC microfluidic device allows for reproducibility as the devices are produced and sold by a biotech company. Three-dimensional models have gained increasing interest due to their ability to recreate precise cellular organizations including, vascular systems[75], blood-brain barrier model[76,77], cancer and immune organs modeling[78,79], respiratory physiology and pathology[80,81], and other organ systems[8,81,82]. To better model how PTCs contribute to CKD, the immortalized PTC (RPTEC/TERT1) microfluidic model will allow us to study kidney physiology and CKD pathology. Furthermore, this system can be utilized in other applications, such as drug efficacy and toxicity studies.

1.7 Summary

The mission of my thesis research work has been to develop a model system to further aid in the quest to elucidate mechanisms underlying chronic kidney disease and

discovering novel, more effective therapeutics. I have focused our research efforts on the specific region of the kidney nephron, the proximal tubule, and proximal tubule cells. To date, I have been pursuing the following goals: (i) distinguishing a human cell line to use for a PT model system, (ii) adapting a commercially available microfluidic device that will mimic the PT and allow the study of PTCs under FSS, (iii) development and validation of assays which characterize the model system for the study of PTCs, and (iv) elucidate the overall genomic changes of human PTCs under the treatment of FSS. My efforts have revolved around the human proximal tubule cell line, RPTEC/TERT1, which have been previously utilized as a proximal tubule cell-like model and validated in-house using fluorescence-based labeling protocols, functional assays, and genetic screening (Chapter II) and ascertaining transcriptional changes following treatment of PTCs in this device at three different fluidic shear stress (Chapter III). I will close with a glimpse into the future research topics such as clinical challenges and fully functional nephron on a lab chip. (Chapter IV).

CHAPTER II

Incorporating renal proximal tubule cells into a microfluidic device for the development of an *in vitro* model

2.1 Introduction

Cellular experimental models are regularly employed as an inexpensive and time-efficient method in both academic research and the pharmaceutical industry to assess the impact of potential drugs on cell or organ systems. These cellular models enable screening chemical compounds in the earlier stages of drug development before developing successful candidates to go into clinical trials. Furthermore, the complexity of the kidney transport machinery to investigate diseases, such as chronic kidney disease (CKD), progression, and pathology, is a continuous challenge for researchers. Currently, the *in vitro* screens for nephrotoxic drugs have focused on proximal tubule cells because this part of the nephron can be an essential target of nephrotoxic injury *in vivo*[72]. Several cell lines have evolved with advancements in cell culture technology and are used for kidney research (Table 2.1). Given their important role in drug metabolism, modeling of PTCs is particularly important for pharmacology research, as new drugs need to be tested for their effects on kidneys, especially proximal tubules, due to their increased contact with potentially nephrotoxic compounds[1]. This Chapter will describe the development of a 3D PTC microfluidic device, including discussing possible cellular options, biomaterial

surface features desirable for cell growth, surface modifications for renal cell attachment, and proliferation conditions.

Table 2.1 Commonly Used Renal Cell Lines

Cell	Source	Cell Type	Availability	PMID References
LLC-PK1	Pig	Primary	High	9773777
MDCK (NBL-2)	Dog	Cell Line	High	5918973
Rodent PTEC	Rat/Mouse	Primary	Veriable	22444643
HK-2	Human	Cell Line	High	8127021
NK1-2	Human	Cell Line	High	23516613
RPTEC/TERT1	Human	Cell Line	Low	18715936
ciPTEC	Human	Cell Line	High	26567716
Stem Cells	Human	Primary	Low	21512642
iPSC	Human	Primary	Low	25217273

Abbreviations: LLC-PK, proximal-like porcine kidney cells; MDCK, Madin–Darby canine kidney; HK2, human kidney 2; NKi-2, human telomerase reverse transcriptase immortalized human renal cortical cells; PTEC, conditionally immortalised proximal tubule epithelial cell; RPTEC, renal proximal tubule epithelial cell; TERT, telomerase reverse transcriptase; iPSC, Induced Pluripotent Stem Cells.

2.2 Cell Sources for Models of the Renal Proximal Tubule

2.2.1 Animal Models of Kidney Biology and Disease

Our understanding of mechanisms of disease and our ability to predict the effectiveness of treatment strategies have largely depended on studies using animal models. Many animals, including dogs, opossums, pigs, mice and particularly rats, have been used to mimic human renal disease[83]. Acute kidney disease and nephropathy events can be induced in various *Rattus* and other animal models by surgery or the administration of drugs or toxins[84,85]. Furthermore, genetically engineered and inbred animal strains provide a platform for investigating complex human nephropathy (for example, IgA nephropathy and diabetic nephropathy)[86,87]. Kidney toxicity is one major cause of clinical drug-trial failure, and drug-induced nephrotoxicity in the clinic is recognized as a significant contributor to both acute kidney injury (AKI) and chronic kidney disease (CKD)[88]. The

efficacy and toxicity of a drug candidate in the human body have been predicted based on the information previously obtained by animal testing. However, inappropriate pharmacokinetic predictions caused by species differences between humans and experimental animals have led to the abandonment of some candidate compounds prior to clinical trials[57]. In addition, information from animal studies is not always predictive of human responses due to distinctive physiology and different cellular functions. For example, renal filtrate clearance in animals is usually much higher than human renal clearance[89]. Using pharmacokinetic data collected from animal models runs the risk of underestimating human nephrotoxicity. Previous dependence on animal-based cellular models has made them unfavorable due to variability[90], environmental[91], and ethical concerns[57,65,92]. Numerous microfluidic systems utilize animal cell lines, such as the Madin–Darby canine kidney (MDCK) and the pig LLC-PK1 (Lilly Laboratories cell, porcine kidney) cells which form tight monolayers and are broadly available[16]. Transcripts expressed levels while under static, 2-dimensional fluid conditions within animal and human cell lines were matched to transcripts selectively expressed in native male Sprague–Dawley rat proximal tubule. Within this comparison, the opossum kidney (OK) cells displayed the highest percentage match (45% of proximal marker genes, TPM threshold = 15), with pig kidney cells (LLC-PK1) close behind (39%)[93,94]. Furthermore, the comparison of the RPTEC/TERT1 cells with the 193 rat genes, over half (90/193) are expressed at an RPKM of 0.5 or higher (a common standard for reliably detected expression)[95]. We also compared expression from RPTEC/TERT cells to expression data generated from human epithelial of proximal tubule primary cells from Thomas Gingeras *et al.* ENCODE project (GEO dataset GSM2343254) (comparison seen in Figure 2.2).

Table 2.2 - RNA-sequencing gene expression comparison of Rat, RPTEC/TERT1, and primary human PTCs.

Gene Symbol	Rat S1 (RPKM)	Rat S2 (RPKM)	Rat S3 (RPKM)	Ensembl ID	RPTEC/TERT1 (RPKM)	Primary PTC (TPM)	Primary PTC (FPKM)
abat	11.2	9.2	3.0	ENSG00000183044	0.20128	0.22	0.91
abcg2	8.9	18.1	1.9	ENSG00000118777	0.06415	0.09	0.37
abhd14a	19.7	183.0	106.2	ENSG00000248487	1.94238	2.52	10.69
acmsd	108.0	91.9	25.0	ENSG00000153086	2.90547	0.04	0.16
acot11	15.8	7.0	0.0	ENSG00000162390	0.30486	0.18	0.76
acss2	31.4	98.0	560.4	ENSG00000131069	40.18003	4.05	17.17
acy3	10.5	144.8	109.6	ENSG00000132744	0.0026	0	0.01
adap2	22.8	10.0	0.0	ENSG00000184060	0.59202	0.61	2.57
afm	0.5	7.9	15.1	ENSG00000079557	0.00162	0	0
agmat	3.6	28.4	80.0	ENSG00000116771	0.33349	0.51	2.15
agxt2	224.2	258.0	390.2	ENSG00000113492	0.00375	0	0
ak4	68.6	204.2	140.3	ENSG00000162433	7.41425	2.67	11.31
aldh2	171.7	464.0	412.7	ENSG00000111275	18.09309	4.99	21.11
aldh8a1	52.9	27.2	20.5	ENSG00000118514	0.4349	0.02	0.08
aldob	5101.4	2930.4	2388.5	ENSG00000136872	0.00834	0	0
alpl	28.9	66.5	114.5	ENSG00000162551	0.04135	0.06	0.24
amacr	5.8	106.3	77.7	ENSG00000242110	0.41847	0.73	3.08
amn	12.1	9.9	4.0	ENSG00000166126	0.95743	0	0
anks4b	43.7	61.3	24.8	ENSG00000175311	0.00605	0	0
anpep	1.5	43.0	141.0	ENSG00000166825	115.06877	5.99	25.38
apmap	5.7	38.2	10.8	ENSG00000101474	55.90779	13.41	56.78
apoe	203.3	32.0	28.6	ENSG00000130203	12.84428	0.79	3.35
aqp11	4.3	16.1	4.2	ENSG00000178301	0.90589	0.13	0.56
aqp7	50.5	26.6	67.6	ENSG00000165269	0.06885	0	0
aspa	13.0	17.5	18.4	ENSG00000108381	0.0005	0	0
aspg	0.0	4.0	22.8	ENSG00000166183	0.32144	0	0
ass1	397.8	250.0	105.4	ENSG00000130707	30.63397	0.84	3.58
baiap2l2	5.1	9.5	21.5	ENSG00000128298	31.66016	24.84	98.93
bhmt	0.3	27.2	9.1	ENSG00000145692	0.18946	0.19	0.82
bhmt2	96.2	129.0	107.9	ENSG00000132840	0.14999	0.37	1.47
c1qtnf3	2.9	10.6	12.8	ENSG00000082196	0.7319	0.04	0.18
cacng5	0.0	0.5	28.5	ENSG00000075429	0	0	0
calml4	822.5	432.7	458.7	ENSG00000129007	2.07224	0.37	1.55
ccr10	13.3	3.2	0.0	ENSG00000184451	0.68781	0.39	1.66
chtf18	0.0	3.0	16.1	ENSG00000127586	3.09112	5.56	23.54
cideb	22.0	17.5	11.6	ENSG00000136305	0	0.16	0.63
cidec	0.2	10.7	11.1	ENSG00000187288	0.00674	0	0
cmbl	214.5	115.0	41.7	ENSG00000164237	20.12817	0.39	1.65
cotl1	131.2	82.4	18.8	ENSG00000103187	44.88324	62.69	249.68
cryl1	295.9	337.9	180.2	ENSG00000165475	23.65619	6.35	25.31
cryz	126.9	320.7	386.3	ENSG00000116791	59.90891	10.07	40.1
csf2rb	0.2	11.2	0.1	ENSG00000100368	0	0	0
cth	6.0	162.2	205.6	ENSG00000116761	15.06656	0.37	1.49
cyp24a1	0.0	17.9	0.8	ENSG00000019186	0.0057	0.1	0.41
cyp2e1	126.0	117.0	28.4	ENSG00000130649	0.63126	0.13	0.5
dao	7.2	50.8	8.4	ENSG00000110887	0.00101	0	0
ddah1	0.0	0.0	0.0	ENSG00000153904	26.18684	3.26	12.97
decr2	406.4	242.9	86.0	ENSG00000242612	2.80629	1.39	5.54
dgkg	16.3	12.4	0.0	ENSG00000058866	0.00049	0.02	0.1
dhfr	61.3	45.6	14.3	ENSG00000228716	4.87338	9.22	36.73
dhrs7	0.6	88.9	330.6	ENSG00000100612	21.67702	7.44	29.62
dnajc22	10.6	20.4	4.5	ENSG00000178401	1.56918	0.08	0.34

dpys	4.4	31.5	28.8	ENSG00000147647	0.00249	0.02	0.08
enpp6	12.1	3.7	2.4	ENSG00000164303	0.00369	0	0
espn	17.7	20.3	42.0	ENSG00000187017	0.47768	0	0.01
fah	82.3	321.7	308.2	ENSG00000103876	5.11161	3.34	13.29
fam151a	21.9	7.1	0.0	ENSG00000162391	0.08533	0	0
fbp1	187.1	246.0	125.5	ENSG00000165140	0	0.2	0.81
fmo1	79.2	89.7	78.2	ENSG00000010932	0.01108	0	0
fmo3	0.8	184.5	275.2	ENSG00000007933	0.00247	0	0
fmo4	6.0	35.2	42.1	ENSG00000076258	2.04733	0.04	0.17
g0s2	15.1	24.0	27.5	ENSG00000123689	6.35192	1.8	7.17
g6pc	78.6	41.8	3.7	ENSG00000131482	0.00142	0	0
galnt14	9.3	14.3	0.0	ENSG00000158089	7.19502	5.52	21.97
gatm	1384.3	898.5	67.7	ENSG00000171766	0.13754	0.35	1.41
gc	0.0	0.0	33.0	ENSG00000145321	0.00454	0	0
gclc	1.3	408.1	635.4	ENSG00000001084	10.58544	1.22	4.88
gemin6	8.6	28.6	1.3	ENSG00000152147	1.80142	0.85	3.39
glyat	1376.8	1289.4	666.0	ENSG00000149124	0.07485	0	0
glyctk	111.1	81.1	54.6	ENSG00000168237	0.79171	0.82	3.25
gng13	1.2	0.0	0.0	ENSG00000127588	0.0692	0.12	0.46
gpx3	17551.3	6338.6	572.0	ENSG00000211445	46.57984	0.86	3.45
grhpr	537.9	423.4	158.9	ENSG00000137106	13.53991	12.57	50.05
gss	32.8	73.9	593.2	ENSG00000100983	44.49755	10.12	40.3
gsta1	581.5	623.0	631.0	ENSG00000243955	0.0168	0	0
gsta2	137.2	123.9	117.9	ENSG00000244067	0.0052	0	0
haao	44.7	678.5	437.2	ENSG00000162882	0.03801	0.28	1.13
hao2	1620.7	2765.4	4401.6	ENSG00000116882	0.00596	0	0
hgd	28.4	170.1	189.4	ENSG00000113924	58.63156	0.32	1.26
hnf4a	20.1	27.6	41.9	ENSG00000101076	0.00119	0	0
hnmt	0.0	12.6	26.3	ENSG00000150540	6.10483	1.2	4.77
hpd	2017.4	715.8	534.1	ENSG00000158104	0.09621	0.01	0.03
hsd11b1	12.6	335.7	321.0	ENSG00000117594	0.0082	0	0
hykk	9.3	27.7	25.9	ENSG00000188266	1.36101	0.95	3.79
igfbp4	6.7	10.5	3.6	ENSG00000141753	8.89936	7.98	31.77
il33	16.0	24.7	15.8	ENSG00000137033	0.0141	0	0
inmt	21.2	63.9	198.4	ENSG00000241644	0	0	0
iqcg	13.5	0.1	0.0	ENSG00000114473	1.21755	0.23	0.93
itga7	15.2	53.0	39.4	ENSG00000135424	0.20058	0.33	1.33
iyd	4.4	34.4	34.7	ENSG00000009765	0.05389	0	0
kcnj15	59.8	58.9	0.7	ENSG00000157551	5.53564	2.08	8.28
khk	24.0	77.0	76.2	ENSG00000138030	0.98485	0.76	3.02
kmo	10.2	36.0	17.1	ENSG00000117009	2.74785	0.93	3.72
mdk	22.6	7.8	0.1	ENSG00000110492	5.86158	42.69	170.02
mep1a	2.3	26.2	111.3	ENSG00000112818	0.00117	0	0
mep1b	0.0	22.7	78.9	ENSG00000141434	0.02949	0	0
metrn	13.5	0.4	0.0	ENSG00000103260	8.14249	7.72	30.75
mettl7b	32.8	118.0	87.1	ENSG00000170439	0.0199	0.02	0.09
miox	1385.9	3849.5	1659.0	ENSG00000100253	18.13953	0	0.02
mrap	0.1	9.2	22.7	ENSG00000170262	0.00627	0	0
msrb1	370.1	535.8	273.6	ENSG00000198736	11.19503	2.68	10.67
nat8	10.6	33.0	65.6	ENSG00000144035	0.05179	0	0
neurl2	16.9	1.0	0.0	ENSG00000124257	0.25438	0.44	1.75
nme4	111.6	20.1	3.0	ENSG00000103202	13.09875	8.54	34.01
nox4	10.1	1.4	0.0	ENSG00000086991	0.07897	0.41	1.65
olfml1	10.1	4.9	8.7	ENSG00000183801	0.00154	0	0

osgin1	0.2	105.0	447.9	ENSG00000140961	3.06161	0.84	3.35
pah	334.0	209.9	12.6	ENSG00000171759	0	0	0
pck1	280.1	375.0	185.5	ENSG00000124253	0.01748	0	0
pdzk1	298.5	256.9	202.7	ENSG00000174827	47.15426	0.32	1.27
pfn3	323.9	898.3	270.3	ENSG00000196570	0.02599	0	0
pla2g6	2.5	31.6	44.6	ENSG00000184381	4.42025	0.31	1.23
pm20d1	9.4	24.6	30.1	ENSG00000162877	0.0384	0	0.02
ppic	0.2	197.5	717.8	ENSG00000168938	20.84012	3.41	13.57
prepl	59.9	129.0	777.9	ENSG00000138078	13.29597	0.43	1.73
proc	14.8	19.5	39.1	ENSG00000115718	0.43358	0.04	0.15
prodh2	62.5	46.1	11.2	ENSG00000250799	0.00143	0	0
pter	106.3	66.3	93.9	ENSG00000165983	18.76291	0.31	1.23
ptprn	4.5	13.8	9.7	ENSG00000054356	0.00102	0.09	0.38
qdpr	314.1	418.5	96.2	ENSG00000151552	8.48598	1.59	6.72
qprt	109.8	75.0	40.8	ENSG00000103485	63.8897	19.85	84.05
rbp1	457.9	35.0	0.3	ENSG00000114115	0.00531	6.06	25.66
rbp4	0.0	0.0	10.7	ENSG00000138207	0.06414	0.37	1.57
rdh16	16.8	31.5	31.8	ENSG00000139547	0.03582	0	0
resp18	0.4	2.4	21.8	ENSG00000182698	0	0	0
rgn	1.7	38.8	173.0	ENSG00000130988	0.31064	0.1	0.43
rpp25	52.6	15.6	0.0	ENSG00000178718	2.1044	2.41	10.21
serpinc1	36.6	2.8	3.7	ENSG00000117601	0.04351	0	0
sfxn1	11.4	44.1	20.2	ENSG00000164466	5.33382	12.44	52.7
slc13a1	79.7	54.1	0.0	ENSG00000081800	0	0	0
slc13a2	2.3	27.0	11.7	ENSG00000007216	0.00034	0	0
slc13a3	42.2	95.4	16.9	ENSG00000158296	0.44039	0.16	0.67
slc16a14	21.9	9.0	2.2	ENSG00000163053	3.54879	0.15	0.62
slc16a2	16.0	9.9	0.0	ENSG00000147100	18.98104	0.72	3.06
slc16a4	15.0	50.2	30.8	ENSG00000168679	1.02672	1.26	5.33
slc17a1	30.3	73.2	11.3	ENSG00000124568	11.29181	0	0
slc17a3	19.0	102.6	103.5	ENSG00000124564	4.52078	0	0
slc22a1	36.6	89.7	9.9	ENSG00000175003	0.20996	0	0.01
slc22a12	1.6	21.6	120.5	ENSG00000197891	0	0	0
slc22a13	0.0	0.0	10.8	ENSG00000172940	0.04601	0	0
slc22a2	31.1	96.5	293.7	ENSG00000112499	0.02307	0	0.01
slc22a6	82.7	105.3	19.8	ENSG00000197901	0	0	0
slc22a8	80.7	152.3	0.7	ENSG00000149452	0	0	0
slc23a1	2.2	23.1	31.8	ENSG00000170482	0.5797	0.01	0.05
slc23a3	0.0	3.6	44.3	ENSG00000213901	1.35053	0.02	0.08
slc25a45	9.8	23.8	0.0	ENSG00000162241	0.40225	0.15	0.65
slc26a1	13.4	33.6	16.6	ENSG00000145217	4.80573	0.17	0.73
slc27a2	13.3	81.5	175.6	ENSG00000140284	2.17246	1.07	4.52
slc29a3	52.2	68.3	163.1	ENSG00000198246	7.73599	1.76	7.46
slc30a2	13.5	11.4	0.0	ENSG00000158014	2.44048	3.28	13.88
slc34a1	333.2	1242.0	214.8	ENSG00000131183	0.11729	0	0
slc34a3	49.1	3.5	0.0	ENSG00000198569	0.52667	0.01	0.04
slc35d1	0.1	12.3	1.9	ENSG00000116704	3.0299	0.73	3.09
slc38a3	0.3	44.0	173.8	ENSG00000188338	0.33852	0	0
slc39a8	1.5	19.4	10.6	ENSG00000138821	8.36981	2.51	10.63
slc3a1	49.6	113.7	709.8	ENSG00000138079	24.39756	2.11	8.94
slc47a1	16.1	73.3	15.6	ENSG00000142494	0.01208	0.23	0.98
slc51a	10.4	26.6	3.1	ENSG00000163959	0.57141	0	0
slc5a10	4.3	54.0	44.1	ENSG00000154025	0.00511	0	0
slc5a11	1.0	39.6	19.4	ENSG00000158865	0.00818	0	0

slc5a12	16.2	0.0	0.0	ENSG00000148942	0	0	0
slc5a2	90.9	8.2	0.5	ENSG00000140675	0.04112	0.01	0.04
slc6a13	4.7	25.0	2.0	ENSG00000010379	9.75523	5.63	23.83
slc6a19	19.8	8.7	0.0	ENSG00000174358	0	0	0
slc7a13	0.3	137.3	780.1	ENSG00000164893	0	0	0
slc7a9	17.5	9.2	3.7	ENSG00000021488	0.03349	0.09	0.39
sod3	114.8	136.0	111.5	ENSG00000109610	143.1643	21.7	91.91
sord	310.7	250.6	80.2	ENSG00000140263	3.46119	4.89	20.72
spink1	39.6	41.3	0.0	ENSG00000164266	0.02572	0.51	2.17
spp2	395.6	157.3	0.3	ENSG00000072080	0.00497	0	0
sult1b1	14.0	8.8	56.4	ENSG00000173597	0.00204	0	0
susd2	10.6	34.4	1.7	ENSG00000099994	0.08384	0.01	0.06
susd3	20.2	27.1	35.2	ENSG00000157303	0.05001	0.19	0.81
syce1	17.3	12.0	2.6	ENSG00000171772	0.00275	0	0
syce2	12.2	3.9	0.0	ENSG00000161860	0.36488	0.03	0.12
sycp3	19.0	4.9	3.2	ENSG00000139351	0.16139	0	0
tff3	4.1	264.9	2658.5	ENSG00000160180	0.0696	0.04	0.18
tgfbi	0.0	0.7	21.7	ENSG00000120708	12.92277	48.96	207.35
thnsl2	15.4	21.6	96.5	ENSG00000144115	2.43824	0.16	0.69
tmem106a	42.3	32.2	2.6	ENSG00000184988	1.40034	0.43	1.84
tmem252	3.7	11.9	8.5	ENSG00000181778	0.62099	0	0
tmigd1	0.0	4.1	16.7	ENSG00000182271	0.00251	0	0
tmlhe	2.6	32.5	162.2	ENSG00000185973	2.37043	1.15	4.86
tnip1	11148.5	3200.9	583.9	ENSG00000145901	31.22135	33.09	140.15
tpmt	96.2	81.4	399.0	ENSG00000137364	13.55631	1.58	6.71
trpv1	34.0	10.1	0.0	ENSG00000196689	0.11426	0.07	0.31
tst	501.0	1098.0	150.5	ENSG00000128311	16.00339	6.57	27.83
ttc36	15.6	76.7	27.3	ENSG00000172425	0.12906	0.22	0.9
upb1	112.0	136.9	197.5	ENSG00000100024	0.00023	0.21	0.82
xdh	15.1	5.8	0.4	ENSG00000158125	4.38739	0.13	0.56
xpnpep2	9.3	11.4	21.5	ENSG00000122121	0	0	0
xylb	16.6	24.6	30.3	ENSG00000093217	0.24434	0.18	0.74
zbtb5	137.7	94.3	43.1	ENSG00000168795	5.69047	1.04	4.16

RPKM expression values of segments of the Rat proximal tubule regions S1, S2, S3 (PMID:25817355) compared to the average RPKM values of RPTEC/TERT1 cell line controls (PMID: 34234242). Further comparison to expression of epithelial cell of primary human proximal tubule cells (most abundant transcript) (GEO dataset GSM2343254).

These primary cells showed a near-identical fraction of those 193 known PTC-specific genes expressed to the RPTEC/TERT1 cells (99/193). Based on this analysis, we have determined that many PTC-specific transcripts are expressed in human immortalized RPTEC/TERT1 cells, as well as primary human PTCs. However, there are some differences between the PTCs in Rat PT regions S1, S2, and S3 and human PTC lines, which may be relevant to interpreting the data.

Despite their value, OK and other animal cells cultured under standard conditions do not fully recapitulate some key aspects of human PTC structure and function[96]. For example, regulation of drug transporter expression (e.g., GLUT2, SGLT1, OCT2) and pharmacokinetic profiles often differ considerably between animals and humans[51,97]. Overall, data from renal studies and clinical drug studies suggest that culture model systems based on human-derived cells are more predictive of human clinical outcomes than an animal tests.

2.2.2 Primary Human Proximal Tubule Cells and Their Challenges

The use of isolated human PTCs from the kidney cortex is currently one of the gold standards for cell-culture models[98,99]. Considering genetic, phenotypic, and functional changes that can result from the techniques of cell immortalization and long-term cell passaging, these offer various advantages, as well as commonly yield far more representative results[100]. Purification and isolation methods of renal epithelial cells from kidney tissue are performed as described previously[98,101–103]. The cortical tissue is dissected away from the kidney section, minced finely, and digested with collagenase. Following the filtration to remove the undigested and fibrous tissue from the cells, they are further separated on a gradient system. After using this filtration method, the proximal tubule fragments form a band near the base of the gradient[99,104]. Additional purification for PT-specific cells can be performed with trypsinization and fluorescence-activated cell sorting (FACS) for the proximal tubular markers leucine aminopeptidase (LAP) and using antibodies dual-labeling for CD10/CD13 markers[103]. Viable human PTCs can be obtained directly from a kidney nephrectomy sample from a cancerous kidney or isolated using a kidney biopsy of a non-cancerous patient. Occasionally, non-transplantable fresh post-

mortem kidneys are available, which provides a more abundant source of fresh cells. However, availability and the time until isolation present a significant challenge[100]. While primary cells are often ideal for cell-culture research studies, it presents its own challenges. Cells in primary cultures may lose their phenotype, stop expressing cell-specific markers, and are prone to dedifferentiation and transporter/receptor expression loss. Primary PTCs cells have minimal expansion capacity, losing their epithelial characteristics with each population doubling in culture. These primary cells display large inter-donor variability (making comparison studies difficult), and their use is limited to the availability of donors[99,105,106]. Furthermore, the limited number of primary cells isolated from human kidney tissue poses another research hurdle. To obtain sufficient cells for use in multiple microfluidic devices, *in vitro* cellular expansion is necessary. Nevertheless, when primary cells are brought into culture, loss of epithelial characteristics and cellular senescence rapidly sets in, thereby severely restricting the functionality of primary cells *in vitro*[51,106]. Due to these complications of availability, maintaining primary cells *in vitro* while retaining their native functionality and endogenous properties, immortalized cell lines are chosen as a more cost-effective and stable alternative.

2.2.3 Immortalized Kidney Proximal Tubule Cell Lines and Their Limitations

Currently, the number of human cell lines generated has increased due to improved molecular techniques and attempt to refine or replace the use of animals in research. Cell lines have been developed relying on different immortalization systems that reduce genetic variability and improve the cells' stability. Some immortalization methods include viral oncogenes (human kidney 2, HK-2 cell line was immortalized using the viral oncogene human papillomavirus 16 (HPV-16) E6/E7), while others were immortalized using a

hybrid adeno-12-Simian virus 40 (SV40) virus (HKC cells)[107,108]. An alternative method to oncogene insertion is the introduction and overexpression of the human telomerase reverse transcriptase (hTERT) (which was used in the development of the RPTEC/TERT1 cells)[108,109]. For example, the human embryonic kidney (HEK and HEK293) cell line originates from an uncharacterized kidney cell in the human embryo transformed with adenovirus type 5 (Ad5) DNA. However, due to the manipulation process, these cells display some properties are associated with a "neuronal lineage" and do not provide a relevant model for comprehensive renal study[110]. Several other well-established human renal models have limited proximal tubular functions, such as the immortalized renal tubular cell line HK-2 (human kidney 2), which has only low-level expression of the SLC22 transporter family and lacks the expression of OAT1, OAT3, OCT2, MRP2, and BCRP, and is therefore not a fully adequate model for nephrotoxicity[111,112].

Relatively new conditional immortalized human PTCs, such as RPTEC/TERT, are suitable models for implementing microfluidic arrays. These cells exhibit the characteristic, tightly packed, epithelial "cobblestone" morphology and developed extensive dome formation at the later time points that are indicative of unidirectional transport of water and solutes and thus of a matured epithelium[113] (Figure 2.1). The immortalized cell line, RPTEC/TERT1, whose shape can be clearly discerned in the light microscope, shows anticipated morphological characteristics of proximal tubular epithelial cells as they are characterized by the tightly compact cobblestone appearance. Furthermore,

fluid dome formation occurred on the monolayer when grown to a high cell density.

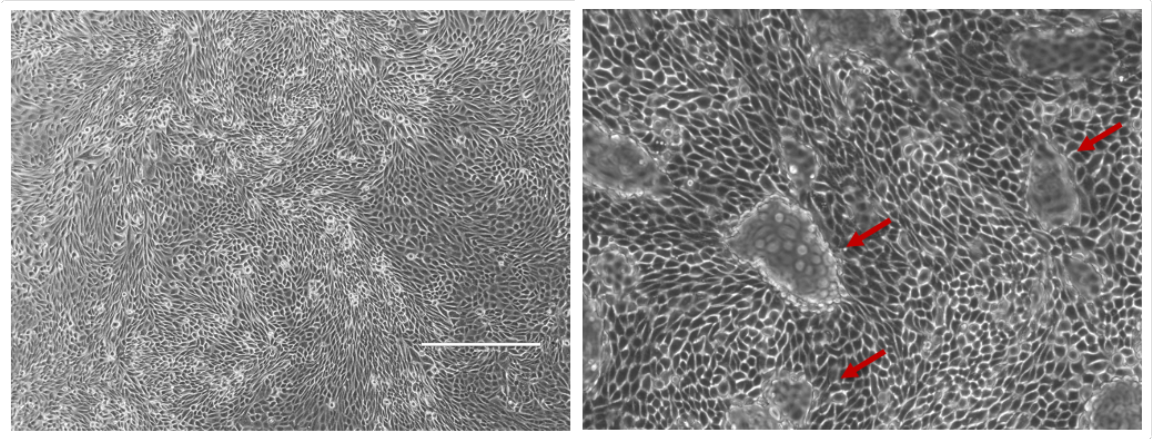

Figure 2.1: RPTEC/TERT1 cell morphology. Immortalized human proximal tubule cells with typical epithelial, cobblestone morphology. Characteristic "domes" formation at the surface of the cells (red arrows).

The original characterization of hRPTECs gives a detailed description of the similarities between these cells and proximal tubules. While it is not a perfect model, their work establishes this cell line as a reasonable model for these renal studies[51,108,109,114–119]. It has been demonstrated that RPTEC/TERT1 cells express many of the proximal tubule drug transport systems, including, and not limited to, the excretion pathway mediated via a complex interplay involving solute carrier (SLC) transporters. This includes the expression of organic cation transporters (OCT2/SLC22A2, OCT3/SLC22A3, and OCTN2/SLC22A5), multidrug and toxin extrusion proteins (MATE1/SLC47A1 and MATE2/SLC47A2), and organic anion transporters (OAT1/SLC22A6, OAT3/SLC22A8, and OATP4C). The PTC transporters responsible for urinary excretion of xenobiotics and the focus of pharmaceutical drug studies are major types of ABC efflux transporters. Several ABC transporters, including MRP1 (ABCB1 (P-glycoprotein, P-gp)) and MRP2 (ABCC2), MRP4/ABCC4, and MRP5/ABCC5)[8,115] are expressed in the RPTEC/TERT1 cell line. Furthermore, this cell line demonstrates an increased capacity for oxidative

respiration, expression of proximal tubule tight junction proteins including claudin 2 and 10 (CLDN2 and -10) and cilia associated proteins including primary ciliary and flagella associated proteins (CFAP20, -300, -410, -53, -44, -36, and PCDP1)[8,115]. Besides waste product excretion and reabsorption of filtered solutes by transporter pathways, these PTCs utilize endocytosis to recycle proteins from the filtrate, such as glucose and albumin. Additional transcriptomic characterization of this cell line and comparison with PTC from fresh human renal tissue will provide insight into its abilities as a valuable human cell model. However, the current characterization and the functional ability of transports, as is present *in situ*, make the RPTEC/TERT1 cell line a valuable tool in developing PTC models for many applications, including drug screening.

2.3 Characterizations of Human Proximal Tubule Cells

2.3.1 Monolayer Culture and Integrity Assessment (ZO-1) by Immunofluorescence from Multiple Cell Sources

The proximal tubule (PT) in the nephron extends the Bowman's capsule and is primarily involved in the reabsorption of approximately 60-65% of the glomerular filtrate, amongst other essential functions[6,120]. These polarized epithelial cells in the tubular structures have distinctive apical and basal plasma membrane domains and specific lateral surfaces that connect cell-to-cell by specialized cellular junctions[121]. Complex extracellular compartments are formed between the interlocking lateral and basal processes between adjacent cells (Figure 2.2). The basal membrane of epithelial cells adheres to the extracellular matrix predominantly by integrins and syndecans (adhesion receptors). In contrast, the lateral surfaces of the epithelial cells interact with each other through lateral cellular junctions[121,122]. Among these lateral cellular junctions are specialized tight junction

proteins (Zona occludens-1 (ZO-1), TJP1), and they create a permeable barrier for molecules selectively dependent on their size, charge, and the type of proteins present. Expression of ZO-1 is essential to the barrier function; thus, a cell lacking clear expression of ZO-1 is expected to have compromised barrier function. Here we use microscopy assessment to monitor these morphological characteristics of primary human proximal tubule cells compared with the immortalized cell line, RPTEC/TERT1. Within 2D culture plate, cells were compared using immunofluorescence labeling of anticipated proteins, cell shape, and polarization (discussed further in Chapter III).

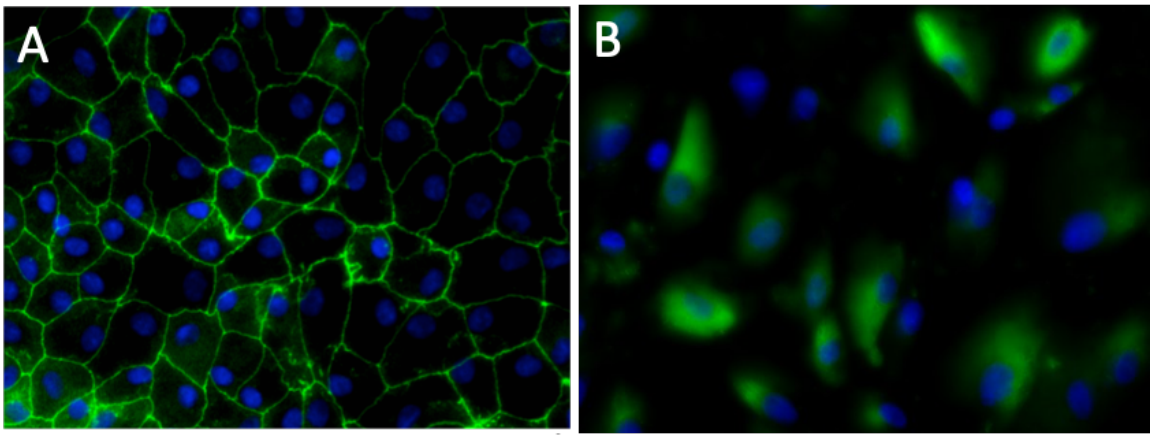

Figure 2.2: Zona Occludens-1 (ZO-1) cellular staining. Human kidney proximal tubular epithelial cell morphology under static conditions. Immunofluorescence staining of the tight junction protein ZO-1 (tight junctions) (green) and DAPI (blue) in (A) immortalized human RPTEC/TERT1 cells and (B) human primary proximal tubule cells.

Consistent expression and integrity of the tight junction marker protein ZO-1 is shown on the outer edges and present in confluent cell monolayers of PTC immortalized cell line, RPTEC/TERT1, thus, indicating that the cells do indeed possess correct PTCs morphology and are interconnected by tight junctions (Figure 2.2A). In contrast, the primary cells would not reach full growth confluency, and cells were elongated, not growing in a pattern resulting in the cobblestone monolayer. Furthermore, the ZO-1 cellular staining seems to be dispersed throughout the cell and does not label the specific protein for ZO-1 (Figure

2.2B). These results indicate that the RPTEC/TERT1 cells morphologically better represent PTC compared to the Primecells Human Primary Tubule cells.

2.3.2 Proximal Tubule Gene Expression using Real-time PCR Validation

Previous studies observed that multiple kidney-specific endothelial genes are highly expressed in freshly isolated primary kidney endothelial tissues and cell culture[8]. We examined the expression of PT-specific markers and genes in the RPTEC/TERT1 using RT-PCR (Real-time PCR). Furthermore, we wanted to determine the genetic expression using RT-PCR corresponded to the expression patterns to RNA-sequencing results; thus, validating our RNA-sequencing results. The PCR amplification of reverse-transcribed mRNA confirmed RPTEC/TERT1 express the PT markers AQP1, BBS7, and CFAP36 were up-regulated and the gene expression of PKD2, MDR2, and GGT1 was down-relegated after the treatment of FSS (Figure 2.3). The expression of a selected set of genes was validated by RT-PCR and confirmed fluid-shear induced increased expression of POLR2A, HSPA4L, EPHX1, UNKL, MDM2, TRIM16L, while DUSP8, ALOX5, IL32, SLC15A1, FSTL3, and LZTS3 expression was decreased by fluid shear stress (Figure 2.4).

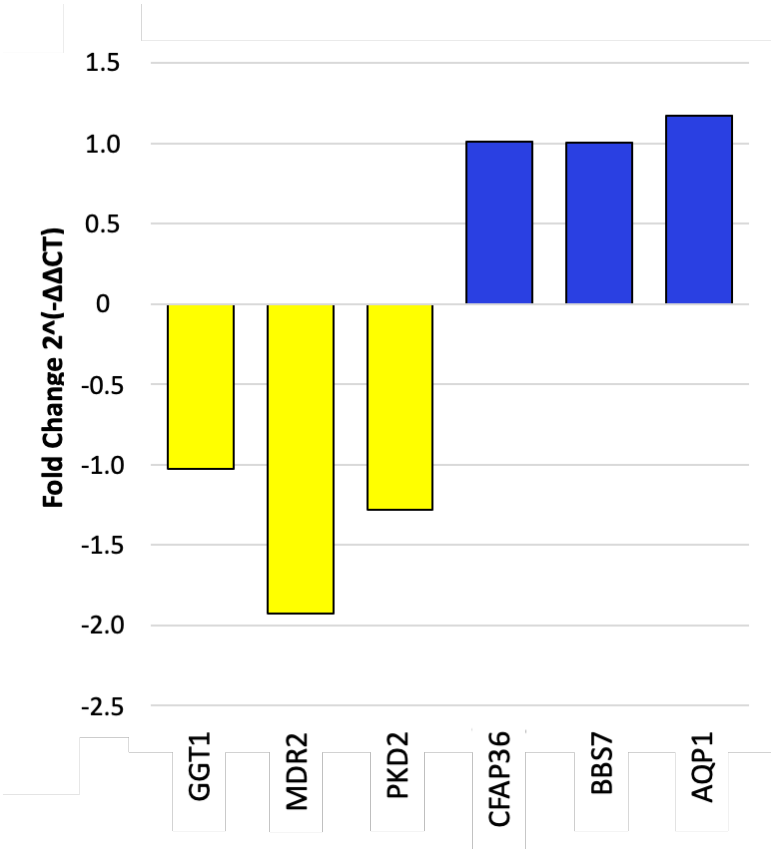

Figure 2.3: Real time-polymerase chain reaction (RT-PCR) of PTC markers. Graph shows the fold change of the genes down-regulated (yellow) and up-regulated (blue) gene.

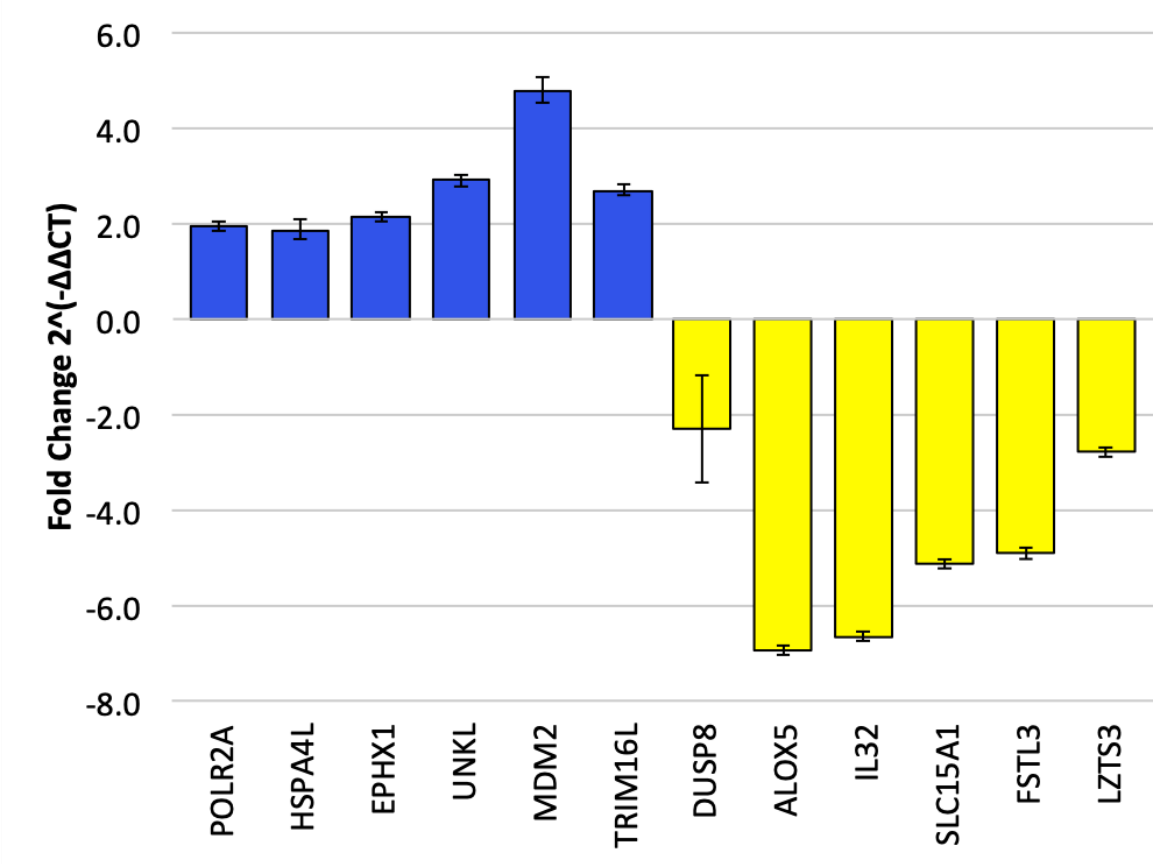

Figure 2.4: Real time-polymerase chain reaction (RT-PCR) validation of highly up-regulated and down-regulated gene transcripts by RNA-sequencing analysis. Graph shows the fold change of the genes down-regulated (yellow) and up-regulated (blue) gene

The gene expression was normalized to the housekeeping gene YWHAZ, providing the relative gene expression. The housekeeping gene YWHAZ was used previously in PTC

research and was identified as maintaining improved specificity comparing static maintained and FSS treated cells[123] (Figure 2.5).

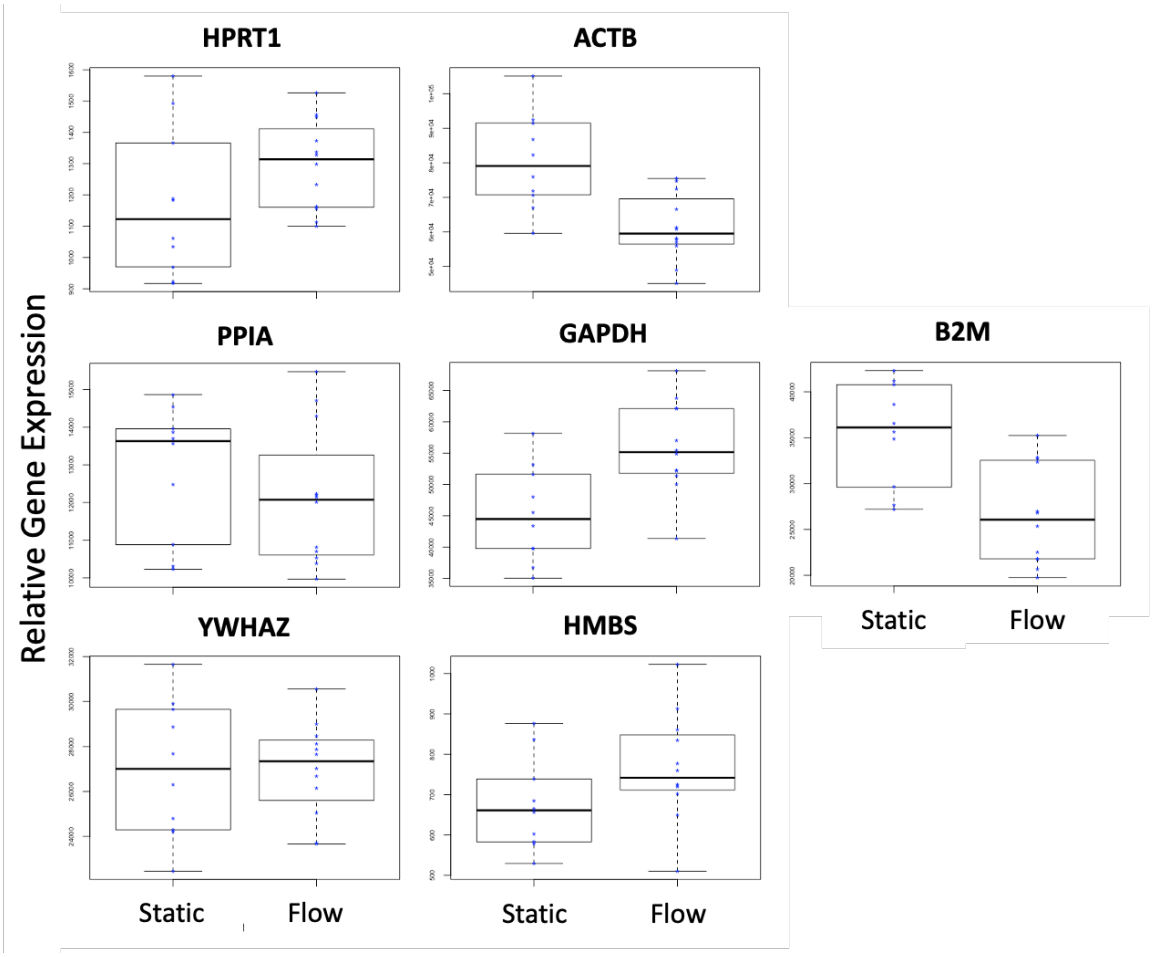

Figure 2.5: Determining housekeeping gene for RT-PCR. Relative gene expression of housekeeping genes from RNA-sequencing comparing static and FSS sample. The housekeeper gene, YWHAZ, was identified as maintaining specificity between the two treatment compared to the other genes.

2.3.3 Proximal Tubule EC_{50} Curve Analysis for Drug Assay Development

Many drugs are known to have adverse kidney phenotypes on different nephron regions. Several review articles have previously been published summing up many known drug outcomes on the [124–130]. Many antibiotics and antifungal agents have nephrotoxicity[131,132]. Many agents, such as metal-based chemicals (platinum, cadmium,

silver) and antimicrobials, have been shown to elicit cytokine responses in the kidney, resulting in inflammation and altered kidney function[133–136]. For validation of the drug response studies with our model system, we directly compared our initial dosing concentrations with *in vivo* studies from databases such as those of the FDA National Center for Toxicological Research (NCTR) Center for Toxicoinformatics, TOXNET, National Toxicology Program, and NIEHS National Center for Toxicogenomics (NCT). However, differences between dosages and responses may be found with this immortalized cell line, RPTEC/TERT1, compared with previously used animal and human cell culture lines.

To distinguish the optimal dosing to use on the RPTEC/TERT1 cell line, we looked at time-dependent and dose-dependent trends for the responses to indicate the *in vivo* responses. Furthermore, we found the approximant EC50 dosage values for the PT

transporter inhibitors using both Calcein-AM and CMFDA assays: Ko143, MK-571, PSC833, and Ceefourin-169,137,138 (Figure 2.6 and 2.7).

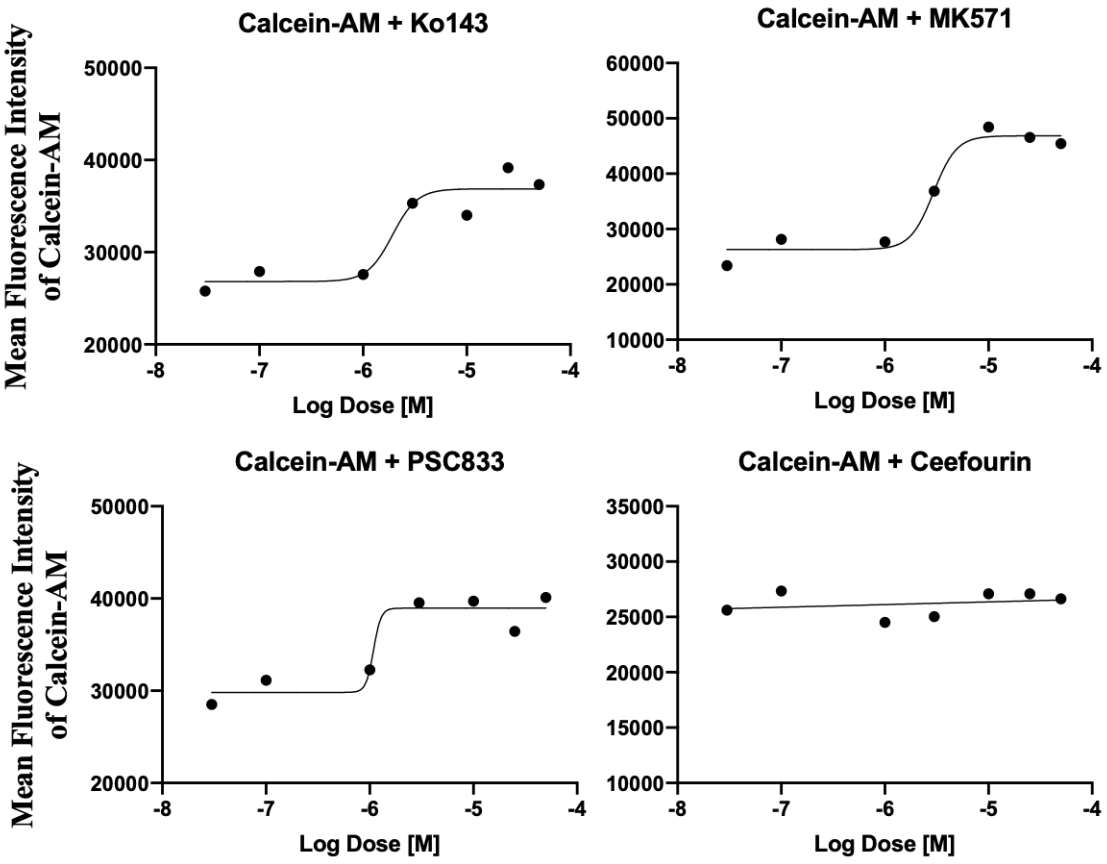

Figure 2.6: Drug dosing curves using fluorescence dye Calcein-AM.

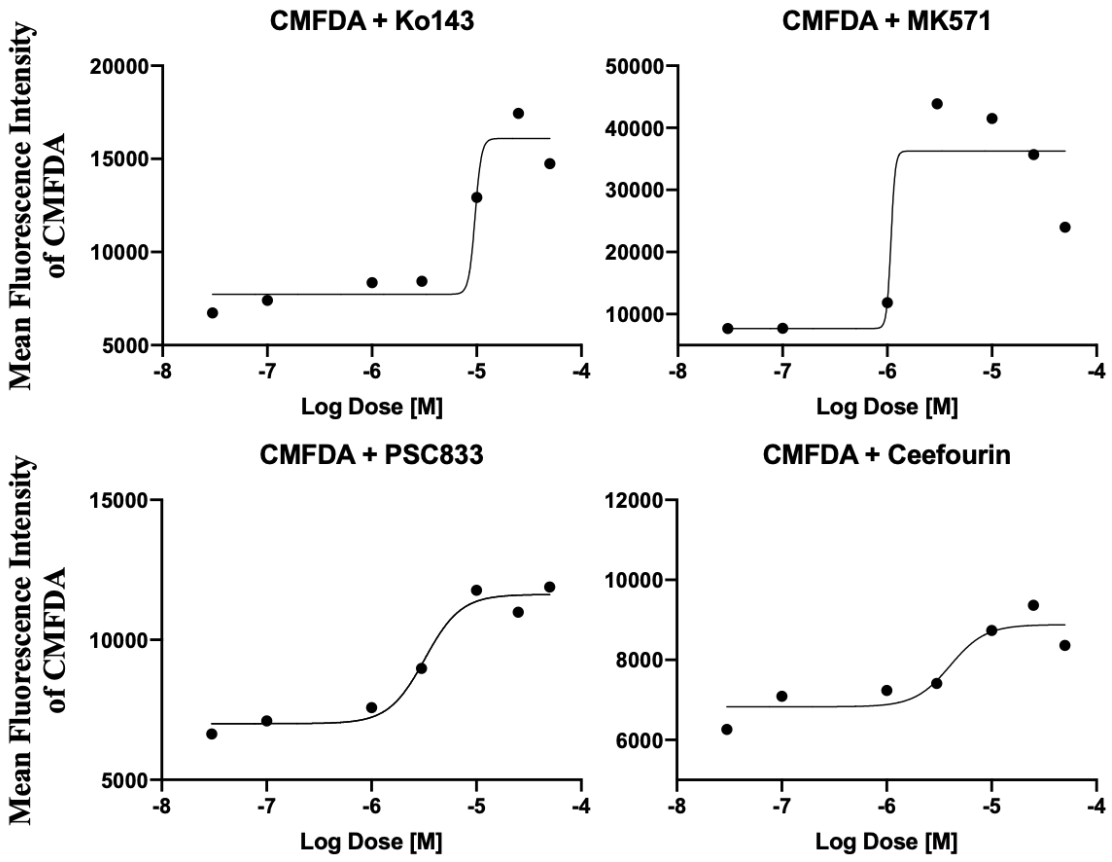

Figure 2.7: Drug dosing curves using CMFDA fluorescence dye.

Toxicological and drug dosing values for the RPTEC/TERT1 immortalized cells included Cisplatin and Polymixin B, which are classical drugs and are cytotoxic to kidney proximal tubule cells. Aspirin was used as the control drug spanning the range of the toxicological curves for the other drugs. In order to establish the range of optimal drug concentrations for toxicity (EC_{50} curves), we first tested the drugs in a well-plate format containing the cells of interest (RPTEC/TERT1). The cell viability assay, CellTiter96 from ProMega, was used to access the cell death, was used to generate a toxicological EC_{50} curve for stagnant

flow cells. The EC_{50} values demonstrated a higher degree of sensitivity in the RPTEC/TERT1 to Polymyxin B dosages compared to the Cisplatin drug (Figure 2.8).

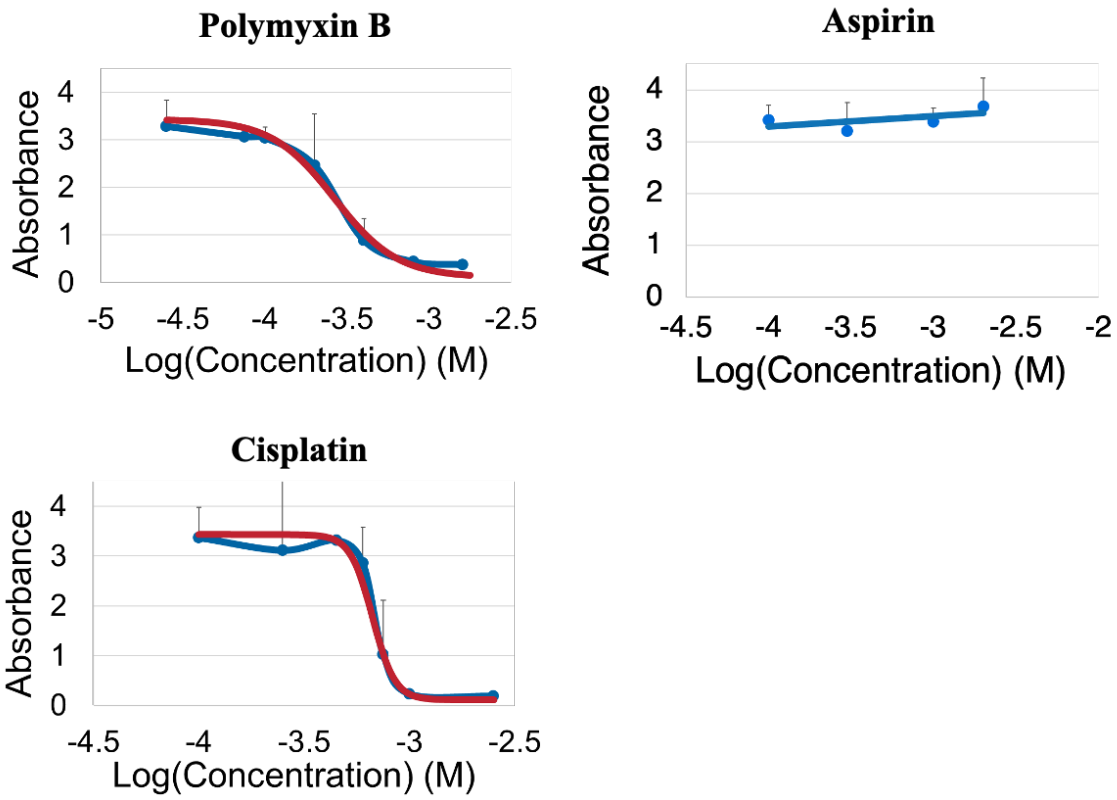

Figure 2.8: Toxicity dosing curves analysis of toxic drugs Polymyxin B and Cisplatin to RPTEC/TERT1. Curves fits were overlaid on the dosing experimental data. Two independent experimental assay experiments were used (red and blue lines). Aspirin dosing was used as a control drug spanning the range of the toxicological curves of the other drugs.

2.4 Fabrication and Preparation of the 3D Microfluidic PTC Device

2.4.1 Overview of Microfluidic Devices

The kidney functions include balancing body fluids, forming urine, and the removal of compounds from the ultra-filtrate for excretion from the body. Specifically, the renal proximal tubule epithelial cells are responsible for active protein trafficking and the reabsorption function of the kidney[10]. Further complicating experimental approaches using model systems, PTC grown in a traditional 2D static cell culture compared to their *in vivo* counterparts often lack or rapidly lose key phenotypic and functional aspects, such as cell

polarity, important apical brush borders, and significant receptor-mediated transport[63]. Fluid shear stress (FSS) has been demonstrated to induce intracellular signaling and transporter function more reflective of the *in vivo* setting[14,139]. To overcome these 2D limitations we proposed developing, demonstrating, and validating a microfluidic *in vitro* PTC model that better emulates human *in vivo* systems and diseased conditions by retaining key phenotypic and functional cellular aspects. This 3D PTC microfluidic device will allow us to better model how PTCs contribute to chronic kidney disease (CKD) utilizing the well-characterized immortalized PTC (RPTEC/TERT1). This RPTEC/TERT1 microfluidic model would allow us to explore GWAS nominated variants in genes. By utilizing PTC generated from CKD patient-derived iPSC, we would discover if the dysfunction begins within the glomerulus and/or proximal tubules (future directions discussed further in Chapter IV). Currently, there are a limited number of commercially available human models mimicking kidney physiology, particularly for capturing the genomic variations in human populations. Different experimental platforms using animal models are typically used – drosophila melanogaster[140], xenopus[141], zebrafish[142,143], rodents[92], devices that could be used with different cell types[108]. Here, we focus on our microfluidic device assembly and preparation for cell attachment and proliferation, as well as on developing a syringe pump system to control the microfluidic flow rate for culturing RPTEC/TERT1 proximal tubule cells under FSS.

2.4.2 Proximal Tubule Device Design

The microfluidic design builds upon SynVivo microfluidic devices, a patented and commercially available cellular platform technology (www.synvivobio.com) developed by CFD Research Corporation. Previously, SynVivo assays have been commercialized for

drug delivery and for inflammation[80,144–146], 3D tumor models[147,148], and blood-brain barrier modeling[76,77]. We adapted their linear channel design for a PT device; with a width of 500µm and a constant depth of 100µm, and a length of 1cm. These devices are made of polydimethylsiloxane (PDMS), which serves as the structural material for the channels bonded to a microscope slide. It is widely regarded that different cell types require different material surface properties for optimal proliferation, viability, and functionality. Briefly, the steps involved in device construction: (a) Spin-coating of photoresist (PR); (b) UV photolithography of the PR; (c) Development of the PR; (d) PDMS casting over-developed PR, followed by PDMS curing; and (e) PDMS bonding to a microscope slide.

2.4.3 Device Coatings and Monolayer Integrity Analysis

Coating a membrane culture surface is a crucial model condition for achieving optimal device performance, particularly in 3D microfluidic models where adhesion under FSS to the substrate is a potential issue. These protein coatings are intended to mimic a basement membrane, a key extracellular component in the PT. The major components of all basement membranes are laminin, collagen IV, entactin/nidogen, and sulfated proteoglycans, which are commonly used in previous kidney models and this dissertation[149]. What concentrations should be used for these coatings in this specific model system have not been established; therefore, some trial-and-error experimentation was required for this study. Various methods of surface treatment have been employed to aid in cell attachment and proliferation of renal cells within the microfluidic device. These treatment methods either increase the presence of functional groups on the surface, increase hydrophilicity, or increase the amount of protein adsorption on the surface of the membranes preferable for PTC cultivation. To find the ideal coating method for the

RPTEC/TERT1 cells, several 24 tissue culture plates were prepared for RPTEC/TERT1 coating environments and concentrations: fibronectin, collagen I, and no coating control conditions (Figure 2.9). Overall, the RPTEC/TERT1 cells grew more optimally and evenly on the collagen I coating system.

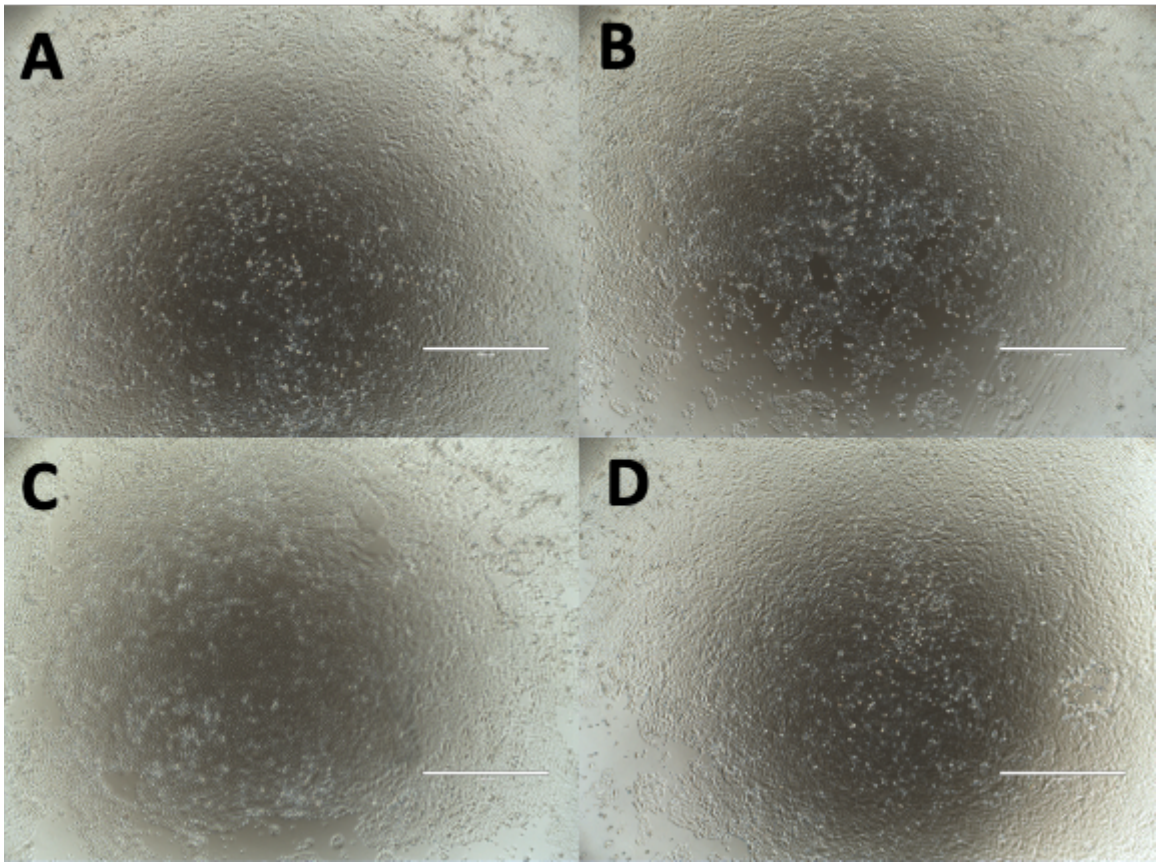

Figure 2.9: Determining coating method for the RPTEC/TERT1 cells. Tissue culture plates were coated with (A) 50 mg/mL Fibronectin, (B) 200 mg/mL Fibronectin, (C) 50 µg/mL Collagen I, and (D) no coating control.

Within the devices, we compared several methods of interest for the current application: protein coatings only, surface plasma treatment using oxygen before protein coating, versus protein coating after pre-treating the surface with positively charged compound (Figure 2.10).

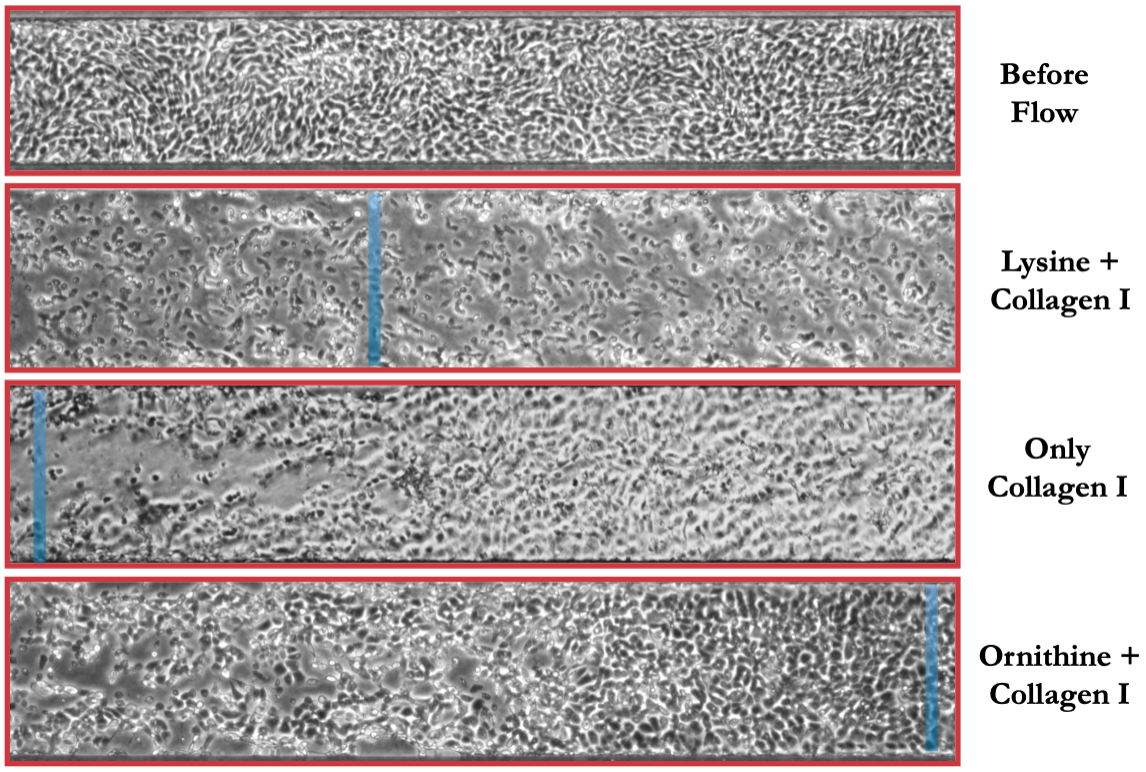

Figure 2.10: Determining improved coating method for the RPTEC/TERT1 cells placed under FSS. Microfluidic devices were treated with Lysine + Collagen I, only Collagen I, and Ornithine + Collagen I. These coating method treatments were compared to the static control.

Additionally, the cells attached and remained attached for more extended periods with the surface plasma treatment using oxygen before protein coating of Collagen I (Figure 2.10). Although the Poly-L-ornithine device base coating under the Collagen I basement membrane provides extended attachment for RPTEC/TERT1 cells, it was not significant enough to add the extra step to the preparation process.

2.4.4 Device Fluid Shear Stress Calculations

Extensive research has been conducted on the biochemical and ultrastructural effects of FSS on multiple cell types. To mimic the PT environment and simulate *in vitro* fluid shear stress, a cell monolayer is subjected to FSS by generating a pressure gradient over the cell surface. In order to calculate FSS on the cells, the mathematical

model assumes a Newtonian fluid in which the shear tensor is proportional to the deformation tensor[150].

For steady flow between infinitely wide parallel plates, wall shear stress τ is calculated. The Fluid Shear Stress passing over the proximal cells was calculated using the equation $\tau = 6\mu Q/bh2$. This equation is derived from the Navier–Stokes momentum equation of two-dimensional flow and the continuity equations[150]. Where τ is FSS, Q is flow rate, μ is medium viscosity, and b and h are channel width and height. Assumptions used in the model were Newtonian fluid (μ= 7.80e-04 Pa·s at 37°C for DMEM media with serum), the no-slip condition, with equal pressure at all outlets[151,152]. A physiologically relevant level of FSS is approximately 1 dyne/cm^2 in the human proximal tubule corresponds to an average flow rate of 63 nl/min, which is 115 mL/min/1.73m^2 [153]. Previous studies have explored broadly divergent FSS on multiple cell types (varying 0.01 dyn/cm^2 to 5.6 dyn/cm^2)[19–21,96]. In humans, a healthy FSS is estimated to vary between 0.3 dyn/cm^2 and 1.2 dyn/cm^2, but can reach high levels of about 1.6 dyn/cm^2 and lower levels (below 0.5 dyn/cm^2) in individuals with renal disease[10].

2.5 Experimental Section

2.5.1 Integrity Assessment (ZO-1) by Immunofluorescence

The Human Primary Tubule cells (#PCKDH01, Primecells) and RPTEC/TERT1 cells were all grown according to manufactures instructions. After cells reached a confluent monolayer, the static wells of cells were quickly rinsed with HBSS, and fixed with 4% paraformaldehyde for 15 min. The fixed cells were permeabilized in 0.1% Triton-X100 and blocked in 5% BSA before being incubated overnight with the antibodies directed against ZO-1 (visualizing tight junction proteins) (Thermo 339100).

2.5.2 Real-time PCR Validation

The RPTEC/TERT1 cells were lysed and RNA extracted using the RNaesay Plus Mini kit (74134, QIAGEN). Concentrations were measured with a Quibit 3.0 (Thermo Scientific) using the Qubit RNA BR Assay Kit (#Q10211, Invitrogen). cDNA was generated with the RevertAid First Strand cDNA Synthesis Kit (#K1622, Thermo Scientific,) using 1ug of total RNA and random hexamer primer following manufacturer's instructions. PCR was performed using primer pairs listed in the TableS1 using AmpliTaq DNA polymerase with Buffer I (#N808-0160, Applied Biosystems). The 20ul reactions were set up to achieve the following final concentrations: 0.2mM each NTP, 0.2uM forward and reverse primer, and 0.5U of enzyme with the following conditions: 2 min 95ºC, 31 cycles of 15 sec 95ºC, 20 sec 57ºC, 20 sec 72ºC, and a final extension performed 2 min 72ºC. The products were separated on 2% agarose gel and visualized with the myECL Imager (Thermo Scientific). Quantitative real-time PCR was performed on the QuantStudio 6 Flex Real-Time PCR system (Applied Biosystems) using primers listed in Table 2.3 using 2x QuantiTect SYBR Green PCR Kit (#204143, QIAGEN) in triplicate. Relative gene expression levels were calculated using the $2^{-\Delta\Delta Ct}$ method[154] and normalized to the housekeeping gene YWHAZ, providing the relative gene expression. For

primer sequences see Table 2.3.

Table 2.3 - RT-PCR primer sequences

Gene	Forward Primers	Reverse Primers
POLR2A	GCCAGAGTGGATGATTGTCA	CAGCCAGTTTGTGAGTCAGG
HSPA4L	CCATAACAGACCTTGTTCCCTA	GGGCAGGATGGTTCTTACAG
EPHX1	AGCCAGGGAGGACGACAG	GTGGGGTGAAACGGAACTTA
UNKL	ACCTGCTGCTCACAGGTTC	GGAAACAAAGTCCCAGATGC
MDM2	GGTGCTGTAACCACCTCACA	TTTTTGTGCACCAACAGACTTT
TRIM16L	GAAGAGTAAGCAGGAGCTGGA	GGGAAGGTGATGTCTTCAGTG
DUSP8	GCATCCTGCCTCACCTCTAC	AGGAGTTGCTGGCGTTGA
ALOX5	AGAAGCACCTGCTGGACAAG	AGCTGGATCTCGCCCAGTT
IL32	GTGGCGGCTTATTATGAGGA	CTCAACATCCGGGACAGG
SLC43A2	ACCTCCTCTTCTCGGCAGTC	CCACTGTGCCATTGGTGAC
FSTL3	AAGTTCTTTGCCCCGAAAAT	CTCCATCGCTCTTAACCACTG
LZTS3	CACCGCAGTATCGTGAGC	CTTGGGTACGACAGGCTTGA
YWHAZ (housekeeping)	AGGAGCCCGTAGGTCATCTT	TGCTTGTGAAGCATTGGGGA

2.5.3 EC_{50} Curve Analysis

The toxicological EC_{50} was determined on static 96 well plates before being assessed in devices. The coating procedure for collagen I was performed as recommended (A1048301, Gibco). The RPTEC/TERT1 cells were seeded and allowed to come to confluency. After cells reached confluency, the cells were left for an additional 24 hours to form tight junction proteins between cells and to activate cell signaling. The cells were treated with polymyxin b or cisplatin at and around toxicological EC_{50} values for these drugs found in the literature. Aspirin was used as a control drug spanning the range of the toxicological curves for the other drugs. Non-drugged and blank controls were also on each plate. Each dose and control were done in triplicate.

CHAPTER III

Three-Dimensional Modeling of Biologically Relevant Fluid Shear Stress in Human Renal Proximal Tubule Cells Mimics *In Vivo* Transcriptional Profiles

This chapter is adapted from the published manuscript and reproduced with permission from Springer Nature: Ross EJ, Gordon ER, Sothers H, Darji R, Baron O, Haithcock D, Prabhakarpandian B, Pant K, Myers RM, Cooper SJ, Cox NJ. Three dimensional modeling of biologically relevant fluid shear stress in human renal tubule cells mimics in vivo transcriptional profiles. Sci Rep. 2021 and has been reproduced with the permission of the publisher. Contributions: E.J.R. conceived and designed the study and experiments and wrote the manuscript. E.R.G. helped prepare figures, devised the statistical analyses, and contributed to writing the manuscript. D.H., B.P., and K.P. generated the devices and provided technical advice and direction. H.S. also helped performed histological and analysis. R.D. and O.B. helped prepare figures. B.P., R.M.M., S.J.C., and N.J.C. contributed to the interpretation of the analyses and manuscript. All authors reviewed the manuscript.

3.1 Introduction

The kidney is essential in the homeostasis regulation of the human body. It enables physiological and regulatory functions, including blood pressure regulation by controlling extracellular fluid volume, maintaining pH balance, keeping appropriate electrolyte balance, hormone production, and waste and xenobiotic removal[10]. Renal proximal tubules (PTs) of the nephron contain proximal tubule cells (PTCs), a specialized cell type responsible for active protein trafficking, and the reabsorption function of the kidney[155]. Given their essential role in drug metabolism, modeling of PTCs is particularly important for pharmacology research, as new drugs need to be tested for their effects on kidneys, especially proximal tubules, due to their increased contact with the excretion pathways involving a complex interplay of solute carrier (SLC) transporters[1,10,156,157]. The

transporters responsible for urinary excretion of xenobiotics and the focus of pharmaceutical drug studies are the four major types of ABC efflux transporters: P-glycoprotein (P-gp, MRP1, ABCB1), multidrug resistance proteins 2 and 4 (MRP2 and MRP4, ABCC2/4), and breast cancer resistance protein (BCRP/ABCG2)[1,157,158]. Together, these efflux transporters eliminate a variety of xenobiotics[159,160]. Besides waste product excretion and reabsorption of filtered solutes by transporter pathways, PTCs use endocytosis to recycle nutrients and proteins from the filtrate, such as glucose and albumin. The proximal tubule function is both complex and crucial for normal kidney function.

Simple monolayer culture systems are widely utilized for the understanding of kidney functions, including drug binding and toxicity. However, alternative models that more closely replicate the *in vivo* environment are likely to further our ability to recapitulate the *in vivo* functions of reabsorption and transportation and better understand how they breakdown in disease. Previous studies of cell culture models show that PTCs studied in traditional, static cell culture often lack or rapidly lose critical phenotypic and functional aspects, such as cell polarity and receptor-mediated transport[67,111]. However, 3D models for PTCs mimic the *in vivo* environment by exposure to Fluid Shear Stress (FSS). These models mimic the glomerular filtrate flow, which is present within the lumen of the PTs as the ultra-filtrate passes through to eventually reach the urinary bladder to be excreted[16,67]. Cells cultured under continuous FSS and three-dimensional (3D) flow models have gained increasing interest due to their ability to recreate precise cellular organizations and previous work has shown that PTC cultures exposed to FSS in a 3D model more closely recapitulate *in vivo* PTs morphology and function; however, these studies have explored widely differing FSS used on diverse cell types (varying between 0.01 dyn/cm^2 to 5.6 dyn/cm^2)[19–

[22]. In humans, a healthy FSS is estimated to vary between 0.3 dyn/cm^2 and 1.2 dyn/cm^2, but can reach high levels of about 1.6 dyn/cm^2 and lower levels (below 0.5 dyn/cm^2) in individuals with renal disease[10,23]. PTCs under fluidic shear have increased transporters' functionality and demonstrate changes in expression of key genes such as solute carrier (SLC) and ABC efflux transporters[156,161]. Nevertheless, the global impact of FSS exposure on human gene expression remains largely unknown, and the effects of FSS at differing rates on the transcriptional profiles in human kidney proximal tubule cells has not been investigated. Furthermore, previous studies of PTCs have used PTs from model and non-human organisms; they showed that the cells were lacking important transporters, receptors, or other physiological attributes[155]. To overcome some of these shortcomings, we studied a novel, reproducible 3D model of human cells derived from proximal tubules that closely the mimics function and transcriptional profiles of primary proximal tubule cells. Our model system uses an immortalized human PTC line (RPTEC/TERT1) combined with a highly reproducible, microfluidic platform developed by our group[109,158].

We characterized epithelial monolayer of RPTEC/TERT1 cells exposed to varying levels of fluid shear stress in a 3D model by using RNA-sequencing and microscopy to demonstrate that this model is excellent for understanding PTC function. We explored transcriptional changes following growth under physiological fluid shear stress of 0.1 dyn/cm^2, 0.25 dyn/cm^2, and 0.5 dyn/cm^2. At this physiologically-relevant level of fluid shear stress, we assessed cell morphology, presence of cilia, and transport functions such as endocytosis and efflux transport. This detailed characterization demonstrates that our 3D model provides a platform for studying human kidney biology and global genomic

factors contributing to PTCs function, indicating that it can serve as a useful tool for evaluating renal biology, pathophysiology, and pharmaceutically-induced nephrotoxicity.

3.2 Results

3.2.1 Fluid Shear Stress Affects Transcriptomic Profiles in Human Kidney Proximal Tubule Cells

To study global gene expression changes induced by fluid shear stress (FSS), we used RNA-sequencing to measure transcriptomic profiles of human proximal tubule-like epithelial cells (RPTEC/TERT1 cells) after 24 hours of exposure to fluidic shear stress of

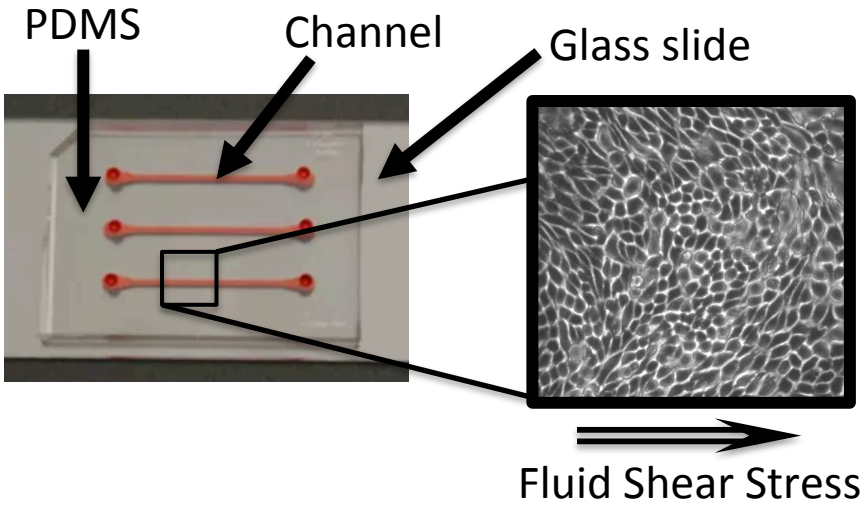

Figure 3.1: Aerial perspective image of linear kidney proximal tubule device. The linear device is assembled on a microscope glass slide with polydimethylsiloxane (PDMS) creating three of the channel walls (red) allowing three independent channels for cellular experiments. Dimensions of cell culture channels (highlighted in red) are 500µm x 100µm x 1cm (width x height x length).

0.1 dyn/cm^2, 0.25 dyn/cm^2, or 0.5 dyn/cm^2 using a 3D microfluidic chip (Figure 3.1). The chip is composed of three parallel channels that allow three-dimensional growth in a tubule-like shape.

We compared each of these FSS conditions to control channels on the same chip maintained under static conditions. We isolated total RNA from these cells and performed

RNA-sequencing. We analyzed the FSS treated samples compared with the static controls to elucidate the overall transcriptomic profiles altered by FSS. We identified 10,444 genes that are significantly differentially expressed (p-adjusted <0.05) between the 12 FSS samples and 10 static control samples (Supplementary Dataset File S2). Of these significantly differentially expressed genes, approximately 56% were up-regulated (5605) and 46% were down-regulated (4839). The top 15 most significantly expressed genes that are involved in the regulation of proximal kidney tubule function are listed in Table 3.1.

Table 3.1 Top significantly expressed genes involved in proximal tubule function and regulation.

Gene Symbol	padj	log2FC	Relationship to Proximal Tubule Cells
AKR1C1	1.60E-142	2.961	Regulation of aldo-keto reductases
CNNM4	9.83E-131	1.167	Mg2R homeostasis
AKR1B10	1.88E-112	4.319	Mitochondrial aldo-keto reductases with activity towards steroids and 3-keto-acyl-CoA conjugates
SLC43A2	3.15E-109	1.937	Essential amino acid transporter (Lat4)
CYP4F11	3.96E-109	2.659	Cytochrome P450 (CYP) enzymes
CYP4F3	6.83E-108	6.305	Cytochrome P450 (CYP) enzymes
PLAU	4.64E-105	-2.089	Preventing calcium salt precipitation
CLCN2	1.50E-91	1.175	Chloride channel 2 (ClC-2)
SLC44A2	1.32E-87	2.020	Drug transporters of the organic anion transporter (OAT) family
NGFR	1.56E-81	5.850	Rapamycin-induced autophagy protects proximal tubular renal cells against proteinuric damage
TRIM16L	3.29E-80	2.154	Regulation of response to stimulus
CABYR	9.63E-69	2.270	Expressed in testes and ciliated cells
TNFRSF10D	9.95E-65	2.278	Biomarker for tubulointerstitial injury
CACNB3	2.23E-62	-0.900	Calcium channel
TRIOBP	3.43E-62	-0.887	Regulation of SGLT expression

Hierarchical clustering representing gene expression level of all 22 samples showed two distinct clusters (log2FC>±1; p-adjusted <0.05): one with FSS-treated samples and the other one with static controls (Figure 3.2).

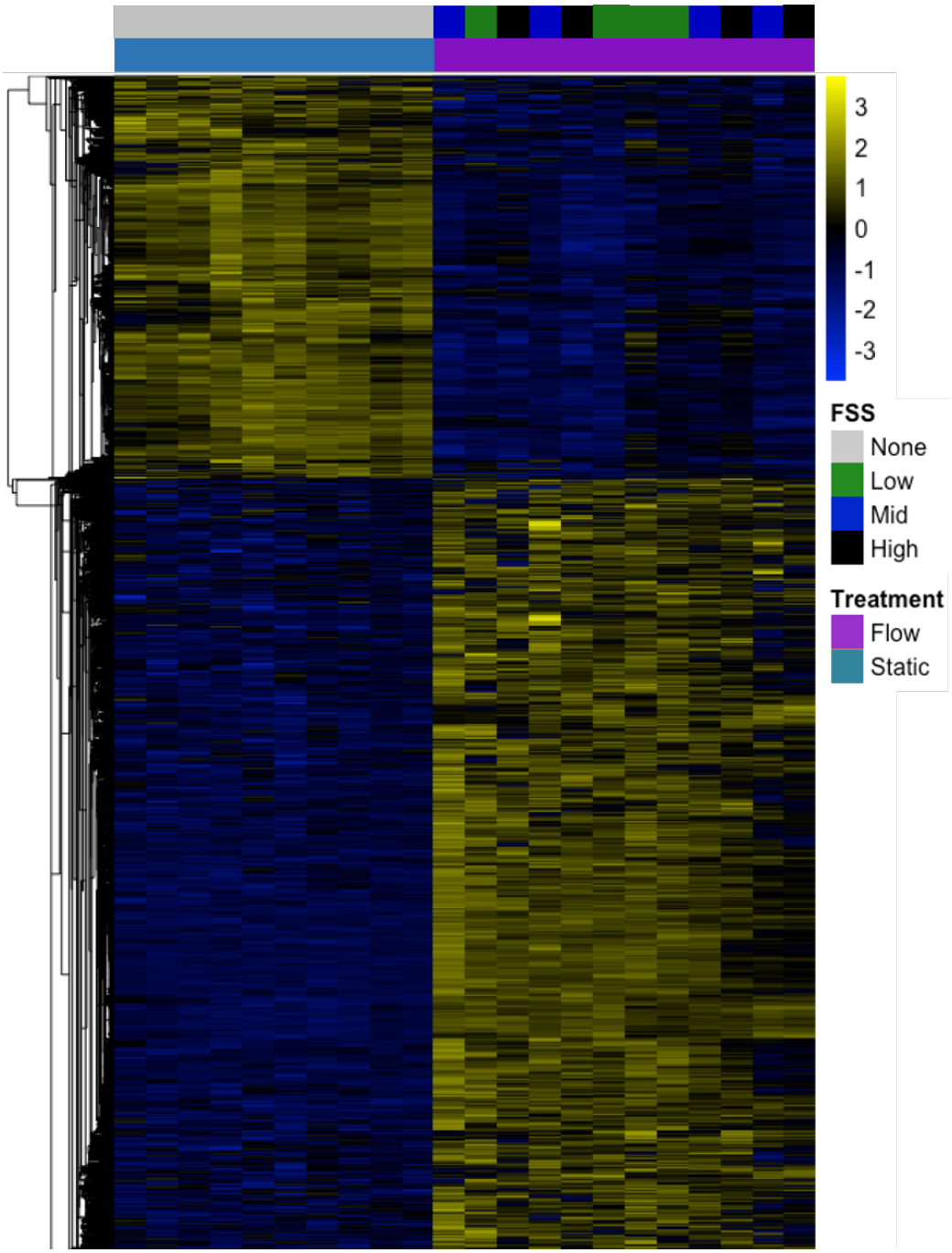

Figure 3.2: Hierarchical clustering heat map. Gene expression profiling shows a strong difference between fluid shear stress treatment RPTEC/TERT1 (purple) and static controls (teal). Heat map showing the expression values (log2FC±1; padj < 0.05) in increasing flow rates 0.1 dyn/cm^2 (green), 0.25 dyn/cm^2 (blue), and 0.5 dyn/cm^2 (biological, black) fluid shear stress treated samples (FSS) and corresponding static controls (gray). Expression values were normalized using DESeq2 R package.

The genes we identified through transcriptomic analysis reveal both known and novel connections to human PTCs function and dysfunction. The volcano plot highlights a subset of highly differentially expressed genes associated with PT genes and previous kidney genome-wide association studies (Fig 3.3).

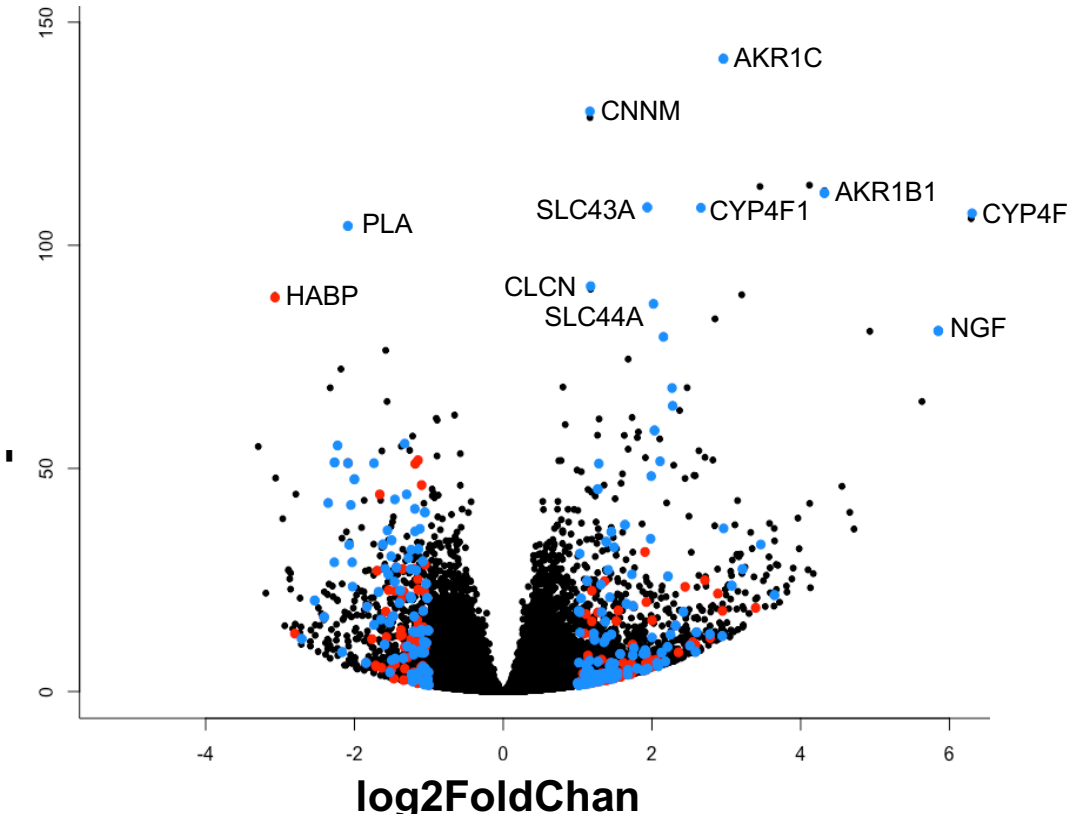

Figure 3.3: Volcano plot displaying differential expressed genes in samples under fluid shear stress conditions and static environment. The y-axis corresponds to the mean expression value of -log10 (padjust value), and the x-axis displays the log2 fold change value. Blue colored points represent most significant genes involved in kidney proximal tubule function. Red colored points represent GWAS (genome-wide association study) hits that denote inherited genetic variants associated with risk of renal diseases. Both subsets groups have padj equals <0.05 and have a log2FC>±1.

Differentially expressed genes observed upon flow treatment revealed 339 genes that have previously been cited in the literature as related to or important for PTs structure, function, and regulation of the cell system (Fig 3.3, blue). Notably, these genes are involved in the

regulation of aldo-keto reductases, magnesium homeostasis, PTCs transporters (including solute carrier family), ATP-binding cassette (ABC) transporters, renal drug metabolism, and cilia (Supplementary Dataset File S3). Furthermore, 156 genes were nearby GWAS (genome-wide association study) hits that denote inherited genetic variants associated with the risk of renal diseases, (Fig 3.3, red). Relevant diseases and symptoms associated with one or more relevant phenotypes described in the NHLBI-GRASP GWAS catalog from the GWAS include, chronic kidney disease, filtration rate, albuminuria, proteinuria, and urinary metabolite imbalance (Supplementary Dataset File S4).

3.2.2 Pathway Analysis of Associated Genes of Fluid Shear Stress Treated Cells

To obtain insights into biological processes influenced by FSS, we used LRPath to determine pathways enriched among our differentially expressed genes. Our analysis of 10,444 significantly differentially expressed genes, up- and down-regulated revealed significant enrichment of expected and novel pathways (GO Analysis Supplementary Dataset File S5-S7). As expected, pathways known to be important for kidney proximal tubule cell function, such as signal transduction, metabolism, cytokine signaling, cell-cell/matrix interaction, tight junction molecule, cell adhesion molecules, extracellular matrix components, and pathways which respond to a stimulus, such as endocytosis were enriched. Furthermore, our data show that genes differentially expressed after treatment with fluid shear stress included critical genes for PTCs function. These included CYP4F3 and CYP4F11, which encode members of the cytochrome P450 superfamily of enzymes involved in the metabolism of fatty acids, xenobiotics, therapeutic drugs, and signaling molecules, and transporters such as SLC47A1 and SLC47A2 which are important for renal excretion of diverse substrates (including drugs), a canonical feature of these cells.

Importantly, these genes are not readily expressed in RPEC/TERT1 cells without the environment of fluid shear stress as observed in the Human Protein Atlas cell RNA expression data (www.proteinatlas.org). Additionally, we observed changes in cell adhesion molecules CLDN2 and CLDN16 which function in tight junction formation critical for role in epithelial barrier function. Defects in these junctions can cause a wide spectrum of kidney diseases, such as hypomagnesemia, hypercalciuria, kidney stones, and hypertension. Furthermore, genes involved in the PT bicarbonate reclamation pathway (SLC4A4 and PCK1) are affected by FSS. This pathway is used by proximal tubules to reabsorb approximately 80% of the filtered bicarbonate ($HCO3^-$) as well as generating new bicarbonate for regulating blood pH.

To summarize and visualize GO terms among the enriched pathways, we used the REVIGO tool to determine semantic clustering of functional categories for up-regulated genes (Fig 3.4A) and down-regulated genes (Fig 3.4B)[162]. Multiple anticipated GO terms associated with PTCs were shown to be enriched and up-regulated, such as channel and transport activity, and nucleic acid binding. Notably, pathways involving cytoskeletal, actin, cell adhesion, and specific channel activity and binding pathways were generally down-regulated under FSS conditions.

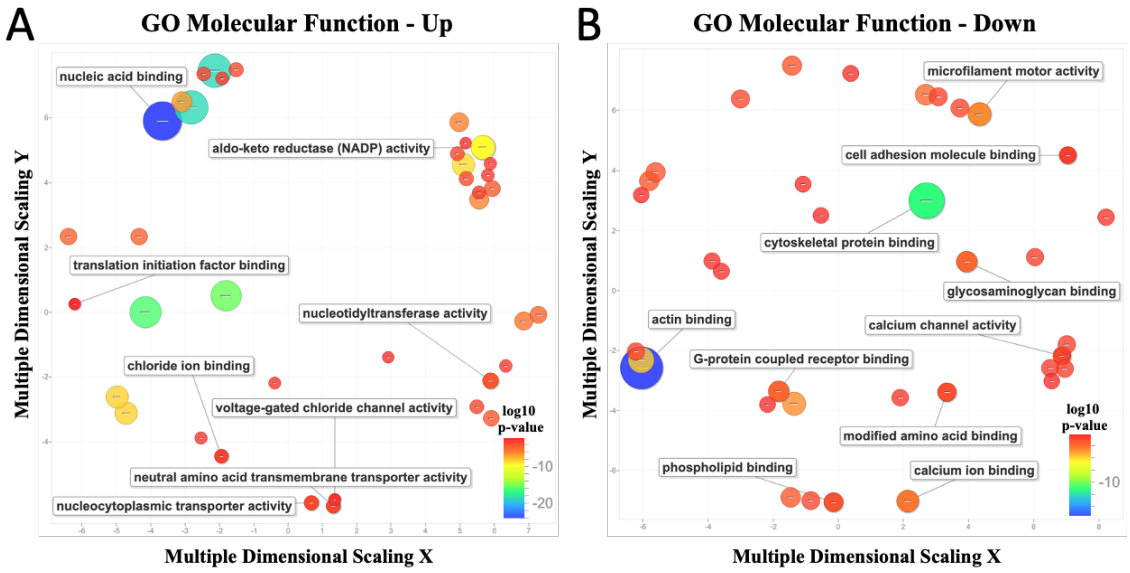

Figure 3.4: GO enrichment analyses of FSS treated and static controls. Scatterplot of enriched pathways for a subset of up-regulated genes (A) and down-regulated (B). To identify similar GO terms among the enriched terms, these were categorized using semantic clustering (REVIGO). The GO terms within the scatterplot are represented as a circle and are related to each other and to a similar process. The circle size symbolizes the amount of GO terms grouped within that cluster and colorization corresponds to the p-value of the enrichment analysis. The red color indicates the highest p-value, and the blue color the lowest p-value.

3.2.3 Identifying Flow Dependent Gene Expression Changes

We examined a set of PT gene expression patterns to identify genes whose expression changes as a function of FSS (Fig 3.5). As with the previous analysis, this approach identified genes important for proximal tubule function and regulation and were affected by FSS in an overall significant gene expression change compared to static. Some examples include ones from the solute carrier (SLC) and claudin gene families, and Aquaporin-4 (AQP4) (e.g. black asterisks). However, expression levels of other genes were impacted on by the shear stress level. Some notable impact of individual FSS on expression are within groups in which the gene expression was increasing or decreasing coordinately with FSS (red asterisks, CYP27B1, IL11, MMP1, CD14, SLIT2). In some cases, gene

expression was impacted in opposite directions at low and high FSS values. (FOXA3 and HEY1, green asterisks). This indicates that the specific FSS impacts gene expression.

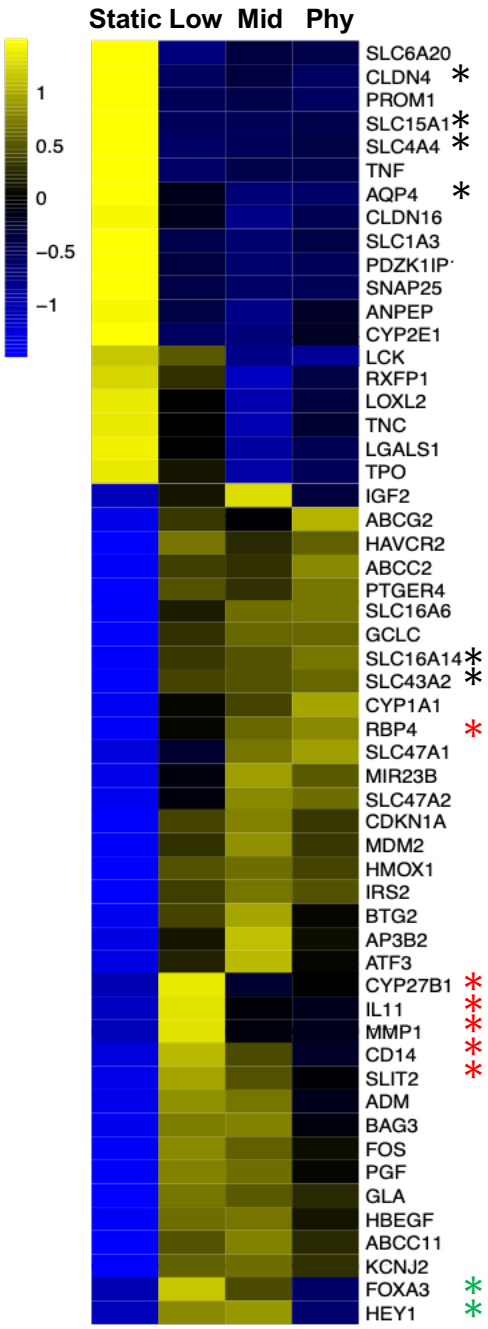

Figure 3.5: Proximal tubule cells under different fluidic shear stress alter expression of example genetic profiles. Statistically significant changes in expression of example genes associated with proximal tubule cells were identified by cross-comparisons of all four conditions (Low (0.1dyn/cm2), Mid (0.25dyn/cm2), Physiological (Phy) level (0.5dyn/cm2), and static baseline). Each column represents data from biological replicates at a specific experimental fluidic shear stress. Example genes were grouped by subtype or directionality. Replica count data for each gene were average across all corresponding samples and plotted as a heat map. More significant values are visualized in the yellow range and lower, less significant values, are visualized in blue.

3.2.4 Proximal Tubule Morphology and Molecular Markers with the Treatment of Fluid Shear Stress

Immunofluorescence microscopic images of the proximal tubule cells after 24 hours of FSS revealed well defined characteristic morphological properties of a confluent epithelial monolayer lined by a continuous, unaltered linear distribution of the tight junction protein, zonula occludens-1 (ZO-1), under both FSS and static culture conditions (Figs 3.6A-B). The ZO-1 (green) outlines each of the cells and surrounds the DAPI labeled nuclei (blue). Consistent expression of the tight junction marker protein ZO-1 in confluent cell monolayers of PTC under both conditions displayed the integrity of intercellular junctions found within healthy, functioning cells. In contrast, treatment with physiological fluid shear stress (0.5 dyn/cm^2) induced noticeable rearrangement in actin cytoskeletal properties (F-actin) of the cells compared to the static channel (Figs 3.6C-D). Similar to observations in animal and human PTC, the FSS caused the F-actin to reorganize to the periphery of the cell compared to diffuse labeling across the cell observed under static conditions. The apical localization of F-actin and intracellular tight-junction protein (ZO-1) indicates appropriate cell polarization in this platform. Furthermore, we found that exposure to FSS left the primary cilia intact (Figs 3.6E and 3.6F). This demonstrates that the primary cilia remain on the RPTEC/TERT1 cell surface, even after the 24-hour treatment of FSS. These data complement the expression data showing that genes corresponding to proximal tubule morphology (tight junctions, F-actin, and cilia) were differentially expressed with FSS (p-adjusted <0.05, $|\log2FC|>1$) (Table 2). These include genes from LPS-TNF-α-ERK1/2 signaling pathway (TNF) and myosin motors (MYO7B)

and/or scaffolding complexes (SGK), which likely play a role in receptor-mediated endocytosis in the PTs.[161]

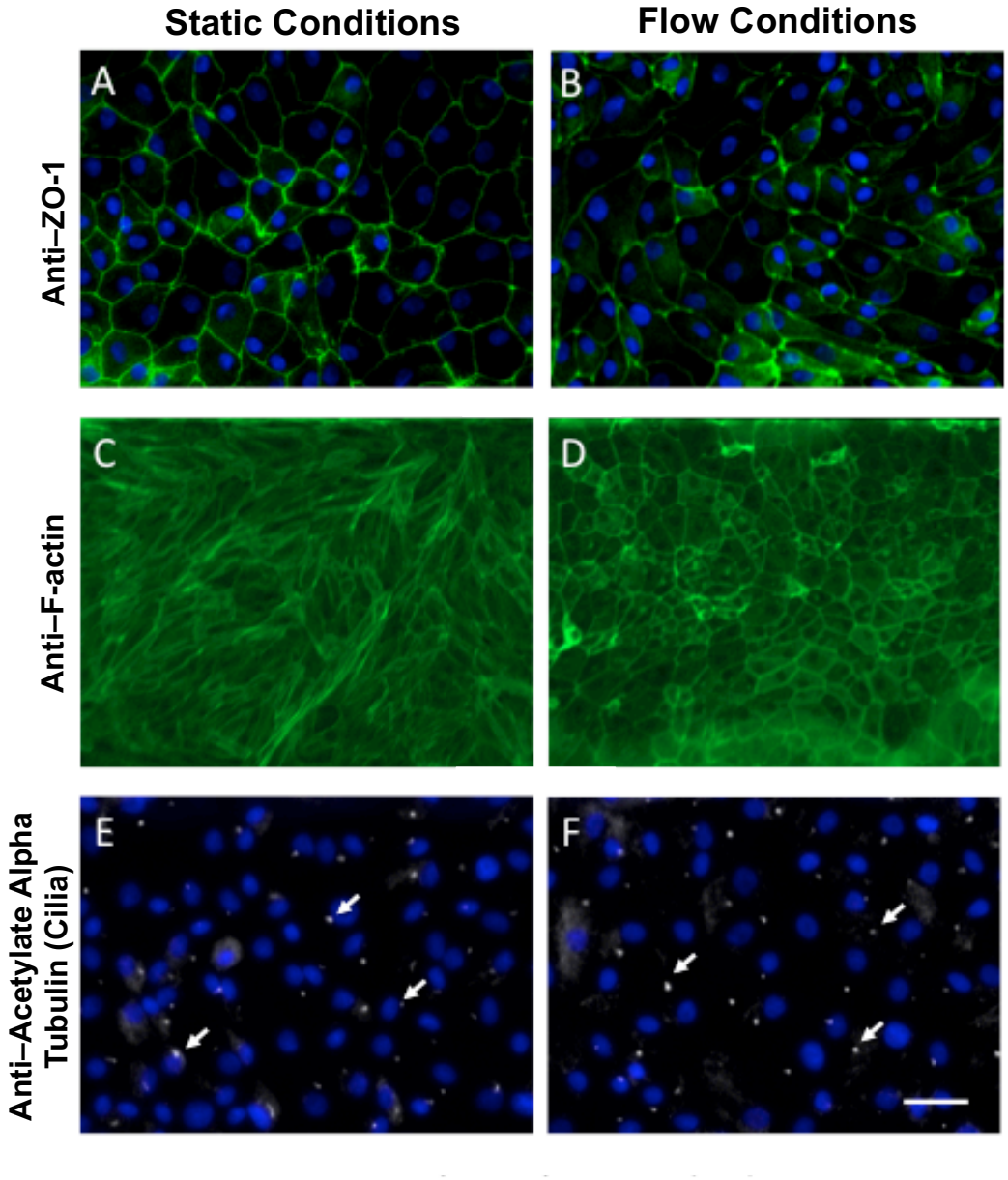

Figure 3.6: Human kidney proximal tubular epithelial cell morphology 24 hours under static conditions versus fluid shear stress. Immunofluorescence staining of the tight junction protein ZO-1 (tight junctions) (green) and DAPI (blue) in static (A) and flow cells (B). Immunofluorescence images of F-actin under static conditions (C) and after 24 hours of exposure to fluid shear stress (D). Under the shear stress, F-actin reorganizes at the periphery of the cells (D). Immunofluorescence staining of acetylated tubulin (white) to visualize primary cilia and DAPI (blue) under static (E) and flow (F) remain similar under both conditions. (Bar = 50μm).

Table 3.2 - Expression of selected genes with mechanistic and functional relevance to tight junctions, f-actin, and cilia in proximal tubules.

Tight Junction and Proximal Tubule

Gene Symbol	padj	log2FC	Description
CLDN16	2.35E-23	-1.384	claudin 16
TNF	7.24E-17	-1.643	tumor necrosis factor
ABCG2	1.17E-07	1.164	breast cancer resistance protein (BCRP)
CLDN2	1.85E-05	-1.099	claudin 2

F-actin and Proximal Tubule

Gene Symbol	padj	log2FC	Description
HPSE	1.31E-33	-2.0710	heparanase
ABCC2	7.27E-22	1.4333	multidrug resistance protein 2 (MDR2)
CCL2	9.78E-08	-1.4992	collagen type I alpha 2 chain
MYO7B	1.44E-09	-2.166	myosin VIIB
COL1A2	0.03265	1.0195	collagen type I alpha 2 chain

Cilia and Proximal Tubule

Gene Symbol	padj	log2FC	Description
ITPKB	8.19E-21	-1.363	inositol-trisphosphate 3-kinase B
CLDN2	1.85E-05	-1.099	claudin 2

3.2.5 Fluid Shear Stress Induces Genes Corresponding to the Endocytosis Process and Reabsorption

Many large, soluble molecules are reabsorbed in the PTCs by receptor mediated endocytosis as a part of essential renal physiology. A subset of genes induced by fluid shear stress (padj <0.05 and a log2FC$>\pm1$) are important for endocytosis (Table 3.3).

Table 3.3: Expression of selected genes with relevance to the process of endocytosis in proximal tubules

Endocytosis and Proximal Tubules

Gene Symbol	padj	log2FC	Description
SLC19A3	1.58E-12	-2.709	sodium–hydrogen exchanger 3 (NHE3, solute carrier family)
SHH	1.61E-28	-1.4367	sonic hedgehog signaling molecule
UGCG	2.67E-25	-1.4590	UDP-glucose ceramide glucosyltransferase
CYP2E1	3.13E-24	-2.0254	cytochrome P450 family 2 subfamily E member 1
CLDN16	2.35E-23	-1.3842	claudin 16
EGF	1.62E-18	1.0292	epidermal growth factor
HMOX1	1.66E-18	1.3240	heme oxygenase 1
ABCG2	1.17E-07	1.1638	breast cancer resistance protein (BCRP)
TG	1.89E-06	1.4330	thyroglobulin
CLCNKA	0.005725	-1.0687	chloride voltage-gated channel Ka
NPHS1	0.02228	1.0809	NPHS1 adhesion molecule, nephrin

These genes are involved in endocytic vesicle coat proteins, lysosomal storage, and receptor families. We tested whether there was evidence for altered endocytic function. Reabsorption of plasma proteins from the glomerular filtrate can be modeled *in vitro* by monitoring FITC-conjugated albumin uptake by PTCs. We measured cellular albumin uptake of the human RPTEC/TERT1 cells in the device after 24 hours of physiological FSS or static conditions. Cells were removed from the flow and treated with FITC-conjugated albumin and uptake was measured using fluorescence microscopy (Figs 3.7A and 3.7B). Uptake of FITC-conjugated albumin of the cells under FSS was significantly higher compared with cells grown under static conditions (Figs 6C, $p<0.001$, Student's T-test). The increased transport of FITC-albumin activity we observed was likely mediated by an increased delivery due to flow dynamic mechanisms, as seen in *in vivo* conditions. Our data are also consistent with previous studies performed on proximal tubules, where fluid shear stress-induced mechanisms have been shown to increase function.[18,63]

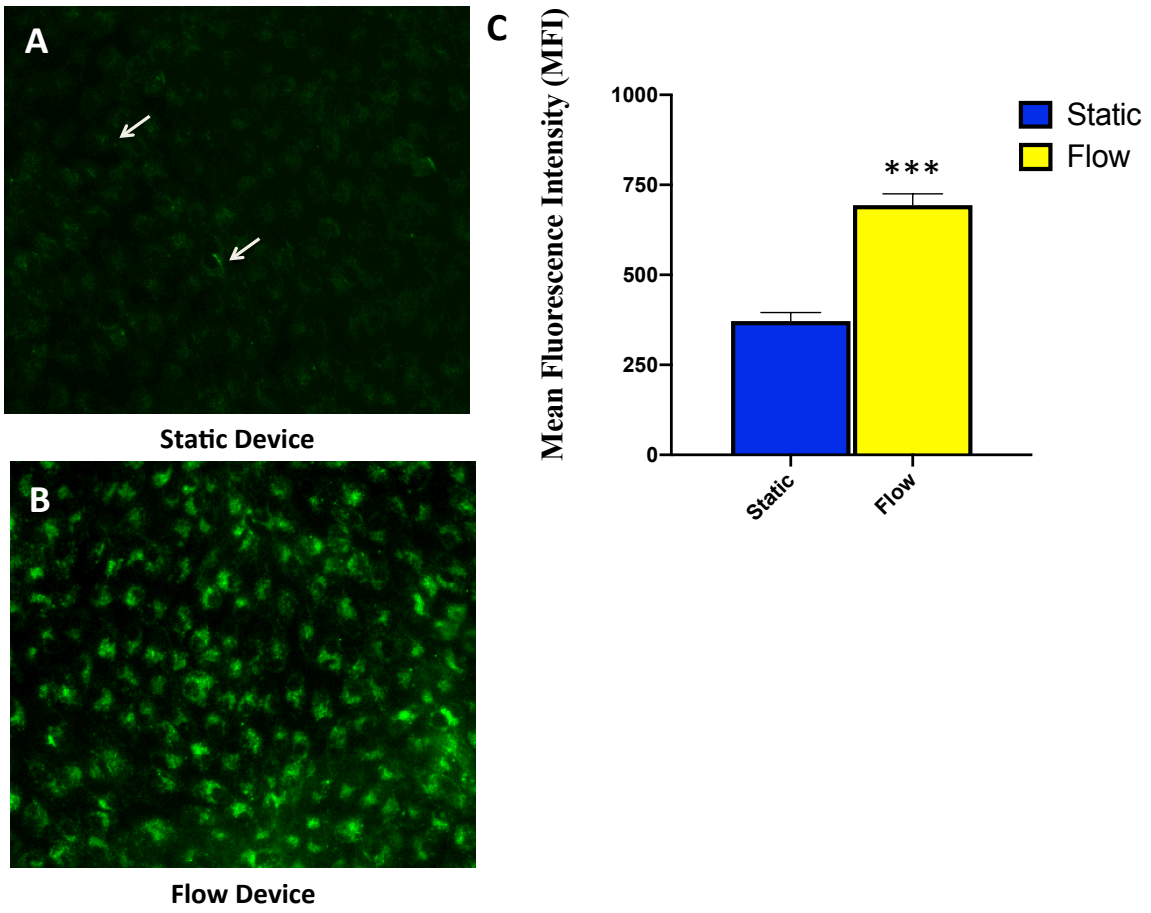

Figure 3.7: Analysis of human proximal tubular albumin reuptake function. Albumin uptake by human proximal tubular epithelial cells after 15 min incubation at 37oC with 50 µg mL-1 of FITC-albumin (green) added to the channel under static conditions (A) and fluid shear stress conditions (B). Mean Fluorescence Intensity (MFI) of RPTEC/TERT1 cells 24 hours after static conditions versus fluid shear stress conditions showing a significant increase in FITC-Albumin fluorescence signal (C) (***$p \leq 0.001$). Transcriptome profiling provides insight to differentially expressed genes corresponding to endocytosis process.

3.2.6 Expression of Xenobiotic Efflux Transporters Changes with Fluid Shear Stress

Transporters that mediate substrate efflux, such as the ATP-binding cassette transport proteins (ABC transporters), are critically important for the canonical PTCs function of xenobiotic efflux[18,138]. Our transcriptomic analysis shows that expression of genes involved in solute carrier (SLC) and ATP-binding cassette (ABC) drug transporters (including the Multi-drug Resistance transporters, MDRs) dramatically change under shear stress with the treatment of FSS (Table 4).

Table 3.4: Significant expression of genes with importance transportation in proximal tubules

Transporters and Proximal Tubules

Gene Symbol	padj	log2FC	Description
SLC43A2	3.1E-109	1.937	solute carrier family 43 member 2
SLC15A1	6.43E-52	-2.086	solute carrier family 15 member 1
ABCA3	7.15E-41	-1.053	ATP binding cassette subfamily A member 3
ABCC2	7.27E-22	1.433	multidrug resistance protein 2 (MDR2)
ABCB1	2.26E-09	-1.085	P-gp, multidrug resistance protein 1 (MDR1)
ABCG2	1.17E-07	1.164	breast cancer resistance protein (BCRP)

We used fluorescence image analysis to measure changes in efflux transport activity with FSS exposure (Figure 3.8). We quantified cellular accumulation of the dyes Calcein-AM, and CMFDA in cells that have been maintained for 24 hours in our device/model under physiological fluid shear stress (0.5 dyn/cm^2) to those maintained under static conditions. As transporters actively efflux the substrate, a decrease in fluorescence is a measure of increased transporter activity. The fluorescent substrate accumulation in the cells cultured under FSS decreased in both Calcein-AM (Fig 3.8A) and CMFDA (Fig 3.8C) compared to static controls (Figs 3.8B and 3.8D, respectively). Decrease of fluorescent substrate accumulation were quantified and demonstrated graphically (Fig 3.8E, $p<0.001$, Student's T-test). As in the case for FITC-albumin uptake rate increase into the cells, these indicate that kidney PTCs under fluidic flow stress display more effective efflux activity of P-glycoprotein (P-gp, MRP1, ABCB1) transporter function and multidrug resistance proteins 2 and 4 (MRP2 and MRP4, ABCC2/4), (using Calcein-AM and CMFDA substrates respectively).

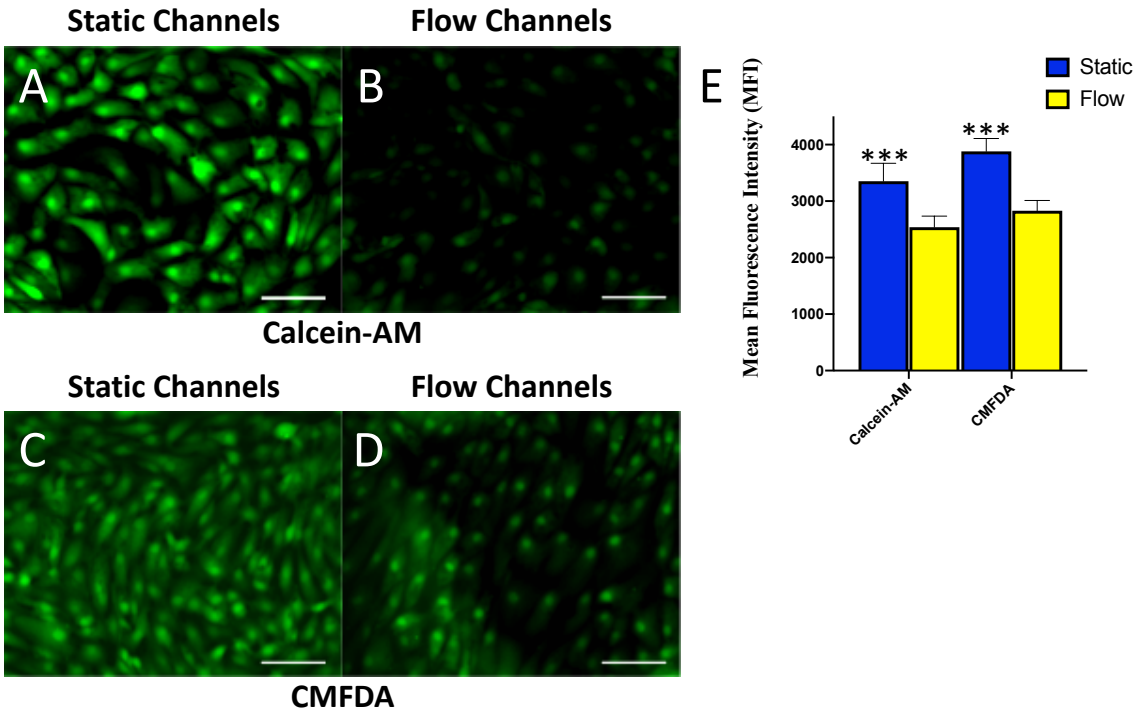

Figure 3.8: Fluorescent transporter substrate Calcein-AM and CMFDA amasses in RPTEC/TERT1 cells under static conditions and dissipates with the application of FSS. Figure (B) and (D) sample fluorescence images demonstrate decreased in Calcein-AM and CMFDA accumulation in cells after 24 hours of FSS treatment prior to staining compared to static channels (A and C) (Bar = 100µm). (E) Quantitative analysis of Mean Fluorescence Intensity (MFI) of Calcein-AM showed a significant decrease after cells were treated with 24 hours of FSS versus static environment (yellow filled bars). Indicating the increased efflux activity after being kept under fluidic conditions (Bar = 100µm; n=4, ***$p \leq 0.001$).

Furthermore, we found that of the 193 genes specifically associated with PTCs in Rat PT regions S1, S2, and S3, over half (90/193) are expressed at an RPKM of 0.5 (a common standard for reliably detected expression) in our RPTEC/TERT1 cells (Supplementary Dataset File S8).[163] Due to the fact that these and other transporters are critical for identifying and understanding drug toxicities and drug–drug interactions, this human PTCs microfluidic device provides an advantageous *in vitro* model for renal physiology, kidney diseases research, pharmaceutical and nephrotoxicity studies.

3.3 Discussion

Renal epithelial cells play a critical role in kidney function and undertake the majority of the kidneys' reabsorptive and secretory burdens. Dysfunction of these cells leads to improper filtration of the proximal tubule and ultimately results in kidney disease. A model of the proximal tubules' normal cellular function under physiological fluid shear stress can add value to *in vitro* drug safety assessments and pathobiology research. While other *in vitro* models have been able to reproduce kidney and PT environments, there are limitations by variable channel size, FSS applied to classical 2D system hybrids and device designs that are difficult to reproduce. Here we utilize a commercially-available device combined with immortalized human RPTEC/TERT1 line – a stable cell line that maintains endogenous expression and functionality of most transporters and metabolic enzymes and has been used extensively for toxicological investigations[2,17,20,100]. The RPTEC/TERT1 immortalized human renal tubule cell line, while applicable to the studies presented here, has its limitations. As with any immortalized *in vitro* cells, the cell line's precision representing the specific cell origin is debatable. Even though the RPTEC/ TERT1 cells were isolated from a healthy male donor and their renal properties were well characterized and functionally similar to proximal tubule cells in the body, it is essential to note that the kidney nephrons are comprised of many different cell types which work together to perform renal functions. Thus, it would be desirable to further define the RPTEC/TERT1 cell line transcriptomic and proteomic profiling compared to other primary renal proximal tubule cells. Our goal was to describe a novel 3D model using transcriptomic and functional assays and demonstrate that this model reproducibly mimics key features of renal proximal

tubule-like cells and would thus be a useful tool in future studies of proximal tubule and renal biology.

We first sought to determine whether our proximal tubule cell line showed altered transcriptional profiles under fluid shear stress compared to the same cells grown under static conditions. Our RNA-sequencing data confirmed previously reported shear stress-induced changes in gene expression of CDH1, COX2 (PTGS2), CCL2 (MCP1), EDN1, EGR1, and SNAI1 in renal epithelial cell[14,21–24]. Furthermore, the expression data reveal over 10,400 other genes altered by fluid shear stress in RPTEC/TERT1 cells. Many of these genes have been linked by GWAS (genome-wide association study) to kidney related traits supporting our hypothesis that FSS induces a gene expression pattern that are relevant for normal PTCs function and also relevant for kidney disease[25,26]. In addition, gene set enrichment analysis on the human PTCs showed strong enrichment for anticipated key processes known to be important for PTCs function including cytoskeletal proteins, endocytic functions, and transporters. Some of the up-regulated molecular functions include voltage-gated chloride channel activity and chloride ion binding, as well as, the aldo-keto reductase superfamily. Both chloride channels and their activity are involved in filtration processes in the proximal tubules together with the process of endocytosis. The aldo-keto reductase superfamily, which reduces aldehydes and ketones, have been previously studied in the podocyte cells of the kidney[164–166]. However, with AKR superfamily involvement in proteinuria and other forms of chronic kidney disease, its being recognized as important to the proximal tubules and more research towards a better understanding of the molecular mechanisms behind kidney function[27]. Interestingly enrichment for down-regulated pathways included the cytoskeletal protein, actin, cell

adhesion binding, and microfilament motor activity (Fig 3). These pathways could contribute to the cytoskeletal reorganization of F-actin and endocytic processes involved in albumin uptake. These pathways and other down-regulated genes involved in PTCs function support further examination of cell responses to fluid shear stress. Of note is that several genes induced by shear stress are members of the solute carrier (SLC) family and ABC transporters, which are important for the kidneys role in homeostasis. They have also been hypothesized to play an important role in sensing metabolites secreted by microorganisms, a function central to the remote sensing and signaling hypothesis[28]. In our study, numerous biological pathways, transporters, and drug-metabolizing enzymes were directly impacted by fluid shear stress – many of which are also involved in drug absorption, distribution, metabolism, and elimination.

The *in vivo* FSS varies from 0.3 – 1.0 dyn/cm^2 or greater in the proximal tubules of healthy individuals (depending on the segment). Changes in flow rate is common in kidney diseases due to hyperfiltration, tubular dilation, and obstruction, which occurs in functional nephrons, to compensate for lost glomeruli and tubules, with diabetic nephropathy and Polycystic Kidney Disease (PKD) as the most common examples[29]. While some genes are induced with any level of FSS (e.g., AQP4, SLC members and CLDN gene family), other genes show increasing expression with increasing FSS. These may be of particular importance for diseases where FSS is reduced which might impact expression of these FSS-dependent genes like RBP4, ABCG2, CYP1A1, and SLC47A1. Loss of retinol-binding protein 4 in urine (RBP4) is a biomarker for loss of function of the human proximal renal tubule[30]. The efflux transporters, Breast Cancer Resistance Protein (BCRP/ABCG2) and Multidrug and Toxin Extrusion (MATE)-type transporter 1 (MATE1, SLC47A1) are

responsible for restricting absorption and enhancing excretion of many pharmaceutical compounds including multiple anticancer drugs[4,31]. Some genes were turned on only by the low- (0.1 dyn/cm^2) and mid- (0.25 dyn/cm^2) of flow (FOXA3 and HEY1). Additional exploration of how these genes might be relevant for kidney development or disease is necessary to fully understand this result.

Functional characterization of RPTEC/TERT1 cells grown in our model system under FSS complements our transcriptomic analysis to demonstrate how this model mimics *in vivo* PTC function. We showed an FSS-dependent increase in formation of tight junctions, an increased albumin uptake, and increased efflux. In our device, tight cell-cell junction proteins were observed between neighboring cells and linked cells in a characteristic cobblestone pattern found *in vivo*[167,168]. Intact actin cytoskeleton (F-actin) is important for regulation of flow dependent ion absorption and endocytosis process of glomerular filtrate proteins is dependent on the integrity of actin cytoskeleton[167,169]. Disruption of F-actin and cytoskeletal organization of PTCs is important to endocytosis the formation of clathrin-coated structures[170]. Additionally, we observed primary cilia in our model, a key feature of PTCs necessary for mechanosensing and regulation of tubular morphology[10,14,170].

In the human kidneys, PTCs reabsorb filtered solutes and proteins, such as glucose, phosphate, amino acids, and urea, from the glomerular filtrate by secondary active transport; however, they reabsorb proteins such as albumin by receptor-mediated endocytosis[73]. We showed that uptake of cellular FITC-albumin fluorescence was flow-dependent. This is physiologically relevant for future use of the model system because

PTCs are responsible for the majority of the glomerular filtrate, and thus, increased expression of these cross epithelial transporters is crucial for its function[16].

Next to active functional albumin reabsorption and uptake, apical efflux transporters are important to understanding kidney physiology and pharmacological studies[18,161]. Interaction of drugs with the ABC efflux transporters can increase the toxicity of co-administered agents and, in fact, new draft United States Food and Drug Administration guidelines require determination of whether a drug candidate is a substrate or inhibitor of P-gp[171]. We showed ABC mediated transport also showed dependence on FSS. This indicates that kidney tubular epithelial cells under fluidic flow display more effective P-gp and MRP2/4 efflux activity under FSS conditions. Thus, a human PTCs microfluidic device might provide an advantageous *in vitro* model for renal physiology, kidney diseases research, pharmaceutical and nephrotoxicities studies. While previous studies have demonstrated a change in proximal tubule cell morphology when exposed to fluidic shear stress, this is the first report of a direct comparison in transport activity between static and fluidic culture conditions in a model using the stably immortalized human cells, RPTEC/TERT1.

Overall, this novel *in vitro* model is valuable for studying renal pharmacology, renal drug transport, and toxicities relevant to the human kidney biology. This device enables direct visualization and quantitative analysis of diverse biological processes similar to the intact kidney tubule in ways that have not been possible in traditional cell culture or animal models.

3.4 Conclusions

This study demonstrates the utility of a 3D model for mimicking *in vivo* function of human renal proximal tubule cells. We used genomics and functional analysis to show that cells under fluidic shear stress in a 3D fluidics device are capable of critical PTCs functions and display expected PTCs transcriptomic profiles including formation of tight junctions, drug efflux, ion and solute transport, and endocytosis. This is the first transcriptomic analysis of response to FSS in RPTEC/TERT1 cells and the varying flow rate also demonstrates differences that may be relevant for kidney disease. Our *in vitro* study demonstrates a comprehensive overview of fluid shear stress altered gene expression in human renal epithelial cells, but is not fully representative for the *in vivo* situation, because of the limitations of immortalized cell lines. Nevertheless, our results and ongoing research of kidney function and disease can benefit from a more biologically relevant PTCs model. This novel *in vitro* model provides a useful approach for studying renal pharmacology, renal drug transport, and toxicities relevant to the human kidney biology.

3.5 Experimental Section

3.5.1 Maintenance of Cell Culture

Human immortalized hRPTECs (RPTEC/TERT1, ATCC CRL-4031) and were cultured and maintained in hTERT Immortalized RPTEC Growth Kit (ATCC ACS-4007), supplemented with Geneticin (Gibco, 10131035), in phenol red free DMEM/F-12 medium (Gibco, 11039021) according to the vendor's instructions. RPTEC/TERT1 cells were passaged 1-2 times per week and subcultured at a 1:2 or 1:3 ratio. Cells were cultured at 37°C in a humidified atmosphere containing 5% CO2.

3.5.2 Mimicking the Human Proximal Tubule Environment On-a-chip (Device Setup)

The hRPTECs were grown to confluency in a microfluidic device obtained from the SynVivo Inc. (www.synvivobio.com, Huntsville, AL) using serum free media. The dimensions utilized were liner channel devices with a width of 500μm, a constant depth of 100μm, and lengths of 1cm. Cells are maintained in their growth medium before experiments in the microfluidic device. The device was pre-coated with the extracellular matrix protein, collagen I (A1048301, ThermoFisher) per vendor's instructions at the concentration of 50 μL/mL. Cells are seeded into the device and are allowed to incubate for approximately 24 hours to allow the cells to attach. After this incubation, a syringe pump (PHD ULTRATH, Harvard Apparatus) is programmed to replace the media volume in the device completely with fresh media every 48 hours (as under static maintenance conditions). Once the cells reached a confluent monolayer in 72-96 hours, channels were placed under multiple levels of fluid shear stress (FSS) conditions, including low flow rates of 0.1dyn/cm^2 or 0.25 dyn/cm^2, and a physiological level of 0.5 dyn/cm^2 [10]. Controls remained under static conditions. Each biological replicate represents cells within an individual channel in a device. Functional characterization and assays were performed after 24 hours of FSS treatment.

3.5.3 Immunofluorescence

After physiological relevant level (0.5 dyn/cm^2) FSS stimulation for 24 hours, the static and flow channels were quickly rinsed with HBSS, and fixed with 4% paraformaldehyde for 15 min. The fixed cells were permeabilized in 0.1% Triton-X100 and blocked in 5% BSA before being incubated overnight with the antibodies directed

against ZO-1 (visualizing tight junction proteins) (Thermo 339100) and acetylated alpha-tubulin (enabling imagining of primary cilia) (Thermo 32-2700).

3.5.4 Chemicals

Albumin–fluorescein isothiocyanate conjugate (A9771), Valspodar (PSC833) (SML0572), and MK-571 sodium salt hydrate (M7571) from Sigma-Aldrich, US. Calcein-AM and Cell Tracker Green CMFDA (Life Technologies, U.S.A.).

3.5.5 Functional Albumin Uptake Study

The human RPTEC/TERT1 cells were under physiological relevant level (0.5 dyn/cm^2) FSS stimulation for 24 hours and were removed from the pump immediately before the endocytosis assay. To investigate albumin endocytosis uptake of cells under static and flow conditions, cells were exposed to 50 ug mL-1 Fluorescein (FITC)-conjugated albumin (A9771, Sigma) for 15 min at 37^{o}C in a humidified atmosphere containing 5% CO2. Rinsing with ice-cold HBSS arrested albumin uptake and fluorescence images were obtained using a microscope (Nikon TE-2000). We acquired four fluorescence images of the FITC channel FITC (200 ms exposure) immediately after washes using Photometrics CoolSnap HQ2 Monochrome CCD Camera (Tucson, AZ) with a 20x/0.75 Plan Fluor Phase Contrast objective, having a total field of 6×8. Fluorescence images were analyzed using ImageJ software (NIH, Version 1.51a) to obtain mean fluorescence intensity (MFI) from one FSS channel and one static control channel in four independent devices for each experimental design.

3.5.6 Efflux Transporter Assays

The transporter substrates, Calcein-AM (1 μM) and CMFDA (1 μM) (both 2% DMSO vehicle), were incubated with serum free culture media at 37 °C for 60 minutes or

30 minutes, respectively after 24 hour treatment of FSS. Transport incubation was stopped by placing the samples on ice and washing three times with cold serum free culture media. After washing, the samples were immediately imaged.

To establish fluorescent substrate uptake in the 3D model system, RPTEC/TERT1 cells remained under physiological relevant level (0.5 dyn/cm^2) FSS stimulation or static conditions for 24 hours and were removed from the pump immediately before efflux transporter assays were performed. The transporter substrates, Calcein-AM (1 μM) and CMFDA (1 μM) (both 2% DMSO vehicle), were incubated using serum free culture media at 37°C for 60 min or 30 min respectively. Transport incubation was stopped by placing the samples on ice and washing three times with cold serum free culture media. Afterward, the samples were immediately imaged. Fluorescent images were obtained as before. Fluorescence images were analyzed using ImageJ software (NIH, Version 1.51a) to obtain mean fluorescence intensity (MFI) from one FSS condition and one static control channel in four independent devices for each experimental design.

3.5.7 Statistical Data Analysis

For statistical analyses, Unpaired t-test was performed using GraphPad InStat software (GraphPad Software Inc., San Diego, CA, USA). All data are presented as means +/- standard error; differences between groups were considered statistically significant when $p < 0.05$.

3.5.8 RNA-seq Sample Preparation

RPTEC/TERT1 cells were grown to confluence and exposed to FSS at the different rates as described above. Total RNA was obtained from cells grown in four independent

device channels after exposure to flow for 24 hours using the ReliaPrep RNA Miniprep Systems (Z6011, Promega) following the manufacturer's instruction.

Total RNA samples were evaluated for concentration by Qubit and for integrity by Bioanalyzer prior to pooling a total of 24 samples over 7 lanes. The RNA-sequencing libraries were generated by the HudsonAlpha Genomic Service Lab (https://gsl.hudsonalpha.org/information/rna) using poly(A) selection and sequencing was performed on an Illumina HiSeq 2500 using paired end reads of 50 bases (Illumina, San Diego, CA, USA) and sequenced an average of 7.6 million reads per sample with an average Q30 score of 94.32%. All samples had an RNA integrity number ranging between 8.8 to 9.8 and 3' or 5' bias above 80% by quality control metrics (https://broadinstitute.github.io/picard/). Any samples which did not pass these quality control mapping were not included into the data set[172].

3.5.9 RNA-seq Analysis

Sequencing reads of 52,463 total genes were aligned using a previously described aRNApipe pipeline (v1.1)[173]. Reads were trimmed with TrimGalore (http://www.bioinformatics.babraham.ac.uk/projects/trim_galore/) prior to alignment with STAR (v2.5.2b)[174] using the hg37 reference genome. Quality control metrics of the alignment process was assessed with Picard (https://broadinstitute.github.io/picard/). All data analysis in R was performed with R version 3.3.1 using RStudio (v1.1.453). To examine gene expression changes, differential expression was determined by using DESeq2 package (v1.12.4)[175] using the default settings in likelihood ratio test (LRT) mode[176]. The most highly differentially expressed gene subset list highlighted in the volcano plot (p-adjust $\geq 1x10^{-30}$ and log2FC $>\pm 1$) was filtered by genes found to be

associated with both PTs and kidney GWAS. To generate gene list containing genes that were previously published in association with the search term proximal tubule, the search engine Geneshot was utilized[177]. In order to compile and filter GWAS that identified specific gene to human kidney disease resistance/susceptibility, the complete 12/16/2019 release of the NHGRI-EBI GWAS database was downloaded from the NHGRI-EBI Catalog website (https://www.ebi.ac.uk/gwas/docs/file-downloads). The *H. sapiens* pathway analysis was conducted using functional enrichment analysis web tool, LRPath with enrichment method GSEA and enrichment category gerontology biological process (no redundant) and advance parameters minimum number of genes equal 20[178–180]. Pathway analysis was run using LRPath[178,181] and pathway analysis was carried out by the top 50 GO terms by p-value separating up- and down-regulated GO terms and visualized using REVIGO (Reduce and Visualize Gene Ontology) available online and run using default parameters[162]. Gene IDs were converted to ENSEMBL gene IDs using R packages biomaRt (v.2.28.0) and biomartr (v.0.7.0)[182]. The R packages pheatmap (v.1.0.10), ggplot2 (v. 3.0.1), edgeR (v.3.14.0), and ggfortify (v.0.4.4) were used for figure preparation.

3.5.10 Data Availability

The RNA sequencing data discussed in this publication have been deposited in NCBI's Gene Expression Omnibus (Edgar et al., 2002) and are accessible through GEO Series accession number GSE172062 (https://www.ncbi.nlm.nih.gov/geo/query/acc.cgi?acc=GSE172062).

CHAPTER IV

Conclusions and Future Directions

4.1 Summary

This thesis demonstrates that the development of a bioartificial microfluidic device utilizing human PTCs is possible from a cellular point of view. By demonstrating functional assays and global transcriptional profiles changes with the treatment of FSS, provides further groundwork towards solute removal through living membranes. However, we cannot estimate if the addition of a bioartificial microfluidic device would make renal replacement therapy more efficient. Nevertheless, the advancement of knowledge often leads to the development of novel insights. Before doing any translation to *in vivo* testing of a device, several crucial aspects deserve future attention.

4.2 Clinical Applications

A new interest in transporter research implemented guidelines for *in vitro* metabolism and transporter-mediated drug-drug interaction studies[183]. Both academia and industry have committed many resources to explore transporter-mediated pharmacological interactions. Considering the high density of transporters in the kidney, more complex interactions could be revealed. Present trends in research are shifting towards dynamic transporter regulation and the mechanisms behind transporter interactions. In pharmacokinetics and pharmacology research, absorption, distribution, metabolism, and excretion (ADME) studies simultaneously incorporate renal transport activity and expression of several transporters in their design[57,184,185]. Furthermore, with the addition of bioinformatics, we can now bring large data sets and transporters regulation, expression,

activity, and interactions together by computational tools for ADME in drug development[186,187]. Overall, research into renal transport can be expected to become more integrative as it tackles clinical questions. This work has demonstrated proof of concept of the assembly of a PT device incorporating human renal cells with characterized transporter expression using RNA-sequencing and functional assays for use in research. Our PTC microfluidic device will allow us to better model how PTCs contribute to CKD utilizing multiple cellular sources, such as well-characterized immortalized PTC (RPTEC/TERT1). In the future, PTCs used in our device can be genetically altered to mimic disease states and use cell lines generated from CKD patients themselves to better recapitulate *in vivo* phenotypes – leading the way to developing personalized medicine for CKD patients.

The use of personalized medicine, targeting differentiation combined with custom-made biomaterials could provide high-quality renal cell prototypes. Genome engineering techniques, for example, clustered regularly interspaced short palindromic repeats and associated gene (CRISPR-Cas9), allows for the precise gene manipulation of living cells. Genes or single nucleotide changes can now be removed and inserted in precise locations. Transporter genes can be added or removed from a cell line on-demand or mutated to represent a polymorphism; the opportunities for genetically modified models to study transporter interactions and regulation are enormous. Further, the technique can also be used *in vivo* by manipulating germ cells and tailoring animals according to the experimental needs. The potential for translational and regenerative medicine of the methodologies exposed here is considerable. Driven mainly by principles of the 3R's, it is likely that tools and innovative approaches derived from kidney tissue engineering will find their way into fundamental renal pharmacological research. CRISPR-Cas9 combined with iPS cell

technology could provide a sustainable and reliable source of high-quality cells for tissue repair and fundamental research.

Genome-wide association studies (GWAS) have advanced our knowledge of the genetic susceptibility to CKD by identifying multiple risk genes. Vanderbilt University provides further gene nomination resources using BioVU DNA databank[188,189]. Pioneer research is already being done using this DNA biobank and electronic medical record resources to identify ADME variants associated with tacrolimus (an immunosuppressive drug prescribed in kidney transplantation) dose requirement[188]. These and other gene nominations, many of the possible identified single nucleotide polymorphisms (SNPs) associated with CKD fall in an area of linkage disequilibrium (LD) blocks that makes it very difficult to identify the causal target variant(s). Thus, our ability to test the specific mechanisms underlying these SNPs associations are limited and requires further testing, including their functional validation.

Furthermore, genetic risks that impact kidney-specific cell types are still currently not well understood. To overcome limitations, the combination of functional microfluidic *in vitro* PTC models that emulate the human *in vivo* system and diseased conditions by PTC generated from genetic engineering or CKD patients, and sibling-derived iPSC is needed. By utilizing PTC generated from CKD patient-derived iPSC, we will discover where function in the nephron is compromised. The use of personalized medicine is a unique opportunity to discover the functional consequences of a variant, which may offer treatment options to individuals carrying the mutation who have not yet required renal transplant[190].

4.5 Integration Towards a Body-on-a-Chip

An emerging branch of microfluidics uses compartmentalization to facilitate interaction between different organs and cell types while simultaneously allowing independent manipulation and observation of the respective cell populations[191,192]. Previously developed physiologically-based pharmacokinetic microfluidics models, such as the model system discussed in this dissertation, allow for the adequate elucidation of absorption, distribution, metabolism, excretion, and toxicity properties relating to multiple organs[192–194]. These body-on-a-chip platforms, also called microphysiological systems, have been developed to model multiple organ types, such as lung, liver, fat, or bone marrow, into isolated chambers while integrating biosensors such as oxygen sensors[195]. A straightforward microfluidic reconfiguration has also been achieved in a single-pass integrated liver-kidney two-organ system using different inlets and outlet combinations for loading different tissue cells and interconnected multiorgan culture[192]. Body-on-chips have been developed to include barrier components representing a 'functional coupling' of four human micro-physiological system models[184]. The intestine, liver, parts of the kidney, and a neurovascular unit were selected, representing major organs involved in the ADME of drugs. This approach utilized transferring media between six institutions with different microphysiological units for subsequent experiment and analysis, rather than the direct coupling of unit to unit. This method circumvents some of the important challenges when trying to integrate multiple organ microphysiological units. One major challenge is implementing a universal medium that can support growth, differentiation, and accurately reproduce organ interactions in the human body. Another microphysiological platform included the kidney, skin, and skeletal muscle[196]. The authors successfully maintained ten

functional multi-microphysiological phenotypic functional platforms for four weeks[196]. In their device, recirculation of media and distribution into each organ module was achieved by a pneumatically driven pump with independently programmable flow rates. Their study illustrates several generalizable designs and operational principles for implementing multi-microphysiological approaches for drug discovery.

These multi-microphysiological systems have been developed to include barrier components representing individual organs and/or organ sections on the same chip. Such a system is yet to be integrated with the multiple, complex components of the nephron to allow simultaneous monitoring of systemic interactions with the whole kidney. There remains much to do to increase reliability and decrease cost, but many academic groups and companies suggest that these achievements in microfluidic platforms are within the near future. Overall, we believe that this technology is beginning to mature and will continue to approach regular use in drug discovery and physiological research.

CHAPTER V

References

1. Yin, J. & Wang, J. Renal drug transporters and their significance in drug-drug interactions. *B* **6**, 363–373 (2016).
2. Kurts, C., Panzer, U., Anders, H.-J. & Rees, A. J. The immune system and kidney disease: basic concepts and clinical implications. *Nat. Publ. Gr.* **13**, (2013).
3. Madrazo-Ibarra, A. & Vaitla, P. Histology, Nephron. *StatPearls* (2020).
4. CJ, M., M, S. & GI, W. Podocyte dedifferentiation: a specialized process for a specialized cell. *Front. Endocrinol. (Lausanne).* **5**, (2014).
5. Julian, B. A. *et al.* Sources of Urinary Proteins and their Analysis by Urinary Proteomics for the Detection of Biomarkers of Disease. *Proteomics. Clin. Appl.* **3**, 1029 (2009).
6. Zhuo, J. L. & Li, X. C. Proximal nephron. *Compr. Physiol.* **3**, 1079–1123 (2013).
7. F, S., L, C., D, A. & M, C. Multidrug and toxin extrusion proteins (MATE/SLC47); role in pharmacokinetics. *Int. J. Biochem. Cell Biol.* **45**, 2007–2011 (2013).
8. Ross, E. J. *et al.* Three dimensional modeling of biologically relevant fluid shear stress in human renal tubule cells mimics in vivo transcriptional profiles. *Sci. Reports* | **11**, 14053 (123AD).
9. AA, E.-S. *et al.* Renal glucuronidation and multidrug resistance protein 2-/multidrug resistance protein 4-mediated efflux of mycophenolic acid: interaction with cyclosporine and tacrolimus. *Transl. Res.* **164**, 46–56 (2014).
10. Wilmer, M. J. *et al.* Kidney-on-a-Chip Technology for Drug-Induced Nephrotoxicity Screening. *Trends Biotechnol.* **34**, 156–170 (2016).
11. A, H. & WJ, N. Adherens and tight junctions: structure, function and connections to the actin cytoskeleton. *Biochim. Biophys. Acta* **1778**, 660–669 (2008).
12. Choucha Snouber, L., Jacques, S., Monge, M., Legallais, C. & Leclerc, E. Transcriptomic analysis of the effect of ifosfamide on MDCK cells cultivated in microfluidic biochips. *Genomics* **100**, 27–34 (2012).

13. Miravète, M. *et al.* Renal tubular fluid shear stress promotes endothelial cell activation. *Biochem. Biophys. Res. Commun.* **407**, 813–817 (2011).
14. Raghavan, V. & Weisz, O. A. Flow stimulated endocytosis in the proximal tubule. *Current Opinion in Nephrology and Hypertension* vol. 24 359–365 (2015).
15. Perry, R. J. *et al.* HHS Public Access. **510**, 84–91 (2015).
16. Nieskens, T. T. G. & Wilmer, M. J. Kidney-on-a-chip technology for renal proximal tubule tissue reconstruction. *Eur. J. Pharmacol.* **790**, 46–56 (2016).
17. Nielsen, R., Christensen, E. I. & Birn, H. Megalin and cubilin in proximal tubule protein reabsorption: From experimental models to human disease. *Kidney Int.* **89**, 58–67 (2016).
18. Dickson, L. E., Wagner, M. C., Sandoval, R. M. & Molitoris, B. A. The proximal tubule and albuminuria: really! *J. Am. Soc. Nephrol.* **25**, 443–53 (2014).
19. Grabias, B. M. & Konstantopoulos, K. Epithelial-mesenchymal transition and fibrosis are mutually exclusive reponses in shear-activated proximal tubular epithelial cells. *FASEB J.* **26**, 4131–41 (2012).
20. Weinbaum, S., Duan, Y., Satlin, L. M., Wang, T. & Weinstein, A. M. Mechanotransduction in the renal tubule. *Am. J. Physiol. Renal Physiol.* **299**, F1220-36 (2010).
21. Kunnen, S. J., Malas, T. B., Semeins, C. M., Bakker, A. D. & Peters, D. J. M. Comprehensive transcriptome analysis of fluid shear stress altered gene expression in renal epithelial cells. *J. Cell. Physiol.* **233**, 3615–3628 (2018).
22. Park, H. J. *et al.* Transcriptional Programs Driving Shear Stress-Induced Differentiation of Kidney Proximal Tubule Cells in Culture. *Front. Physiol.* **11**, 587358 (2020).
23. Jansen, J. *et al.* A morphological and functional comparison of proximal tubule cell lines established from human urine and kidney tissue. *Exp. Cell Res.* **323**, 87–99 (2014).
24. CDC. Chronic Kidney Disease in the United States, 2019. *Cdc* **1**, 1–6 (2019).
25. Chronic Kidney Disease in the United States, 2021. https://www.cdc.gov/kidneydisease/publications-resources/ckd-national-facts.html.
26. Robinson, B. *et al. 2016 USRDS Annual Data Report*.

https://www.usrds.org/2016/download/Acknowledgments_17_04_14.pdf.

27. Hsu, R. K. & Hsu, C. THE ROLE OF ACUTE KIDNEY INJURY IN CHRONIC KIDNEY DISEASE. *Semin. Nephrol.* **36**, 283 (2016).
28. Norris, K. & Nissenson, A. R. Race, Gender, and Socioeconomic Disparities in CKD in the United States. *J. Am. Soc. Nephrol.* **19**, 1261–1270 (2008).
29. Mehrotra, R., Kermah, D., Fried, L., Adler, S. & Norris, K. Racial Differences in Mortality Among Those with CKD. *J. Am. Soc. Nephrol.* **19**, 1403–1410 (2008).
30. Levin, A., Lancashire, W. & Fassett, R. G. Targets, trends, excesses, and deficiencies: refocusing clinical investigation to improve patient outcomes. *Kidney Int.* **83**, 1001–9 (2013).
31. Wuttke, M., Schaefer, F., Wong, C. S. & Köttgen, A. Genome-wide association studies in nephrology: using known associations for data checks. *Am. J. Kidney Dis.* **65**, 217–22 (2015).
32. Fanelli, C., Dellê, H., Cavaglieri, R. C., Dominguez, W. V. & Noronha, I. L. Gender Differences in the Progression of Experimental Chronic Kidney Disease Induced by Chronic Nitric Oxide Inhibition. *Biomed Res. Int.* **2017**, (2017).
33. Nicholas, S. B., Kalantar-Zadeh, K. & Norris, K. C. Socioeconomic Disparities in Chronic Kidney Disease. *Adv. Chronic Kidney Dis.* **22**, 6 (2015).
34. Harris, R. C. & Zhang, M.-Z. The role of gender disparities in kidney injury. *Ann. Transl. Med.* **8**, 514–514 (2020).
35. NR, K. & LA, P. Racial differences in the use of invasive cardiovascular procedures: review of the literature and prescription for future research. *Ann. Intern. Med.* **135**, 352–366 (2001).
36. EC, S. *et al.* Racial differences in cardiac revascularization rates: does 'overuse' explain higher rates among white patients? *Ann. Intern. Med.* **135**, 328–337 (2001).
37. K, K.-Z., G, B., MH, H. & JD, K. Reverse epidemiology of cardiovascular risk factors in maintenance dialysis patients. *Kidney Int.* **63**, 793–808 (2003).
38. Wolf, M. *et al.* Impact of Activated Vitamin D and Race on Survival among Hemodialysis Patients. *J. Am. Soc. Nephrol.* **19**, 1379–1388 (2008).
39. Hsu, C., Lin, F., Vittinghoff, E. & Shlipak, M. G. Racial Differences in the

Progression from Chronic Renal Insufficiency to End-Stage Renal Disease in the United States. *J. Am. Soc. Nephrol.* **14**, 2902–2907 (2003).

40. L, G. *et al.* The Role of Place in Disparities Affecting Black Men Receiving Hemodialysis. *Kidney Int. reports* **6**, 357–365 (2020).
41. C, Z. *et al.* Genetic susceptibility of hypertension-induced kidney disease. *Physiol. Rep.* **9**, (2021).
42. ML, N., KR, B.-P., GI, O., RV, K. & I, C. Survival of the Fittest: Addressing the Disparities in the Burden of Chronic Kidney Disease. *Cureus* **12**, (2020).
43. L, A. & P, E. Racial and ethnic disparities in end-stage kidney failure-survival paradoxes in African-Americans. *Semin. Dial.* **20**, 577–585 (2007).
44. C, D. *et al.* Reassessing the Inclusion of Race in Diagnosing Kidney Diseases: An Interim Report From the NKF-ASN Task Force. *Am. J. Kidney Dis.* **78**, 103–115 (2021).
45. A, B. & M, M. Impact of gender and gender disparities in patients with kidney disease. *Curr. Opin. Nephrol. Hypertens.* **28**, 178–182 (2019).
46. G, C. *et al.* Sex and gender differences in chronic kidney disease: progression to end-stage renal disease and haemodialysis. *Clin. Sci. (Lond).* **130**, 1147–1163 (2016).
47. JJ, C., M, H., NC, C. & KJ, J. Sex and gender disparities in the epidemiology and outcomes of chronic kidney disease. *Nat. Rev. Nephrol.* **14**, 151–164 (2018).
48. JJ, C., M, H., I, U., L, S. & B, T. Chronic Kidney Disease, Gender, and Access to Care: A Global Perspective. *Semin. Nephrol.* **37**, 296–308 (2017).
49. MM, B. & B, S. Gender bias in renal transplantation: are women alone donating kidneys in India? *Transplant. Proc.* **39**, 2961–2963 (2007).
50. OP, S. & DR, M. Sex differences in pharmacokinetics and pharmacodynamics. *Clin. Pharmacokinet.* **48**, 143–157 (2009).
51. Soo, J. Y. C., Jansen, J., Masereeuw, R. & Little, M. H. Advances in predictive in vitro models of drug-induced nephrotoxicity. *Nature Reviews Nephrology* vol. 14 378–393 (2018).
52. D, H., LD, B., KM, S. & SJ, R. Tissue engineering: strategies, stem cells and scaffolds. *J. Anat.* **213**, 66–72 (2008).

53. F, B., TJ, M. & ML, Y. Tissue engineering and regenerative medicine: history, progress, and challenges. *Annu. Rev. Chem. Biomol. Eng.* **2**, 403–430 (2011).
54. MA, N., NJ, C., MW, P. & LG, Z. 3D printing of novel osteochondral scaffolds with graded microstructure. *Nanotechnology* **27**, (2016).
55. AS, M. & DJ, M. Regenerative medicine: Current therapies and future directions. *Proc. Natl. Acad. Sci. U. S. A.* **112**, 14452–14459 (2015).
56. Wang, X., Sun, Q. & Pei, J. Microfluidic-Based 3D Engineered Microvascular Networks and Their Applications in Vascularized Microtumor Models. *Micromachines* **9**, 493 (2018).
57. Kimura, H., Sakai, Y. & Fujii, T. Organ/body-on-a-chip based on microfluidic technology for drug discovery. *Drug Metab. Pharmacokinet.* **33**, 43–48 (2018).
58. Liu, D., Cheng, F., Pan, S. & Liu, Z. Stem cells: a potential treatment option for kidney diseases. *Stem Cell Res. Ther. 2020 111* **11**, 1–20 (2020).
59. J, L. & JJ, G. The rebirth of interest in renal tubular function. *Am. J. Physiol. Renal Physiol.* **310**, F1351–F1355 (2016).
60. Lian, Y., Zhou, Q., Zhang, Y. & Zheng, F. VEGF ameliorates tubulointerstitial fibrosis in unilateral ureteral obstruction mice via inhibition of epithelial-mesenchymal transition. *Acta Pharmacol. Sin. 2011 3212* **32**, 1513–1521 (2011).
61. J, J. *et al.* Biotechnological challenges of bioartificial kidney engineering. *Biotechnol. Adv.* **32**, 1317–1327 (2014).
62. Liu, D., Cheng, F., Pan, S. & Liu, Z. Stem cells: a potential treatment option for kidney diseases. *Stem Cell Res. Ther.* **11**, 249 (2020).
63. Homan, K. a *et al.* Bioprinting of 3D Convoluted Renal Proximal Tubules on Perfusable Chips. *Sci. Rep.* **6**, 34845 (2016).
64. Song, J. J. *et al.* Regeneration and Experimental Orthotopic Transplantation of a Bioengineered Kidney. *Nat. Med.* **19**, 646 (2013).
65. Campuzano, S. & Pelling, A. E. Scaffolds for 3D Cell Culture and Cellular Agriculture Applications Derived From Non-animal Sources. *Front. Sustain. Food Syst.* **0**, 38 (2019).
66. Little, M. H. Growing kidney tissue from stem cells: how far from 'party trick' to medical application? *Cell Stem Cell* **18**, 695 (2016).

67. Nieskens, T. T. G. & Sjögren, A. K. Emerging In Vitro Systems to Screen and Predict Drug-Induced Kidney Toxicity. *Seminars in Nephrology* vol. 39 215–226 (2019).
68. Little, M. H. & Combes, A. N. Kidney organoids: accurate models or fortunate accidents. *Genes Dev.* **33**, 1319 (2019).
69. Zhang, L. *et al.* Drug Delivery A novel biosensor based on intestinal 3D organoids for detecting the function of BCRP A novel biosensor based on intestinal 3D organoids for detecting the function of BCRP. (2017) doi:10.1080/10717544.2017.1381199org/10.1080/10717544.2017.1381199.
70. Kang, H. M. *et al.* Effective reconstruction of functional organotypic kidney spheroid for in vitro nephrotoxicity studies. *Sci. Rep.* **9**, 1–17 (2019).
71. M, W., A, H., S, H., J, K. & S, H. 3D organ models-Revolution in pharmacological research? *Pharmacol. Res.* **139**, 446–451 (2019).
72. JY, S., J, J., R, M. & MH, L. Advances in predictive in vitro models of drug-induced nephrotoxicity. *Nat. Rev. Nephrol.* **14**, 378–393 (2018).
73. Jang, K.-J. *et al.* Human kidney proximal tubule-on-a-chip for drug transport and nephrotoxicity assessment. *Integr. Biol.* **5**, 1119 (2013).
74. Ashammakhi, N., Wesseling-Perry, K., Hasan, A., Elkhammas, E. & Zhang, Y. S. Kidney-on-a-chip: untapped opportunities. *Kidney Int.* **94**, 1073–1086 (2018).
75. Lamberti, G. *et al.* Adhesion patterns in the microvasculature are dependent on bifurcation angle. *Microvasc. Res.* **99**, 19–25 (2015).
76. B, P. *et al.* SyM-BBB: a microfluidic Blood Brain Barrier model. *Lab Chip* **13**, 1093–1101 (2013).
77. Deosarkar, S. P. *et al.* A Novel Dynamic Neonatal Blood-Brain Barrier on a Chip. *PLoS One* **10**, e0142725 (2015).
78. Pradhan, S. *et al.* A Microvascularized Tumor-mimetic Platform for Assessing Anti-cancer Drug Efficacy. *Sci. Rep.* **8**, 3171 (2018).
79. Soroush, F. *et al.* A novel microfluidic assay reveals a key role for protein kinase C δ in regulating human neutrophil-endothelium interaction. *J. Leukoc. Biol.* **100**, 1027–1035 (2016).
80. Kolhar, P. *et al.* Using shape effects to target antibody-coated nanoparticles to lung

and brain endothelium. *Proc. Natl. Acad. Sci.* **110**, 10753–10758 (2013).

81. Liu, Z. *et al.* Co-cultured microfluidic model of the airway optimized for microscopy and micro-optical coherence tomography imaging. *Biomed. Opt. Express* **10**, 5414 (2019).
82. M, J. *et al.* Detachment of ligands from nanoparticle surface under flow and endothelial cell contact: Assessment using microfluidic devices. *Bioeng. Transl. Med.* **3**, 148–155 (2018).
83. TD, H., T, O. & GJ, B. Small animal models of kidney disease: a review. *Methods Mol. Biol.* **466**, 41–57 (2009).
84. Ortiz, E., Gurrola, G. B., Schwartz, E. F. & Possani, L. D. Scorpion venom components as potential candidates for drug development. *Toxicon* **93**, 125 (2015).
85. AP, S. *et al.* Animal models of acute renal failure. *Pharmacol. Rep.* **64**, 31–44 (2012).
86. B, F., A, M. & N, C. BCG-associated heterologous immunity, a historical perspective: intervention studies in animal models of infectious diseases. *Trans. R. Soc. Trop. Med. Hyg.* **109**, 52–61 (2015).
87. Kiryluk, K. *et al.* Discovery of new risk loci for IgA nephropathy implicates genes involved in immunity against intestinal pathogens. *Nat. Genet.* **46**, 1187–96 (2014).
88. Awdishu, L. & Mehta, R. L. The 6R's of drug induced nephrotoxicity. *BMC Nephrology* vol. 18 1–12 (2017).
89. Kim, S. & Takayama, S. Organ-on-a-chip and the kidney. *Kidney Res. Clin. Pract.* **34**, 165 (2015).
90. O, S., Y, P. & F, G. Human collagen produced in plants: more than just another molecule. *Bioengineered* **5**, (2014).
91. Kraham, S. J. Environmental Impacts of Industrial Livestock Production. *Int. Farm Anim. Wildl. Food Saf. Law* 3–40 (2017) doi:10.1007/978-3-319-18002-1_1.
92. Becker, G. J. & Hewitson, T. D. Animal models of chronic kidney disease: useful but not perfect. *Nephrol. Dial. Transplant.* **28**, 2432–2438 (2013).
93. Lee, J. W., Chou, C.-L. & Knepper, M. A. Deep Sequencing in Microdissected Renal Tubules Identifies Nephron Segment-Specific Transcriptomes. *J Am Soc*

Nephrol **26**, 2669–2677 (2015).

94. Khundmiri, S. J., Chen, L., Lederer, E. D., Yang, C.-R. & Knepper, M. A. Transcriptomes of Major Proximal Tubule Cell Culture Models. *J. Am. Soc. Nephrol.* **32**, 86–97 (2021).
95. Lee, J. W., Chou, C. L. & Knepper, M. A. Deep sequencing in microdissected renal tubules identifies nephron segment-specific transcriptomes. *J. Am. Soc. Nephrol.* **26**, 2669–2677 (2015).
96. HJ, P. *et al.* Transcriptional Programs Driving Shear Stress-Induced Differentiation of Kidney Proximal Tubule Cells in Culture. *Front. Physiol.* **11**, (2020).
97. Rahmoune, H. *et al.* Glucose transporters in human renal proximal tubular cells isolated from the urine of patients with non-insulin-dependent diabetes. *Diabetes* **54**, 3427–3434 (2005).
98. Baer, P. C., Nockher, W. a, Haase, W. & Scherberich, J. E. Isolation of proximal and distal tubule cells from human kidney by immunomagnetic separation. *Kidney Int.* **52**, 1321–1331 (1997).
99. DA, V., W, Q., X, C., CA, P. & DW, J. Isolation and primary culture of human proximal tubule cells. *Methods Mol. Biol.* **466**, 19–24 (2009).
100. Mihevc, M., Petreski, T., Maver, U. & Bevc, S. Renal proximal tubular epithelial cells: review of isolation, characterization, and culturing techniques. *Molecular Biology Reports* vol. 47 9865–9882 (2020).
101. Van der Hauwaert, C. *et al.* Isolation and Characterization of a Primary Proximal Tubular Epithelial Cell Model from Human Kidney by CD10/CD13 Double Labeling. *PLoS One* **8**, 2–11 (2013).
102. Sánchez-Romero, N. *et al.* A simple method for the isolation and detailed characterization of primary human proximal tubule cells for renal replacement therapy. *Int. J. Artif. Organs* **43**, 45–57 (2020).
103. M, M., T, P., U, M. & S, B. Renal proximal tubular epithelial cells: review of isolation, characterization, and culturing techniques. *Mol. Biol. Rep.* **47**, 9865–9882 (2020).
104. N, F. *et al.* Application of physiological shear stress to renal tubular epithelial

cells. *Methods Cell Biol.* **153**, 43–67 (2019).

105. Li, Y. *et al.* An in vitro method for the prediction of renal proximal tubular toxicity in humans. *Toxicol. Res. (Camb).* **2**, 352–365 (2013).
106. Schophuizen, C. TOWARDS A BIOARTIFICIAL KIDNEY Insights in uptake and elimination of cationic solutes by proximal tubule epithelial cells.
107. Kramann, R., Kusaba, T. & Humphreys, B. D. Who regenerates the kidney tubule? *Nephrol Dial Transpl.* **30**, 903–910 (2015).
108. Slyne, J., Slattery, C., McMorrow, T. & Ryan, M. P. New developments concerning the proximal tubule in diabetic nephropathy: In vitro models and mechanisms. *Nephrol. Dial. Transplant.* **30**, iv60–iv67 (2015).
109. Wieser, M. *et al.* hTERT alone immortalizes epithelial cells of renal proximal tubules without changing their functional characteristics. *Am J Physiol Ren. Physiol* **295**, F1365-75 (2008).
110. Thomas, P. & Smart, T. G. HEK293 cell line: A vehicle for the expression of recombinant proteins. *J. Pharmacol. Toxicol. Methods* **51**, 187–200 (2005).
111. Jenkinson, S. E. *et al.* The limitations of renal epithelial cell line HK-2 as a model of drug transporter expression and function in the proximal tubule. *Pflugers Arch. Eur. J. Physiol.* **464**, 1–11 (2012).
112. Faria, J., Ahmed, S., Gerritsen, K. G. F., Mihaila, S. M. & Masereeuw, R. Kidney-based in vitro models for drug-induced toxicity testing. *Arch. Toxicol. 2019 9312* **93**, 3397–3418 (2019).
113. Aschauer, L. *et al.* Delineation of the Key Aspects in the Regulation of Epithelial Monolayer Formation. *Mol. Cell. Biol.* **33**, 2535–2550 (2013).
114. Simon-Friedt, B. R. *et al.* The RPTEC/TERT1 cell line as an improved tool for in vitro nephrotoxicity assessments HHS Public Access. *Biol Trace Elem Res* **166**, 66–71 (2015).
115. Aschauer, L. *et al.* Application of RPTEC/TERT1 cells for investigation of repeat dose nephrotoxicity: A transcriptomic study. *Toxicol. Vitr.* **30**, 106–116 (2015).
116. Wilmes, A. *et al.* Mechanism of cisplatin proximal tubule toxicity revealed by integrating transcriptomics, proteomics, metabolomics and biokinetics. *Toxicol. Vitr.* **30**, 117–127 (2015).

117. Secker, P. F., Luks, L., Schlichenmaier, N. & Dietrich, D. R. RPTEC/TERT1 cells form highly differentiated tubules when cultured in a 3D matrix. *ALTEX* **35**, 223–234 (2018).
118. Limonciel, A. *et al.* Comparison of base-line and chemical-induced transcriptomic responses in HepaRG and RPTEC/TERT1 cells using TempO-Seq. **92**, 2517–2531 (2018).
119. M, P. *et al.* Empagliflozin Inhibits Basal and IL-1β-Mediated MCP-1/CCL2 and Endothelin-1 Expression in Human Proximal Tubular Cells. *Int. J. Mol. Sci.* **21**, 1–17 (2020).
120. Breshears, M. A. & Confer, A. W. The Urinary System. *Pathol. Basis Vet. Dis.* 617 (2017) doi:10.1016/B978-0-323-35775-3.00011-4.
121. Pozzi, A. & Zent, R. ZO-1 and ZONAB Interact to Regulate Proximal Tubular Cell Differentiation. *J. Am. Soc. Nephrol.* **21**, 388 (2010).
122. Morgan, M. R., Humphries, M. J. & Bass, M. D. Synergistic control of cell adhesion by integrins and syndecans. *Nat. Rev. Mol. Cell Biol. 2007 812* **8**, 957–969 (2007).
123. Nair, A. R. *et al.* Renal cells exposed to cadmium *in vitro* and *in vivo* : normalizing gene expression data. *J. Appl. Toxicol.* **35**, 478–484 (2015).
124. Welch, H. K., Kellum, J. A. & Kane-Gill, S. L. Drug-Associated Acute Kidney Injury Identified in the United States Food and Drug Administration Adverse Event Reporting System Database. *Pharmacother. J. Hum. Pharmacol. Drug Ther.* **38**, 785–793 (2018).
125. Joyce, E. L., Kane-Gill, S. L., Fuhrman, D. Y. & Kellum, J. A. Drug-associated acute kidney injury: who's at risk? *Pediatr. Nephrol. 2016 321* **32**, 59–69 (2016).
126. R, J. & AM, H. Renal toxicity of therapeutic drugs. *J. Clin. Pathol.* **62**, 505–515 (2009).
127. SG, Y. & MA, P. Drug-induced crystal nephropathy: an update. *Expert Opin. Drug Saf.* **7**, 147–158 (2008).
128. D, C. & Z, A. Drug-associated renal dysfunction and injury. *Nat. Clin. Pract. Nephrol.* **2**, 80–91 (2006).
129. MA, P. Drug-induced renal failure: update on new medications and unique

mechanisms of nephrotoxicity. *Am. J. Med. Sci.* **325**, 349–362 (2003).

130. MA, P. Drug-induced nephropathy: an update. *Expert Opin. Drug Saf.* **4**, 689–706 (2005).
131. Downes, K. J. *et al.* Mechanisms of antimicrobial-induced nephrotoxicity in children. *J. Antimicrob. Chemother.* **75**, 1 (2020).
132. Morales-Alvarez, M. C. Nephrotoxicity of Antimicrobials and Antibiotics. *Adv. Chronic Kidney Dis.* **27**, 31–37 (2020).
133. Ramesh, G. & Reeves, W. B. TNF-α mediates chemokine and cytokine expression and renal injury in cisplatin nephrotoxicity. *J. Clin. Invest.* **110**, 835 (2002).
134. EJ, P. *et al.* Repeated-dose toxicity and inflammatory responses in mice by oral administration of silver nanoparticles. *Environ. Toxicol. Pharmacol.* **30**, 162–168 (2010).
135. Simon, B. R., Wilson, M. J., Blake, D. A., Yu, H. & Wickliffe, J. K. Cadmium alters the formation of benzo[a]pyrene DNA adducts in the RPTEC/TERT1 human renal proximal tubule epithelial cell line. *Toxicol. Reports* **1**, 391–400 (2014).
136. AR, N. *et al.* Renal cells exposed to cadmium in vitro and in vivo: normalizing gene expression data. *J. Appl. Toxicol.* **35**, 478–484 (2015).
137. Masereeuw, R. *et al.* Screening of Drug-Transporter Interactions in a 3D Microfluidic Renal Proximal Tubule on a Chip. doi:10.1208/s12248-018-0247-0.
138. Caetano-Pinto, P. *et al.* Fluorescence-Based Transport Assays Revisited in a Human Renal Proximal Tubule Cell Line. *Mol. Pharm.* **13**, 933–944 (2016).
139. S, M., K, S., M, K.-N., T, T. & S, T. Fluid shear triggers microvilli formation via mechanosensitive activation of TRPV6. *Nat. Commun.* **6**, (2015).
140. B, U., K, C. & HJ, B. Drosophila tools and assays for the study of human diseases. *Dis. Model. Mech.* **9**, 235–244 (2016).
141. Lienkamp, S. S. Using Xenopus to study genetic kidney diseases. *Semin. Cell Dev. Biol.* **51**, 117–124 (2016).
142. N, H. *et al.* 'Zebrafishing' for novel genes relevant to the glomerular filtration barrier. *Biomed Res. Int.* **2013**, (2013).
143. L, E., A, O., K, H., C, B. & K, T. Zebrafish: a model system for the study of vertebrate renal development, function, and pathophysiology. *Curr. Opin. Nephrol.*

Hypertens. **20**, 416–424 (2011).

144. N, D. *et al.* Flow and adhesion of drug carriers in blood vessels depend on their shape: a study using model synthetic microvascular networks. *J. Control. Release* **146**, 196–200 (2010).
145. G, L. *et al.* Bioinspired microfluidic assay for in vitro modeling of leukocyte-endothelium interactions. *Anal. Chem.* **86**, 8344–8351 (2014).
146. G, L. *et al.* Adhesion patterns in the microvasculature are dependent on bifurcation angle. *Microvasc. Res.* **99**, 19–25 (2015).
147. B, P. *et al.* Synthetic tumor networks for screening drug delivery systems. *J. Control. Release* **201**, 49–55 (2015).
148. Prabhakarpandian, B., Shen, M.-C., Pant, K. & Kiani, M. F. Microfluidic devices for modeling cell–cell and particle–cell interactions in the microvasculature. *Microvasc. Res.* **82**, 210–220 (2011).
149. JH, M. Renal basement membrane components. *Kidney Int.* **56**, 2016–2024 (1999).
150. Ha, L., Jang, K.-J. & Suh, K.-Y. Chapter 2 Kidney on a Chip. in *Microfluidics for Medical Applications* 19–39 (The Royal Society of Chemistry, 2015). doi:10.1039/9781849737593-00019.
151. C, W., H, L. & MA, S. A novel in vitro flow system for changing flow direction on endothelial cells. *J. Biomech.* **45**, 1212–1218 (2012).
152. JD, H., D, D., A, V., E, L. & M, L. Effects of serum deprivation on the mechanical properties of adherent vascular smooth muscle cells. *Proc. Inst. Mech. Eng. H.* **222**, 761–772 (2008).
153. V, R., Y, R., NM, P.-S., MD, C. & OA, W. Shear stress-dependent regulation of apical endocytosis in renal proximal tubule cells mediated by primary cilia. *Proc. Natl. Acad. Sci. U. S. A.* **111**, 8506–8511 (2014).
154. Livak, K. J. & Schmittgen, T. D. Analysis of Relative Gene Expression Data Using Real-Time Quantitative PCR and the 2−ΔΔCT Method. *Methods* **25**, 402–408 (2001).
155. Aschauer, L., Carta, G., Vogelsang, N., Schlatter, E. & Jennings, P. Expression of xenobiotic transporters in the human renal proximal tubule cell line RPTEC/TERT1. *Toxicol. Vitr.* **30**, 95–105 (2015).

156. Y-C Soo, J., Jansen, J., Masereeuw, R. & Little, M. H. *Advances in predictive in vitro models of drug-induced nephrotoxicity*. www.nature.com/nrneph (2018) doi:10.1038/s41581-018-0003-9.
157. Masereeuw, R. & Russel, F. G. M. Regulatory Pathways for ATP-binding Cassette Transport Proteins in Kidney Proximal Tubules. *AAPS J.* **14**, 883–894 (2012).
158. Saib, S., Hodin, S., He, Z., Delézay, O. & Delavenne, X. Is the human model RPTEC/TERT1 a relevant model for assessing renal drug efflux? *Fundam. Clin. Pharmacol.* fcp.12631 (2020) doi:10.1111/fcp.12631.
159. Caetano-Pinto, P., Jansen, J., Assaraf, Y. G. & Masereeuw, R. The importance of breast cancer resistance protein to the kidneys excretory function and chemotherapeutic resistance. *Drug Resist. Updat.* **30**, 15–27 (2017).
160. Fletcher, J. I., Williams, R. T., Henderson, M. J., Norris, M. D. & Haber, M. ABC transporters as mediators of drug resistance and contributors to cancer cell biology. *Drug Resist. Updat.* **26**, 1–9 (2016).
161. Eshbach, M. L. & Weisz, O. A. Receptor-Mediated Endocytosis in the Proximal Tubule. *Annu. Rev. Physiol* **79**, 425–48 (2017).
162. Supek, F., Bošnjak, M., Škunca, N. & Šmuc, T. REVIGO Summarizes and Visualizes Long Lists of Gene Ontology Terms. *PLoS One* **6**, e21800 (2011).
163. Lee, J. W., Chou, C. L. & Knepper, M. A. Deep sequencing in microdissected renal tubules identifies nephron segment-specific transcriptomes. *J. Am. Soc. Nephrol.* **26**, 2669–2677 (2015).
164. Lewko, B. *et al.* Osmolarity and glucose differentially regulate aldose reductase activity in cultured mouse podocytes. *Exp. Diabetes Res.* **2011**, 11 (2011).
165. Shaw, N., Yang, B., Millward, A., Demaine, A. & Hodgkinson, A. AKR1B10 is induced by hyperglycaemia and lipopolysaccharide in patients with diabetic nephropathy. *Cell Stress Chaperones* **19**, 281–287 (2014).
166. Chen, W.-D. & Zhang, Y. Regulation of Aldo–Keto Reductases in Human Diseases. *Front. Pharmacol.* **3**, 35 (2012).
167. Duan, Y. *et al. Shear-induced reorganization of renal proximal tubule cell actin cytoskeleton and apical junctional complexes*. www.pnas.org/cgi/content/full/ (2008).

168. Jaramillo-Juárez, F. *et al.* F-Actin Distribution Changes Provoked by Acetaminophen in the Proximal Tubule in Kidney of Adult Male Rat. *Microsc. Res.* **4**, 39–45 (2016).
169. Van de Water, B., Jaspers, J. J., Maasdam, D. H., Mulder, G. J. & Nagelkerke, J. F. In vivo and in vitro detachment of proximal tubular cells and F-actin damage: consequences for renal function. *Am. J. Physiol.* **267**, F888-99 (1994).
170. Bhattacharyya, S. *et al.* Cdc42 activation couples fluid shear stress to apical endocytosis in proximal tubule cells. *Physiol. Rep.* **5**, e13460 (2017).
171. International Transporter Consortium, T. I. T. *et al.* Membrane transporters in drug development. *Nat. Rev. Drug Discov.* **9**, 215–36 (2010).
172. Conesa, A. *et al.* A survey of best practices for RNA-seq data analysis. *Genome Biology* vol. 17 (2016).
173. Alonso, A. *et al.* ARNApipe: A balanced, efficient and distributed pipeline for processing RNA-seq data in high-performance computing environments. *Bioinformatics* **33**, 1727–1729 (2017).
174. Dobin, A. *et al.* STAR: Ultrafast universal RNA-seq aligner. *Bioinformatics* **29**, 15–21 (2013).
175. Love, M. I., Huber, W. & Anders, S. Moderated estimation of fold change and dispersion for RNA-seq data with DESeq2. *Genome Biol.* **15**, 550 (2014).
176. Marioni, J. C., Mason, C. E., Mane, S. M., Stephens, M. & Gilad, Y. RNA-seq: An assessment of technical reproducibility and comparison with gene expression arrays. *Genome Res.* **18**, 1509–1517 (2008).
177. Lachmann, A. *et al.* Geneshot: search engine for ranking genes from arbitrary text queries. *Nucleic Acids Res.* **47**, W571–W577 (2019).
178. Kim, J. H. *et al.* LRpath analysis reveals common pathways dysregulated via DNA methylation across cancer types. *BMC Genomics* **13**, (2012).
179. Newton, M. A., Quintana, F. A., Den Boon, J. A., Sengupta, S. & Ahlquist, P. RANDOM-SET METHODS IDENTIFY DISTINCT ASPECTS OF THE ENRICHMENT SIGNAL IN GENE-SET ANALYSIS. **1**, 85–106 (2007).
180. Lee, C., Patil, S. & Sartor, M. A. RNA-Enrich: A cut-off free functional enrichment testing method for RNA-seq with improved detection power.

Bioinformatics **32**, 1100–1102 (2016).

181. Sartor, M. A., Leikauf, G. D. & Medvedovic, M. LRpath: A logistic regression approach for identifying enriched biological groups in gene expression data. *Bioinformatics* **25**, 211–217 (2009).
182. Durinck, S., Spellman, P. T., Birney, E. & Huber, W. Mapping identifiers for the integration of genomic datasets with the R/ Bioconductor package biomaRt. *Nat. Protoc.* **4**, 1184–1191 (2009).
183. Huang, S.-M. In Vitro Metabolism-and Transporter-Mediated Drug-Drug Interaction Studies Guidance for Industry DRAFT GUIDANCE. (2009).
184. Vernetti, L. *et al.* Functional Coupling of Human Microphysiology Systems: Intestine, Liver, Kidney Proximal Tubule, Blood-Brain Barrier and Skeletal Muscle. *Sci. Rep.* **7**, (2017).
185. Nigam, S. K. & Bush, K. T. Uraemic syndrome of chronic kidney disease: altered remote sensing and signalling. *Nature Reviews Nephrology* vol. 15 301–316 (2019).
186. Xia, X. Bioinformatics and Drug Discovery. *Curr. Top. Med. Chem.* **17**, 1709 (2017).
187. A, D., O, M. & V, Z. SwissADME: a free web tool to evaluate pharmacokinetics, drug-likeness and medicinal chemistry friendliness of small molecules. *Sci. Rep.* **7**, (2017).
188. Birdwell, K. A. *et al.* Use of a DNA Biobank Linked to Electronic Medical Records to Characterize Pharmacogenomic Predictors of Tacrolimus Dose Requirement in Kidney Transplant Recipients. *Pharmacogenet. Genomics* **22**, 32 (2012).
189. DM, R. *et al.* Development of a large-scale de-identified DNA biobank to enable personalized medicine. *Clin. Pharmacol. Ther.* **84**, 362–369 (2008).
190. Schuler, B. A. & Medical College of Wisconsin. Strengths and weaknesses in the application of next-generation sequencing to patient care : three cases in clinical genomics. (2015).
191. Y, I., E, Y. & K, S. Micro total bioassay system for oral drugs: evaluation of gastrointestinal degradation, intestinal absorption, hepatic metabolism, and

bioactivity. *Anal. Sci.* **28**, 197–200 (2012).

192. Sung, J. H. *et al.* Recent advances in body-on-a-chip systems. *Anal. Chem.* **91**, 330 (2019).
193. LM, S., ML, S., JG, B. & A, G. A cell culture analogue of rodent physiology: Application to naphthalene toxicology. *Toxicol. In Vitro* **9**, 307–316 (1995).
194. H, K., Y, S. & T, F. Organ/body-on-a-chip based on microfluidic technology for drug discovery. *Drug Metab. Pharmacokinet.* **33**, 43–48 (2018).
195. K, V., A, S. & ML, S. Development of a microscale cell culture analog to probe naphthalene toxicity. *Biotechnol. Prog.* **20**, 316–323 (2004).
196. CD, E. *et al.* Interconnected Microphysiological Systems for Quantitative Biology and Pharmacology Studies. *Sci. Rep.* **8**, (2018).